CARBON DIOXIDE CAPTURE ON NITROGEN-DOPED CARBON NANOPARTICLE DERIVED FROM AROMATIC COMPOUNDS VIA SOLUTION PLASMA AND NITRIDATION

Mr. Phuwadej Pornaroontham

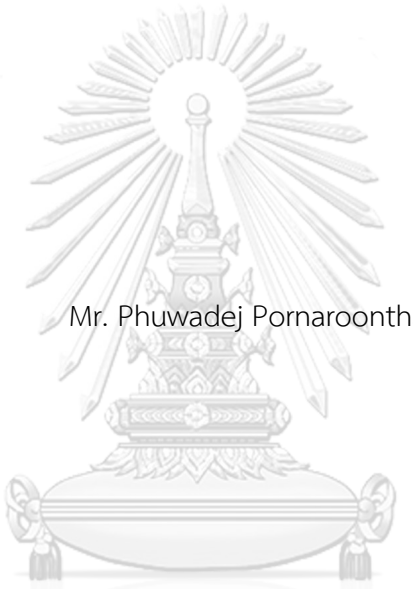

จุฬาลงกรณ์มหาวิทยาลัย
CHULALONGKORN UNIVERSITY

A Dissertation Submitted in Partial Fulfillment of the Requirements
for the Degree of Doctor of Philosophy in Chemical Technology
Department of Chemical Technology
Faculty of Science
Chulalongkorn University
Academic Year 2018

Copyright of Chulalongkorn University

การจับยึดคาร์บอนไดออกไซด์บนอนุภาคคาร์บอนระดับนาโนเมตรเจือด้วยไนโตรเจนที่เตรียมจากสารประกอบแอโรแมติกผ่านกระบวนการโซลูชันพลาสมาและไนไตรเดชัน

นายภูวเดช พรอรุณธรรม

จุฬาลงกรณ์มหาวิทยาลัย
CHULALONGKORN UNIVERSITY

วิทยานิพนธ์นี้เป็นส่วนหนึ่งของการศึกษาตามหลักสูตรปริญญาวิทยาศาสตรดุษฎีบัณฑิต
สาขาวิชาเคมีเทคนิค ภาควิชาเคมีเทคนิค
คณะวิทยาศาสตร์ จุฬาลงกรณ์มหาวิทยาลัย
ปีการศึกษา 2561
ลิขสิทธิ์ของจุฬาลงกรณ์มหาวิทยาลัย

Thesis Title	CARBON DIOXIDE CAPTURE ON NITROGEN-DOPED CARBON NANOPARTICLE DERIVED FROM AROMATIC COMPOUNDS VIA SOLUTION PLASMA AND NITRIDATION
By	Mr. Phuwadej Pornaroontham
Field of Study	Chemical Technology
Thesis Advisor	Professor NATTAYA PONGSTABODEE, Ph.D.
Thesis Co Advisor	Professor Nagahiro Saito, Ph.D.

Accepted by the Faculty of Science, Chulalongkorn University in Partial Fulfillment of the Requirement for the Doctor of Philosophy

..... Dean of the Faculty of Science
(Professor POLKIT SANGVANICH, Ph.D.)

DISSERTATION COMMITTEE

..... Chairman
(Associate Professor PRASERT REUBROYCHAROEN, Ph.D.)

..... Thesis Advisor
(Professor NATTAYA PONGSTABODEE, Ph.D.)

..... Thesis Co-Advisor
(Professor Nagahiro Saito, Ph.D.)

..... Examiner
(Associate Professor CHAWALIT NGAMCHARUSSRIVICAI, Ph.D.)

..... Examiner
(Associate Professor NAPIDA HINCHIRANAN, Ph.D.)

..... External Examiner
(Gasidit Panomsuwan, Ph.D.)

จุฬาลงกรณ์มหาวิทยาลัย
Chulalongkorn University

ภูวเดช พรอรุณธรรม : การจับยึดคาร์บอนไดออกไซด์บนอนุภาคคาร์บอนระดับนาโนเมตรเจือด้วยไนโตรเจนที่เตรียมจากสารประกอบแอโรแมติกผ่านกระบวนการโซลูชันพลาสมาและไนไตรเดชัน. (CARBON DIOXIDE CAPTURE ON NITROGEN-DOPED CARBON NANOPARTICLE DERIVED FROM AROMATIC COMPOUNDS VIA SOLUTION PLASMA AND NITRIDATION) อ.ที่ปรึกษาหลัก : ศ. ดร.ณัฐธยาน์ พงศ์สถาบดี, อ.ที่ปรึกษาร่วม : ศ. ดร.นากาฮิโระ ไซโตะ

งานวิจัยนี้ศึกษาการดูดซับคาร์บอนไดออกไซด์บนตัวดูดซับคาร์บอนระดับนาโนเมตรที่เตรียมสารประกอบเบนซีน (C) และของผสมระหว่างเบนซีนและน้ำมันหล่อเย็น (oC) ผ่านกระบวนการโซลูชันพลาสมา โดยตัวดูดซับที่ได้จากกระบวนการมีความสามารถในการดูดซับคาร์บอนไดออกไซด์ต่ำก่อนการดัดแปรด้วยการให้ความร้อนในบรรยากาศแอมโมเนียที่อุณหภูมิสูง หลังจากการดัดแปรพบว่าความสามารถในการดูดซับสูงสุดที่ 1.63 มิลลิโมลต่อกรัมตัวดูดซับที่อุณหภูมิการดูดซับ 25 องศาเซลเซียสบนตัวดูดซับที่เตรียมจากของผสมระหว่างเบนซีนและน้ำมันหล่อเย็นในอัตราส่วนร้อยละ 15 โดยปริมาตรผ่านกระบวนการโซลูชันพลาสมาดัดแปรภายใต้บรรยากาศแอมโมเนียที่อุณหภูมิ 800 องศาเซลเซียส (noC15(800)) การศึกษาคุณลักษณะของตัวดูดซับสังเคราะห์ด้วยเทคนิคต่างๆพบว่าค่าการดูดซับขึ้นกับรูพรุนขนาดไมโคร และปริมาณหมู่ฟังก์ชันไนโตรเจนบนคาร์บอนเป็นสำคัญ การศึกษาอุณหพลศาสตร์ของการดูดซับทำให้ทราบถึงกลไกลการดูดซับพบว่า การดูดซับบน noC15(800) เป็นการดูดซับทางกายภาพ เป็นกระบวนการคายความร้อน และเกิดขึ้นเองได้ โดยมีแรงจับยึดกับโมเลกุลของตัวถูกดูดซับที่แข็งแรงกว่าตัวดูดซับที่ไม่ผ่านการดัดแปร อีกทั้งยังเพิ่มความสามารถในการเลือกจับคาร์บอนไดออกไซด์ได้ดีกว่าการเลือกจับไนโตรเจนหลังการดัดแปร สามารถนำกลับมาใช้ใหม่ได้เมื่อผ่านกระบวนการฟื้นฟูด้วยอุณหภูมิและสุญญากาศ มีเสถียรภาพต่อการนำไปใช้เป็นวัฏจักร การศึกษาไอโซเทอมของการดูดซับพบว่า การดูดซับเป็นแบบชั้นเดียว เกิดบนพื้นผิวตัวดูดซับวิวิธพันธ์ และจากการศึกษาโดยใช้สถิติศาสตร์พบว่า ความเป็นรูพรุนระดับไมโคร และหมู่ฟังก์ชันไนโตรเจนส่งผลทางบวกต่อค่าการดูดซับ อีกทั้งอันตรกิริยาระหว่างตัวแปรเป็นชนิดเสริมฤทธิ์กัน

สาขาวิชา เคมีเทคนิค ลายมือชื่อนิสิต .....

ปีการศึกษา 2561 ลายมือชื่อ อ.ที่ปรึกษาหลัก .....

ลายมือชื่อ อ.ที่ปรึกษาร่วม .....

5772838523 : MAJOR CHEMICAL TECHNOLOGY

KEYWORD: Carbon dioxide, Adsorption, Solution plasma process, Carbonaceous material

Phuwadej Pornaroontham : CARBON DIOXIDE CAPTURE ON NITROGEN-DOPED CARBON NANOPARTICLE DERIVED FROM AROMATIC COMPOUNDS VIA SOLUTION PLASMA AND NITRIDATION. Advisor: Prof. NATTAYA PONGSTABODEE, Ph.D. Co-advisor: Prof. Nagahiro Saito, Ph.D.

The carbon dioxide (CO_2) adsorption on nanocarbon (C), oxygen-doped nanocarbon synthesized from benzene and a mixture of benzene and metal working fluid (MWF), respectively, via solution plasma process (SPP) have been revealed in this study. Firstly, they showed low CO_2 adsorption capacity at 25 °C. However, their capacities were enhanced by nitridation under ammonia atmosphere at high temperature. The maximum CO_2 adsorption capacity of 1.63 mmol g^{-1} was achieved on nitrogen-oxygen-codoped nanocarbon obtained from SPP discharging a mixture containing 15 vol% MWF nitrided at 800 °C (noC15(800)). The characterizations revealed that the micropososity and nitrogen functionality on the adsorbent are crucial parameters affecting the CO_2 capacity. From thermodynamics insights, the adsorption on noC15(800) was physisorption, exothermic, spontaneous and with better selectivity of CO_2/N_2 compared to unmodified. noC15(800) also showed good stability over multi-cycle of use. The adsorption isotherm on noC15(800) over the whole pressure range at all temperatures was best fitted to the Toth isotherm referring monolayer adsorption on heterogenous surface. From the statistical analysis, micropore and nitrogen content had positive synergistic effect on adsorption capacity.

จุฬาลงกรณ์มหาวิทยาลัย
Chulalongkorn University

Field of Study: Chemical Technology Student's Signature .....

Academic Year: 2018 Advisor's Signature .....

Co-advisor's Signature .....

ACKNOWLEDGEMENTS

I would like to use this opportunity to express my deepest gratitude with special thanks to the people who contributed and fulfilled my PhD life.

Firstly, I would like to thank with deepest appreciation to my advisor, Prof Nuttaya Pongstabodee, PhD, as well as my co-advisor, Prof. Nagahiro Saito, PhD,who gave me the great supervision and encouragement. He also gave me a golden opportunity to have a short-term experience in Saito laboratory at Nagoya University to complete this wonderful project, which also helped me in doing a lot of research and I came to know about so many new things I am really thankful to them.

Secondly, I would like to thank Gasidit Panomsuwan, PhD, for introducing Solution Plasma process and giving helpful suggestion to initiate the idea of this project.

Thirdly, I am grateful to my colleagues in Nuttaya's lab group at Chulalongkorn University and Saito's lab at Nagoya University who gave me their careful guidance both theoretically and practically to surpass all problem. I also really thank them for extending their friendship towards to me and sharing good moment during PhD life.

Besides, I would like to thank the 100th Anniversary Chulalongkorn University Fund for Doctoral Scholarship, the 90th Anniversary of Chulalongkorn University Fund (Ratchadaphiseksomphot Endowment Fund) and the PETROMAT Fund for financial support over years. I also thank Department of Chemical technology, Chulalongkorn University, and the Department of Chemical Systems Engineering, Nagoya University, for instrumental support.

Lastly, my PhD degree could not be achieved without heartening, love and care from my family. This PhD symbolized their success of parenting me to achieve this PhD degree.

Phuwadej Pornaroontham

จุฬาลงกรณ์มหาวิทยาลัย
Chulalongkorn University

TABLE OF CONTENTS

Page

.....iii

ABSTRACT (THAI).....iii

.....iv

ABSTRACT (ENGLISH).....iv

ACKNOWLEDGEMENTS.....v

TABLE OF CONTENTS.....vi

LIST OF TABLES.....x

LIST OF FIGURES.....xi

CHATER I INTRODUCTION.....1

1.1 Background.....1

1.2 Objectives.....3

1.3 Scope of dissertation.....3

1.4 Methodology.....3

CHAPTER II RELATED THEORIES AND LITERATURE REVIEWS.....5

2.1 CO_2 capture technologies.....5

2.2 Solid-gas adsorption.....7

2.2.1 Physical adsorbent.....8

2.2.2 Chemical adsorbent.....8

2.2.2.1 CO_2 adsorption in absence of water.....9

2.2.2.2 CO_2 adsorption in presence of water.....9

2.2.3 Example of CO_2 adsorbent.....11

จุฬาลงกรณ์มหาวิทยาลัย
Chulalongkorn University

2.2.3.1 Zeolitic materials 11
2.2.3.2 Mesoporous silica 12
2.2.3.3 Carbonaceous materials 13
2.2.3.3.1 Hard-templated method 15
2.2.3.3.2 Soft-templated method 15
2.2.3.3.3 Template-free synthesis 16
2.2.3.3.4 Physical and chemical deposition 16
2.2.3.3.5 Solution plasma process 17
2.3 Porosity 19
2.4 Swing adsorption process 23
2.4.1 Temperature swing adsorption, TSA 24
2.4.2 Pressure swing adsorption, PSA 24
2.4.3 Vacuum swing adsorption, VSA 25
2.4.4 Concentration swing adsorption, CSA 25
2.4.5 Hybrid process 26
2.5 Adsorption isotherm 26
2.5.1 Langmuir isotherm 26
2.5.2 Freundlich isotherm 27
2.5.3 Sips isotherm 27
2.2.4 Toth isotherm 28
2.6 Thermodynamics of adsorption 29
2.7 Literature Review 32
CHATPER III EXPERIMENTAL 35
3.1 Chemicals 35

จุฬาลงกรณ์มหาวิทยาลัย
Chulalongkorn University

3.2 Solution plasma process (SPP) set up 35
3.3 Preparation of nanocarbons 36
3.4 Nitriding process 36
3.5 CO_2 adsorption measurement 37
3.6 Characterization 37
3.7 Thermodynamic studies 39
3.8 Isotherm studies 39
3.9 Regeneration test 40
3.10 Statistical analyses 40
CHAPTER IV RESULTS AND DISCUSSION 41
4.1 Characterization of synthesized sorbent 41
4.1.1 Crystallinity determination by XRD technique 41
4.1.2 Bulk and surface elemental composition 43
4.1.3 Textural properties of synthesized nanocarbons 45
4.1.4 CO_2 adsorption experiment 50
4.1.5 Raman spectroscopy 51
4.1.6 Transmission electron microscopy 53
4.1.7 Chemical state of heteroatom on nanocarbons examined by XPS 54
4.2 Thermodynamic studies 56
4.2.1 Isosteric enthalpy of adsorption 58
4.2.2 Henry's law region 59
4.2.3 Selectivity of CO_2 over N_2 64
4.2.4 Regenerability and stability test 65
4.3 Isotherm studies 66

จุฬาลงกรณ์มหาวิทยาลัย
Chulalongkorn University

4.4 Statistical analyses 70
4.4.1 First screening 70
4.4.2 Second screening 73
4.4.3 Response surface methodology (RSM) 75
4.5 Deeper studies 80
4.5.1 Influence of micropores on CO_2 adsorption potential 80
4.5.2 Influence of nitrogen atom in carbon framework on CO_2 adsorption mechanism 82
CHAPTER V CONCLUSION 85
5.1 Synthesis of nanocarbon for CO_2 adsorption 85
5.2 CO_2 adsorption mechanism 85
5.3 Influence of factors on CO_2 adsorption capacity 85
REFERENCES 87
VITA 98

จุฬาลงกรณ์มหาวิทยาลัย
Chulalongkorn University

LIST OF TABLES

Page

Table 1 Structural properties obtained from XRD technique 42

Table 2 Elemental composition of SPP-derived carbons 45

Table 3 Textural properties calculated by BET and t-plot methods 49

Table 4 Degree of graphitization expressed in term I_d/I_g and in-plane crystallite size 52

Table 5 Deconvolution results of the XPS spectra at C 1s, O 1s and N 1s for synthesized samples 56

Table 6 Thermodynamic parameters of CO_2 adsorption on C and noC15(800) at different temperatures 63

Table 7 Henry constants on N_2 and CO_2 adsorption and selectivity 65

Table 8 Parameters of fitting the CO_2 adsorption on noC15(800) data 69

Table 9 Twelve observations and its condition used for making statistical analysis ... 71

Table 10 ANOVA table of 1st screening 72

Table 11 Sixteen observations and its condition used for making statistical analysis. 74

Table 12 ANOVA table of 2nd screening 75

Table 13 ANOVA table of response surface analysis 77

Table 14 Comparison of actual response and predicted response 80

จุฬาลงกรณ์มหาวิทยาลัย
CHULALONGKORN UNIVERSITY

LIST OF FIGURES

Page

Figure 1 Global greenhouse gas emissions based on global emission from 2010 (a) by type of gases and (b) by economic sector 6

Figure 2 Trend in atmospheric concentration of CO_2 6

Figure 3 Carbon capture and storage technologies 7

Figure 4 Reaction mechanism of CO_2 and primary or secondary amine in absence of water 9

Figure 5 Reaction mechanism of CO_2 and tertiary amine in presence of water 10

Figure 6 Reaction routes for CO_2 and primary amine or secondary amine with and without water 11

Figure 7 The framework structures of Zeolite 12

Figure 8 Mesoporous silica with different types of structure 13

Figure 9 Carbon allotropes (a) diamond, (b) graphite, (c) lonsdaleite, (d) C60 buckminsterfullerene, (e) C540 Fullerite, (f) C70 g) amorphous carbon and (h) single-walled carbon nanotube 14

Figure 10 Nitrogen containing functional groups on carbon framework 14

Figure 11 Schematic diagram of hard-templated and soft-soft-templated synthesis 16

Figure 12 A schematic diagram of solution plasma 18

Figure 13 Reaction routes from aliphatic and aromatic molecules 19

Figure 14 Pore types on a porous material 20

Figure 15 IUPAC Classification of physisorption isotherms 21

Figure 16 Classification of hysteresis loops 22

Figure 17 Adsorption isotherm at different temperatures 24

จุฬาลงกรณ์มหาวิทยาลัย
CHULALONGKORN UNIVERSITY

Figure 18 Adsorption isotherm at different regions of operating pressure 25

Figure 19 Schematic of solution plasma process 36

Figure 20 Temperature-time course utilized for nitriding process 37

Figure 21 XRD patterns of synthetic nanocarbons at (a) different MWF ratio and different nitriding temperatures of (b) C series, (c) oC5 series, (d) oC15 series and (e) oC25 series 43

Figure 22 N_2 adsorption-desorption isotherm of synthetic nanocarbons at -196 °C for (a) C series, (b) oC5 series, (c) oC15 series and (d) oC25 series 48

Figure 23 CO_2 adsorption capacities of SPP-derived carbons at 25 °C for (a) non-nitrided samples and (b) nitrided samples at different temperatures 50

Figure 24 Representative Raman spectra of the different adsorbents 53

Figure 25 Representative TEM images of (a, b) C, (d, e) nC(800), (g, h) oC15 and (j, k) noC15(800) and SAED patterns of (c) C, (f) nC(800) (i) oC15 and (l) noC15(800) 54

Figure 26 Representative XPS spectra of the C, oC15, nC(800) and noC15(800) samples for the (a) C 1s, (b) O 1s and (c) N 1s regions of the nitrided samples (nC(800) and noC15(800)) 55

Figure 27 CO_2 adsorption capacity as a function of the pressure at various temperatures 57

Figure 28 Isostere plots of (a) C and (b) noC15(800) 59

Figure 29 Isosteric enthalpy of adsorption over CO_2 loading on (a) C and (b) noC15(800) 59

Figure 30 Van't Hoff plot of C and noC15(800) 61

Figure 31 N_2 and CO_2 adsorption isotherm at 25 °C on (a) C and (b) noC15(800) 65

Figure 32 CO_2 adsorption capacities on noC15(800) over 5 cycles of use 66

Figure 33 Fitting of CO_2 adsorption isotherms of noC15(800) at different temperatures with four selected isotherm models 68

จุฬาลงกรณ์มหาวิทยาลัย
Chulalongkorn University

Figure 34 Overestimation of maximum capacity when using model without correction 68

Figure 35 Residual plot (a) and Studentized residual by row number plot (b) for 1st screening analysis 72

Figure 36 Residual plot (a) and Studentized residual by row number plot (b) for 2nd screening analysis 73

Figure 37 Residual plot (a) and Studentized residual by row number plot (b) for response surface analysis 77

Figure 38 Half normal plot showing contribution of factors 78

Figure 39 Pareto plot 78

Figure 40 Interaction plot of 3 main effects 79

Figure 41 Surface response of interactions between (a) Vmicro and Temp, (b) Vmicro and %N (c) %N and Temp 79

Figure 42 Sorption potentials on (a) micropore, (b) mesopore and (c) macropore 82

Figure 43 Molecular orbital diagram and the shape of orbitals of the CO_2 molecule 83

Figure 44 Adsorption mechanism of CO_2 on the noC15(800) adsorbent based on electron donation and backdonation 84

จุฬาลงกรณ์มหาวิทยาลัย
Chulalongkorn University

CHATER I

INTRODUCTION

1.1 Background

The level of carbon dioxide (CO_2) in atmosphere is quite low compared to the other gases. However, its concentration keeps increasing for centuries, especially since industrial revolution. The main CO_2 emission was caused by anthropogenic activities. The excess presence of CO_2 in atmosphere caused climate to change. With its characters, polar bond C=O which absorb and re-emit infra-red radiation from the earth's surface making global temperature rising. CO_2 is now considered to be a major greenhouse gas that should be controlled according to Paris agreement in the 2015 United Nations Climate Change Conference, COP21 [1]. In the past, CO_2 from several processes, e.g. post-combustion process, were controlled by reaction with solution of amine or so-called amine scrubbing. However, this method showed many drawbacks in term of equipment corrosion, high energy consumption for generation of solution and requirement on large space for installation scrubbing unit [2, 3]. Thus, recently it has changed to adsorption on solid sorbent with the advantages of ease of handling and transporting, low energy consumption for regeneration. The solid sorbent use in this application should possess the properties of highly thermal and chemical stability for several cycles of use, high surface area to its volume ratio and selective to CO_2. Many researches have been done on studies of amine-functionalized mesoporous solid supports such as zeolites [4], silicas [5, 6], activated carbons [7], and polymers [8]. The performance of CO_2 adsorption on solid sorbent depends on the pore structure, type of amine, and amount of active site. The amine-type sorbents could obtain high CO_2 capture capacities and selective for CO_2 molecule due to specific acid-base reaction between amine functional group and CO_2 molecule to form stable carbamate [9, 10] and/or bicarbonate species [2, 11]. However, the big problem was some amine removed from the surface due to high temperature requirement for regeneration. Thus, the capacity dropped after a while. The alternative way to beat this disadvantage is to making nitrogen atom strongly bonded to solid support by doping nitrogen atom to the framework of support. N-

จุฬาลงกรณ์มหาวิทยาลัย
Chulalongkorn University

doped carbonaceous materials were successfully proved that they had highly thermal stable and can be regenerated at milder condition compared to amine because of weaker binding energy to CO_2 molecule [12-14]. Therefore, they can be used last longer. To synthesize carbon support, carbonization was introduced but it still needs very high temperature and take long time. Some researches introduced a way to synthesize carbon support by using aromatic organic compounds via solution plasma process (SPP) [15]. It is a cold or non-equilibrium plasma in liquid phase [23] by discharging bipolar pulse at specific frequency into liquid phase. The large temperature difference between plasma core and the bulk liquid caused phase changing of matter to be quenched. While it has enough energy to creates activated species initiating chemical reaction to occur. The organic solution is a key-factor to synthesize carbon material. Kang, J. and group [15] synthesized carbon nanoparticles from pure benzene at different applied frequency. Their carbon material exhibited high surface area and contained some mesoporosity at discharging at 25 kHz. At this point, it seems that carbon particles from this method has potential to be CO_2 adsorbent. Since mesoporosity acts as a pathway to diffuse sorbate molecule to store inside [16]. However, those surface areas are mainly external surface area which is not suitable for adsorb CO_2 molecule. Previous studies revealed that microporosity [17, 18] was the key to adsorb CO_2 with high capacity combining with mesopore [19, 20] and/or changing its skeleton to nanoscale [21, 22] which provide fast kinetics. Thus, carbons from SPP needs further activation to open the micropores. Doping nitrogen atom to carbon matrix was also proved to promote CO_2 adsorption [23, 24] which was achieved by nitriding process which is a treatment with ammonia at high temperature. However, the amount of nitrogen atom doped in carbon framework is proportional to surface oxygen density [25]. The application of SPP can also synthesize heteroatom-doped carbonaceous materials with various mixing substances to organic solutions [26, 27]. Therefore, mixing metal working fluid (MWF), which contains high level of carbon and oxygen resources from its based oil and additives, with aromatic solution under SPP discharging in attempt to increase oxygen surface density to synthesized carbon. Moreover, MWF is completely miscible with benzene making solution homogeneous. From all mentioned above, we are

presenting CO_2 adsorption on carbonaceous material synthesized via SPP by using solution of benzene mixed with MWF followed by nitriding process with the study of adsorption mechanism by using isotherm studies and thermodynamic studies.

1.2 Objectives

1.2.1 To synthesize N-doped carbon via solution plasma process and followed by nitriding process

1.2.2 To investigate adsorption mechanism on N-doped carbon by thermodynamic and isotherm studies

1.3 Scope of dissertation

1.3.1 Synthesis of oxygen-doped carbon from benzene aromatic compound and mixture of benzene and metal working fluid using solution plasma process

1.3.2 Doping nitrogen atom onto carbon-based sorbent using nitridation

1.3.3 Investigation on CO_2 adsorption of sorbent with studying adsorption mechanism by using thermodynamic aspect

1.3.4 Testing regenerability and stability over multi-cycle of use on sorbent

1.4 Methodology

จุฬาลงกรณ์มหาวิทยาลัย
Chulalongkorn University

1.4.1 Studying related literature reviews

1.4.2 Synthesizing carbon-based adsorbent using pure benzene and mixture of benzene and metal working fluid (MWF) at different ratios (0 – 25 vol%) via solution plasma process (SPP)

1.4.3 Surface modifications on synthesized carbon-based adsorbent by nitridation at different temperatures, 600 – 800 °C

1.4.4 Testing CO_2 adsorption by volumetric analysis at 25 °C

1.4.5 Characterizations on synthesized sorbents

1.4.5.1 X-ray diffractometry (XRD)

– To identify the intrinsic crystallinity of the sorbent

1.4.5.2Transmitted electron microscopy (TEM)

– To analyze the morphology of the sorbent

1.4.5.3Raman spectroscopy

– To investigate the defect site of the sorbent

1.4.5.4CHN analysis

– To find the elemental composition of the sorbent

1.4.5.5X-ray photoelectron spectroscopy (XPS)

– To evaluate the surface chemical state of the sorbent

1.4.5.6N_2 physisorption measurement

– Surface properties analysis

1.4.6 Revealing CO_2 adsorption mechanism by using thermodynamic and equilibrium studies

1.4.7 Studying selectivity of CO_2 over N_2

1.4.8 Testing stability on multi-cycled adsorption

1.4.9 Writing manuscripts and dissertation

จุฬาลงกรณ์มหาวิทยาลัย
Chulalongkorn University

CHAPTER II

RELATED THEORIES AND LITERATURE REVIEWS

2.1 CO_2 capture technologies

The global warming has become the serious problem since the emission of greenhouse gases (GHGs) has been dramatically increased within decades. This is because of that an increasing in world populations, more requirements of the basic human needs which is leading to more energy to be consumed. Most of energy resources is now fossil fuel which causes a lot of environmental problems. It is surprising that not only the earth's average temperature has been increasing, but also the global sea level has been rising. Most of the observed increase in globally averaged temperatures since the mid-20th century is due to the observed increase in greenhouse gases concentration in the atmosphere. This is discernible that human influences now extend to other aspects of climate, accompany with ocean warming, continental-average temperatures, temperature extremes, and change in wind patterns.

The greenhouse gases are the gases that can absorb infrared radiation from the earth's surface which is normally reflected to the space. This is called the greenhouse effect. There are many well-known GHGs such as methane, oxides of nitrogen, unburnt hydrocarbons, water vapor, fluorinated gases (e.g. CFCs) and carbon dioxide (CO_2). The effect of greenhouse gases depends on its residence time, ability to absorb the radiation and its atmospheric concentration. CO_2 has been considered as one of the major GHGs since CO_2 is contributing more than 70% of global greenhouse gas emissions shares [28] (Figure 1) which were mainly released from energy production. IPCC said that the atmospheric CO_2 concentration has increased 30 percent since preindustrial era and that the present concentration has not been exceeded during the past 420,000 years likely not during the past 20 million years. This encourages an increase in global temperature. About three-quarters of the emissions of CO_2 is attributed to the combustion fossil fuel. The National Oceanic and Atmospheric Administration – NOAA [29] showed that carbon dioxide level has been rising from 318 ppm in 1960 to 408 ppm in 2018 or 28% increased as shown in

Figure 2. According to the 21st Conference of Parties, COP21, also known as the 2015 Paris Climate Conference, they aim to achieve a legally binding and universal agreement on climate, with the aim of keeping global warming below 2°C [1]. GHGs emission for each country must be limited. It is then necessary to control the amount of CO_2 before release to the atmosphere. Therefore, the scientists invented the technologies that solve this problem which is called Carbon Capture and Storage (CCS).

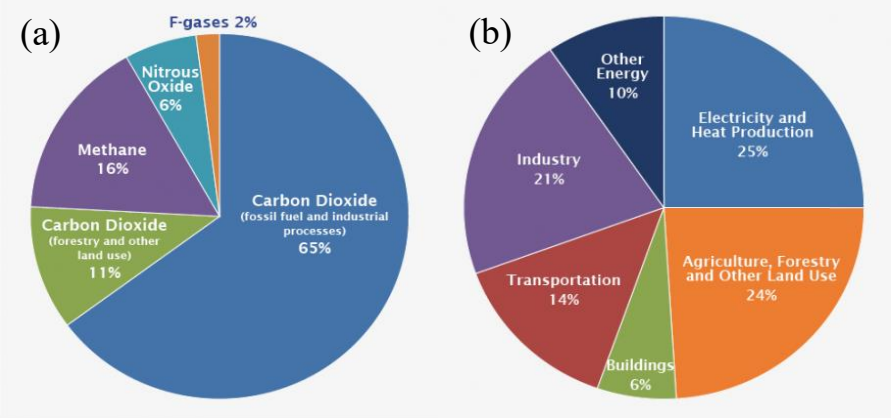

Figure 1 Global greenhouse gas emissions based on global emission from 2010 (a) by type of gases and (b) by economic sector [30]

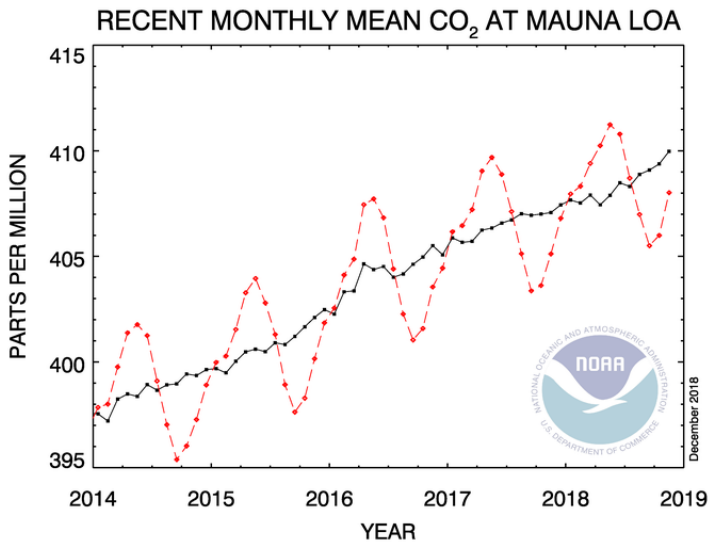

Figure 2 Trend in atmospheric concentration of CO_2 [29]

Figure 3 shows some of CO_2 capture technologies for post-combustion process. Conventionally, CO_2 can be captured via chemical absorption using amine solvent, which is based on the fact that amine is a base and CO_2 is acidic, by flowing CO_2 gas into amine-scrubbing unit as shown in However, this method showed many drawbacks in term of equipment corrosion, high energy consumption for regeneration, requirement of a large space for installing scrubbing-unit [2, 3], and loss of amine-solution. Many searches focus on an adsorption on porous solid sorbent due to its ease of handling, low energy consumption for regeneration. To overcome these drawbacks, CO_2 technology has been developed by using solid sorbent adsorption because of less space needed, lower regenerating energy consumption and high durability.

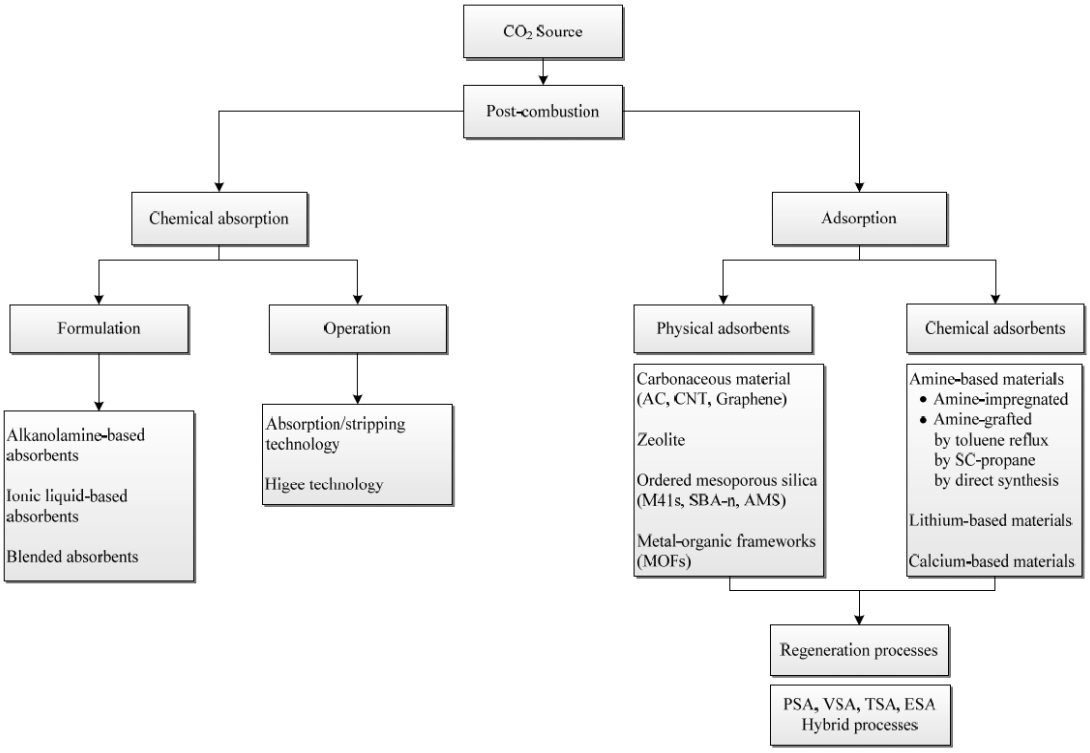

Figure 3 Carbon capture and storage technologies [31]

2.2 Solid-gas adsorption

Solid-gas adsorption is a concept that the gaseous adsorbate molecule is attracted to the solidus adsorbent surface by forces of attraction. There are two

major types of adsorption which are physical adsorption and chemical adsorption. For physical adsorption, so called physisorption, the adsorbate attracted to the adsorbate by weak forces leading to high possibility for regeneration. This type of adsorption is normally operating under high pressure to push more adsorbate stay inside porous adsorbate. Low temperature is also required in this kind of adsorption. On the other hand, chemisorption is adsorption where the adsorbate and adsorbent interact each other chemically. The performance of adsorption relies on amount of the active site and porosity of adsorbent. It usually operates at atmospheric pressure and suitable temperature which sometimes at high temperature due to activation requirement. In addition, there is some good points for chemical adsorption which are better efficiency and higher selectivity of CO_2 capture. This can be enhanced by functionalizing amine on the surface of solid sorbents.

2.2.1 Physical adsorbent

Physical adsorbent is adsorbent that interact with adsorbate molecule, CO_2, by weak Van der Waals forces. It usually has enthalpy of adsorption less than 40 kJ mol^{-1}. Normally, this kind of adsorbent needs high pressure to operate and the adsorption capacity relies on textural properties of them, which are total surface area and porosity. Although it has weak binding forces to CO_2 molecule, it has benefit of that the adsorption is reversible which means regeneration is highly possible.

จุฬาลงกรณ์มหาวิทยาลัย
Chulalongkorn University

2.2.2 Chemical adsorbent.

Another type of adsorbent is chemical adsorbent where the CO_2 molecule is bonded to the chemical active site via chemical bonding. It usually has the enthalpy of adsorption above 80 kJ mol^{-1}. These active sites normally involved the basic functionalities because CO_2 is acidic, so the acid-base interaction is possible. For the inorganic base, most of them are metal oxide or metal hydroxide, while the organic base is amine. Therefore, the adsorption performance of adsorbent relies on the amount of active site mainly.

There are many studies that focuses on amine-modified adsorbent. Typically, they immobilized amine on a solid support via different method, such as simple-impregnation, functionalization, grafting and polymerization. There are varieties of support have been studied, mesoporous silicas [3, 5, 6], zeolites [4], polymers (polymethacrylate, polystyrene) [8] and carbonaceous materials [7, 32, 33]. With this, the adsorption capacity could be enhanced and increase its selectivity to CO_2 over N_2 and/or CH_4 from the mixture of gases. The chemistry between amine and CO_2 are expressed below:

2.2.2.1 CO_2 adsorption in absence of water

Primary amine or secondary amine reacts with CO_2 via neutralization to form alkylammonium carbamate with stoichiometric ratio of 1:2. It caused by nitrogen atom on amine, which is Lewis base, donates electron to interact with positive pole of CO_2 molecule on C atom forming zwitterion. Then it reacts further with another amine group to form carbamate as shown in Figure 4.

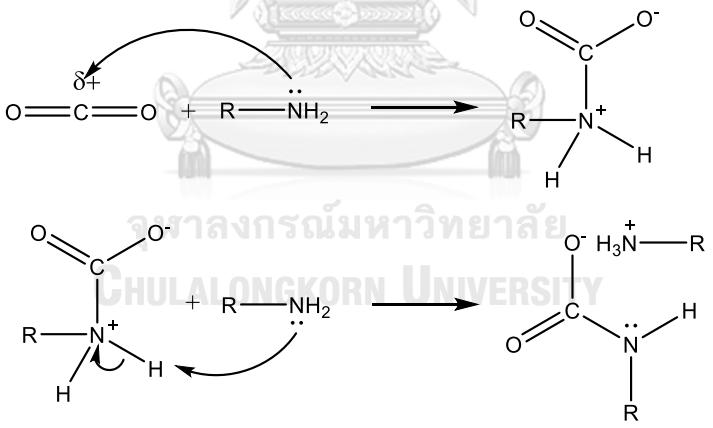

Figure 4 Reaction mechanism of CO_2 and primary or secondary amine in absence of water

2.2.2.2 CO_2 adsorption in presence of water

For tertiary amine water is needed to react with CO_2 forming alkylammonium bicarbonate species as described in Figure 5 with the stoichiometric ratio of 1:1:1 for

amine, CO_2 and H_2O, respectively. Formation of bicarbonate species is happened for primary amine and secondary amine also but in presence of water. It firstly forms carbamate species as described above and then a carbamate salt further reacts with water to form bicarbonate species which release 1 amine group. As a result, amine and CO_2 reacts 1:1 ratio. Furthermore, these amines also directly react with water and CO_2 with the ratio 1:1:1 to form bicarbonate species. This means adsorption capacity can be enhanced by moisture. However, to form bicarbonate needs more energy to overcome activation energy. Therefore, their kinetics is slower and need higher temperature of operation. The formation of carbamate is fast and irreversible at low temperature while bicarbonate formation is slower and reversible [34]. Thus, for regeneration process bicarbonate is somehow preferred. Moreover, the reaction between ammonia/amine group also lead to carbonate species formation but the reaction is much slower than bicarbonate formation. Thus, carbamate and bicarbonate play an important role for CO_2 adsorption chemically as summarized in Figure 6

.

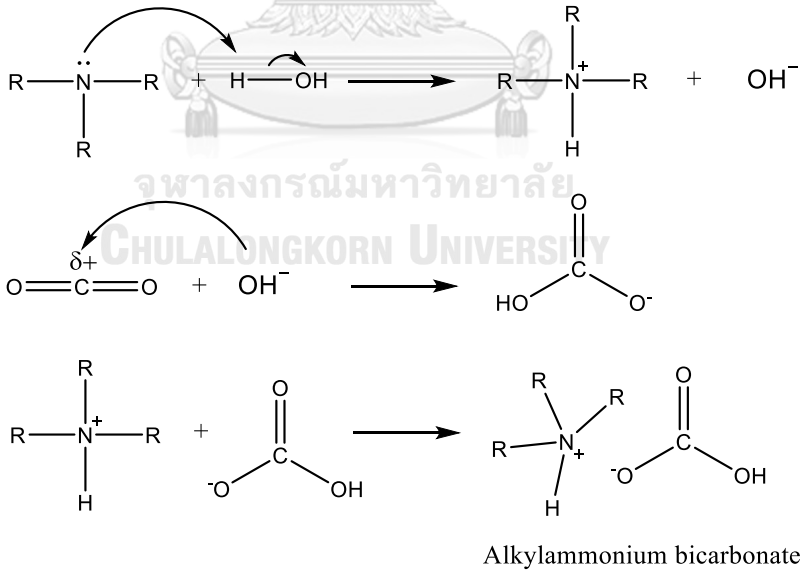

Figure 5 Reaction mechanism of CO_2 and tertiary amine in presence of water

จุฬาลงกรณ์มหาวิทยาลัย
Chulalongkorn University

Although the chemisorption relies on amount of active site, however the transport of gas to the surface is also important factor. Thus, textural property of adsorbent is still a main factor needed to be determined.

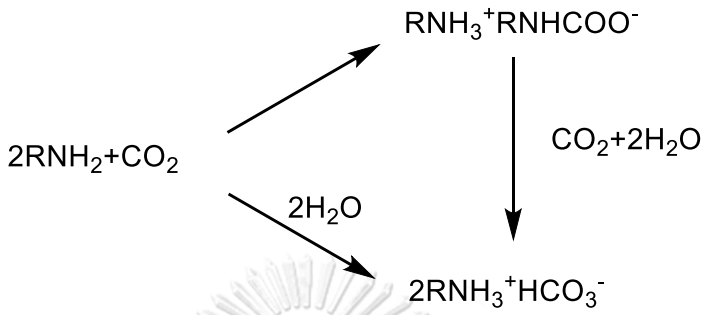

Figure 6 Reaction routes for CO_2 and primary amine or secondary amine with and without water

2.2.3 Example of CO_2 adsorbent

From this point, the examples of adsorbent that have been studied are described as follows:

2.2.3.1 Zeolitic materials

Zeolites is a mineral that can be found naturally, and it can also be synthesized by chemical processes. They are mainly composed of aluminium, silicon and oxygen, so called aluminosilicate, which have high microporosity. Its pores are containing various positive ions that can be exchanged with the others causing different acidity and catalytic activity. Zeolites are also called as molecular sieve due to that its size and pore size are tunable. Therefore, it is normally used to separate single component from the mixture such as oxygen, nitrogen or argon from ordinary air. The type of zeolites was categorized based on its structures and frameworks. Till now, it has more than 200 types of zeolite according to Structure commission of International Zeolite Association (IZA). There are many researches study on CO_2 adsorption on zeolite. Some have modified the surface of zeolite to be more selective on CO_2 molecule by replacing alkaline and/or alkaline-earth metal ion to

จุฬาลงกรณ์มหาวิทยาลัย
Chulalongkorn University

the framework [35-37]. The advantages of using zeolite is that it can withstand high temperature condition which is suitable for post-combustion flue gas. However, its drawbacks are moisture-sensitive which reduces adsorption capacity, and high temperature is needed for regeneration.

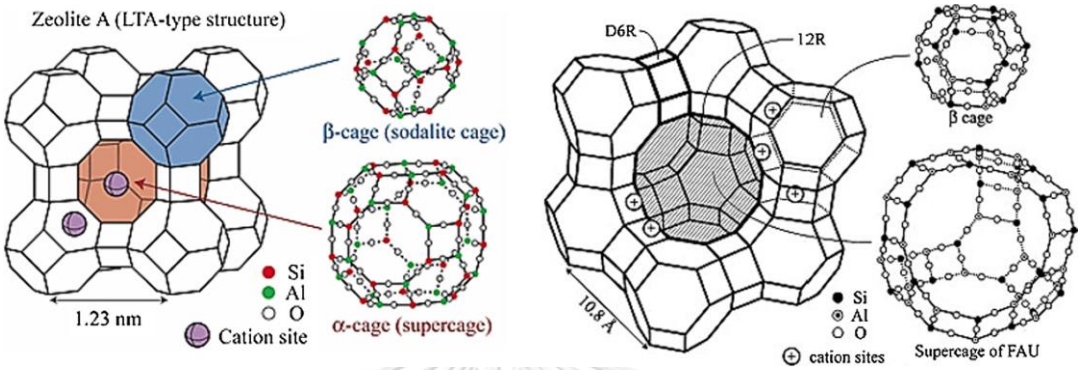

Figure 7 The framework structures of Zeolite [38]

2.2.3.2 Mesoporous silica

A silicate material made of SiO_2 is well-known and widely used for many applications, such as supports for catalysis, selective adsorption, separation and hosts to confine guest molecule. With the advantages of customizable pore structure, high surface area, narrow pore size distributions and high stability to heat and water. Its porosity is mesoporous with pore size in range of 2 to 50 nm which is larger than micropore (<2 nm) of zeolites. The variation of structure depends on the type and the ratio of templating agent, structure-directing agent and space-filling species [39]. In CO_2 adsorption field, there are many researchers studied functionalized mesoporous silica supports with different amine to enhance the adsorption capacity and selectivity which were mainly contributed by type of amine used and the textural property of silica.

จุฬาลงกรณ์มหาวิทยาลัย
Chulalongkorn University

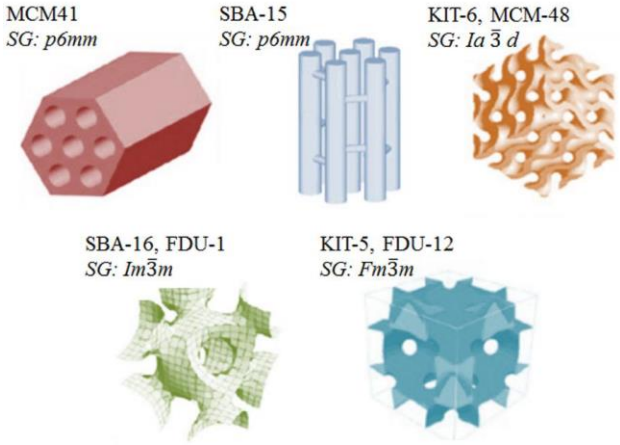

Figure 8 Mesoporous silica with different types of structure [40]

2.2.3.3 Carbonaceous materials

Carbon is an abundant material in the world. It can form many allotropes due to its valency. For example, a carbon atom bonds with other 4 carbon atoms tetrahedrally with sp^3 hybridization to form diamond, a very hard material. Also, it can form to other 3 carbon atoms in hexagonally flat-ringed structure with sp^2 in chemical bonding state as a graphene. Many graphene sheets stack together to form a graphite which the properties are much different from diamond. Some of the allotropes of carbon were shown in Figure 9. Recently, carbonaceous material used for adsorbent is popular due to its high surface area to its volume ratio, high thermal and chemical stability, and ultra-light weigh, such as graphene, carbon nanoparticles and carbon nanotubes. It can be modified to gain more active sites to improve their surface more selective and more reactive to capture CO_2 using organic chemistry. There are many studies about N-doped carbon which is carbon framework containing nitrogen atom. They have found that the presence of nitrogen atoms could increase the affinity of adsorption. Normally doping nitrogen atom into carbon framework can be done by using nitridation or nitriding which is a treatment of carbon under ammonia atmosphere at high temperature. The type of nitrogen containing on carbon framework were shown in Figure 10. Each functional group has different acidity and basicity; thus, the type of nitrogen functional group also affects affinity of adsorption.

จุฬาลงกรณ์มหาวิทยาลัย
Chulalongkorn University

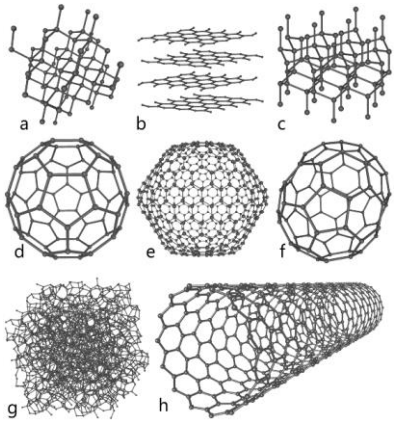

Figure 9 Carbon allotropes (a) diamond, (b) graphite, (c) lonsdaleite, (d) C60 buckminsterfullerene, (e) C540 Fullerite, (f) C70 g) amorphous carbon and (h) single-walled carbon nanotube [41]

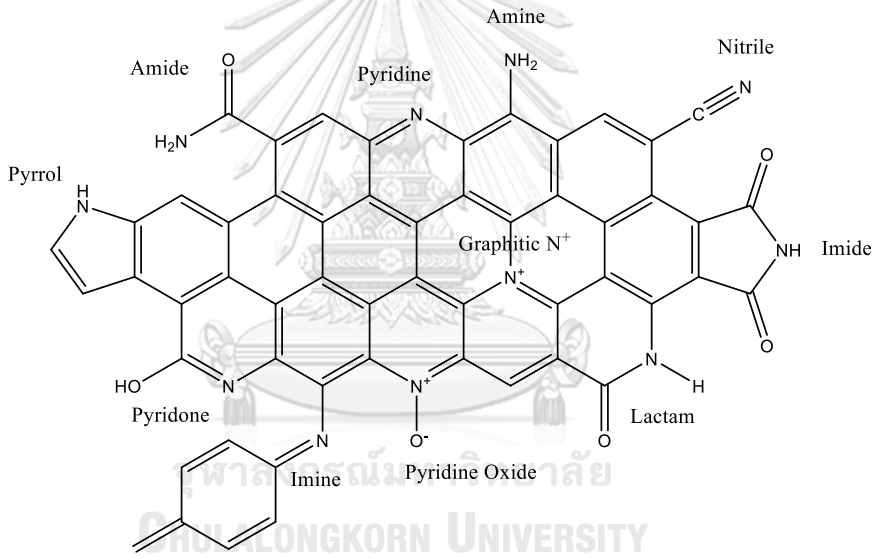

จุฬาลงกรณ์มหาวิทยาลัย
Chulalongkorn University

Figure 10 Nitrogen containing functional groups on carbon framework

There are many ways to synthesize structure-controlled carbon such as hard templated, soft-templated, free-templated, physical vapor deposition (PVD) and chemical vapor deposition (CVD). The general information of those synthesis method will be explained below.

2.2.3.3.1 Hard-templated method

Synthesis of carbon using a rigid material that has a well-ordered structure as a template, for example: mesoporous silica, was called hard-templated synthesis or nanocasting. It was done by using mesoporous support to be filled up with precursor. Then it was carbonized at high temperature to make carbon filling in the hole of template followed by removing template using appropriate method. In case of mesoporous silica as a template, hydrofluoric acid was used to eliminate a template. The good point of this method is the morphology of carbon obtained is precisely controlled and uniform. Therefore, with this method, reproduction is possible and stable. However, it used hazardous chemical during removal of template, thus it could damage the structure of obtained carbon, also the particle would be smaller.

2.2.3.3.2 Soft-templated method

Soft-templated method was also called direct-synthesis. It is different from hard-templated synthesis by that the template is not rigid material. Normally, it used surfactant as a structure-directing agent by using a concept of complicated sol-gel chemistry to form micelles as a template. High polymer and biopolymer were also used in some studies. This method provided a template that was made during synthesis. It is different from hard-templated which was prepared before used. Thus, removal of template is much easier than hard-templated. However, due to that the template is not rigid, so the external conditions (temperature, pH, humidity) would affect structure of template leading to lower controllability compared to hard-templated. Furthermore, the precursor filled in the template should polymerize itself stably to prevent collapsing of structure when template is removed. This is leading to lower controllability and less unity of obtained porous material. The diagram below is presenting synthesis pathways via hard templated and soft templated.

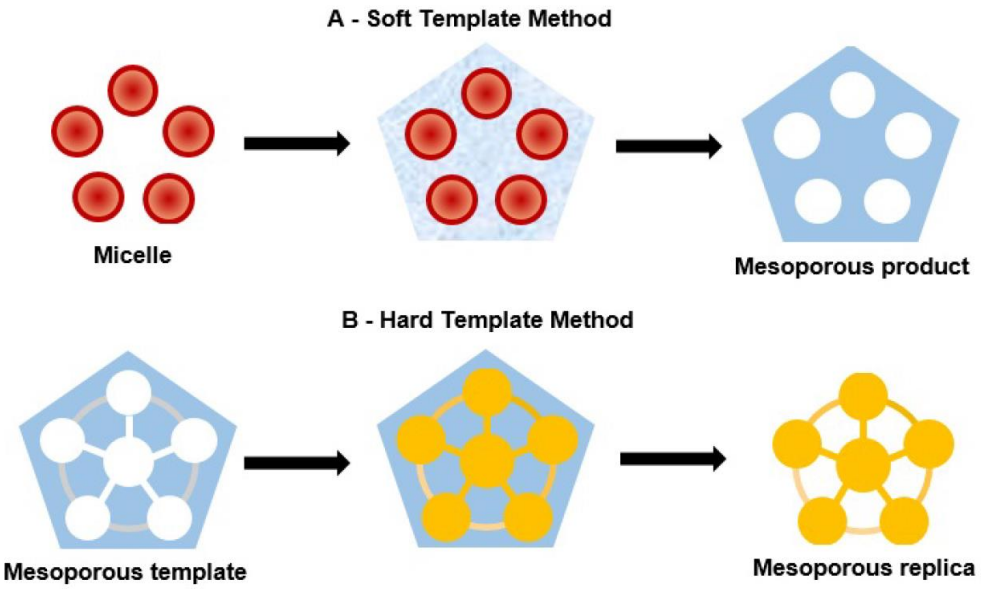

Figure 11 Schematic diagram of hard-templated
and soft-soft-templated synthesis [42]

2.2.3.3.3 Template-free synthesis

This method has a challenge to match up the chemicals that can be self-assembly without templates. The molecules of precursors are link together by polymerization or cross-linking into an organic gel based on sol-gel chemistry. There are reports of synthesis of porous carbon for CO_2 adsorption by mixing two or more chemicals to self-polymerized [43-45]. Then it was activated or carbonized at a suitable condition. There is also a study that using protic salt as a template-free precursor in one-step synthesis of N-doped carbon [46]. This method was done without further process of template removal.

2.2.3.3.4 Physical and chemical deposition

Both PVD and CVD use the same concept of that the product was growing on a suitable substrate. The difference is that PVD is a change in phases physically from the source material, but CVD is a change in carbon precursor which is usually gas (i.e. methane, acetylene) decompose and deposit on substrate. For example, in PVD, it converts liquid or gas source materials into gaseous state, then it condenses back to

thin-film and deposit on a substrate where nucleation and growth of nanostructure take place. The solid formed has different morphology to the initial source. The processes involving in PVD are sputtering and evaporate. A mechanism for producing graphene using PVD on Cu substrate under H_2 annealing has been proposed by Narula, U. and group [47]. In case of CVD, carbon precursors gas would react with a metal catalyst on substrate to grow forming by-product gas which is eliminated by vacuum and use of carrier gas. For the reaction, using heat, laser or plasma also be useful. Finally, obtained carbon was removed from substrate with elimination of metal catalyst by etching. It is highly risky to cause the defect on the crystal while removing nanostructure material from a substrate. Li, X. and group [48, 49] successfully grew graphene layer on copper substrate using CVD of methane and hydrogen gases. These methods are suitable for synthesizing high-quality graphene, carbon nanotubes which those obtained products are uniform. However, it is difficult to make it into mass-production and it needs high-technology.

2.2.3.3.5 Solution plasma process

Solution plasma process (SPP) is re-defined from the term plasma discharge in liquid by Takai and Saito [50-52]. It is thermal non-equilibrium system where the temperature and density of electron is much greater than ions generated in glow discharge regime. This make the temperature of a liquid not getting higher much, so called cold plasma. The chemical reaction exerted by electron mainly. It is unlikely to thermal equilibrium where the temperature and density of electron is are equal similar to ions. Because of the higher mass of ion, so the chemical reaction is induced by thermal effect. This causes the temperature of medium increases rapidly when discharge started, called hot plasma. SPP was conducted by using bipolar pulse power supply connecting to electrode and discharge in a liquid. It was generated under high voltage but low current conditions. The tunable parameters are pulse frequency and pulse width. The model of solution plasma is shown in Figure 12. At the plasma core is very hot about 4000 K surrounded by liquid molecules, which plasma passed through, they absorb the plasma energy adequately

จุฬาลงกรณ์มหาวิทยาลัย
Chulalongkorn University

and consequently are activated to excited molecules and radical species. These activated molecules play likewise an initiator to induce a chemical reaction at the interface between plasma and solution.

The use of SPP can be applied to many fields, such as synthesis of metal nanoparticle in aqueous solution, synthesis of metal-doped carbon and synthesis of heteroatom-doped carbon material. Saito and group [15, 53, 54] successfully synthesized carbon nanoparticle by using SPP discharging in liquid benzene. They have also found that aromatic compound gives better yield of carbon nanoparticle compared to aliphatic compound due to the smaller energy gap between highest occupied molecular orbital (HOMO) and lowest unoccupied molecular orbital, LUMO, of aromatic compound that electron can be excited by plasma because of delocalization of **π**-system from the study of density of state (DOS). They also found the suitable energy gap is around 7 eV. To synthesize carbon particles from SPP, the type of organic solution has an important role for designing the desired species in the carbon framework. From previous works, a mixture of pure organic liquid is applied to synthesize heteroatom-doped carbonaceous materials via SPP [26, 27]

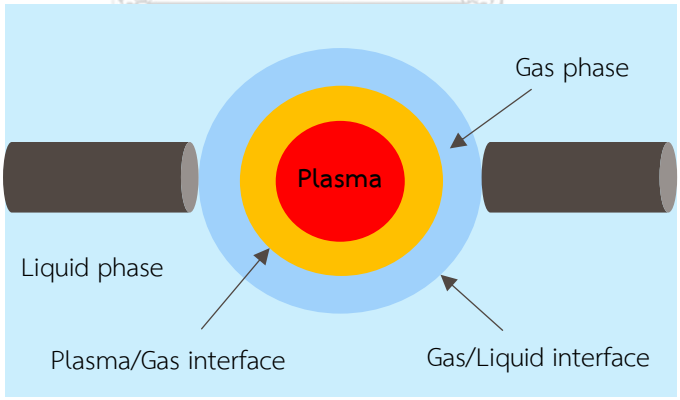

Figure 12 A schematic diagram of solution plasma

The mechanism to synthesize carbon nanoparticles from benzene was purposed by Saito [53]. They found that the pathway for linear molecules and ring molecules are different. Carbon from linear molecules are from carbonization at plasma core. While ring molecule with conjugated **π**-system is polymerization,

shown by Figure 13. The species that play an important role is benzene cation radical which was generated by plasma. It initiates chemical reaction taking place by combining with other molecules or radicals resulting a larger carbon framework. In addition, because different pathway of synthesis, carbon from each route also has difference in structure.

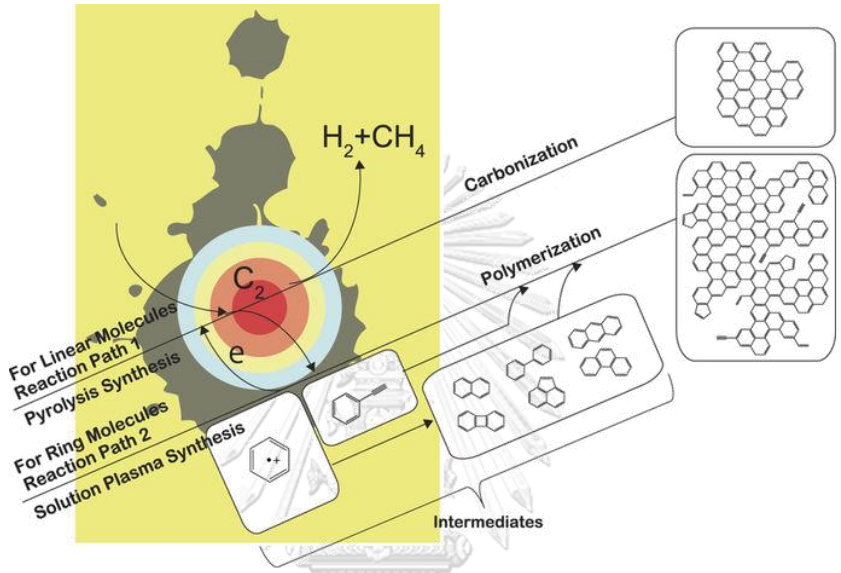

Figure 13 Reaction routes from aliphatic and aromatic molecules [53]

จุฬาลงกรณ์มหาวิทยาลัย
Chulalongkorn University

2.3 Porosity

One of structural properties that is very essential for adsorption application is porosity. On the shows Figure 14 the pore types on a porous material which includes mainly open pore, interconnected pore and closed pore. According to IUPAC classifications, nanopores are categorized into 3 types; micropore, mesopore and macropore. For micropore, it means the pore with a diameter less than 2 nm which can be subdivided into 2 more types: supermicropore with diameter range of 0.7 to 2 nm, while another one is ultramicropore with a diameter less than 0.7 nm. Mesopore is a pore with diameter from 2 to 50 nm. This kind of pore causes the capillary effect during adsorption-desorption analysis. It can be detected by hysteresis loop in physical adsorption isotherm. It can obviously be seen in case of ink-bottle pore

which is a pore that has entrance smaller than its chamber. The last type of nanopore is macropore where the diameter of pore is larger than 50 nm. In adsorption, macropore does not play an important role compared to mesopore and micropore. When the particles are connecting, there might be pores between aggregated particles, so-called interparticle pore or interparticle void. It was usually found in very fine-powdered material. For the closed pore, it was not connected to pathway of gas stream. So, this kind of pore cannot hold any substance in there, but it was also advantageous in term of that it reduces density of material.

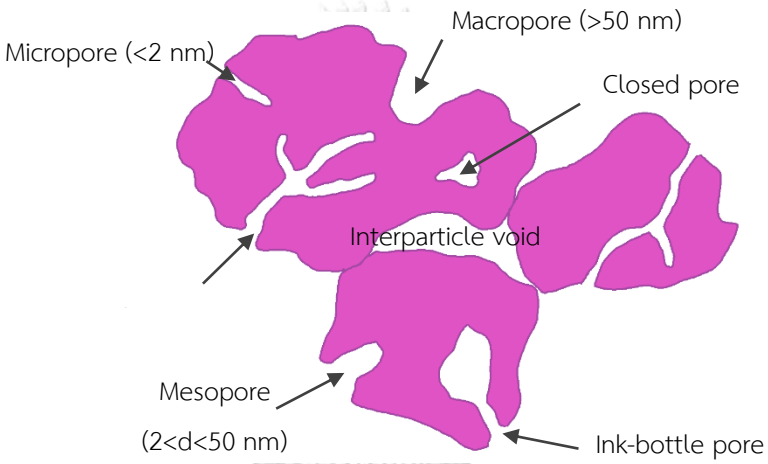

Figure 14 Pore types on a porous material

จุฬาลงกรณ์มหาวิทยาลัย
Chulalongkorn University

To examine the porosity of material, it is normally conducted by N_2 adsorption-desorption analysis at a boiling temperature of N_2 at -196 C. It gives us an isotherm of physical adsorption of N_2 on that material. The type of pores was interpreted from the statistical calculation based on number of layers of N_2 adsorbed extracted from the isotherm. IUPAC classified physical adsorption isotherm into 6 types presenting in Figure 15. The detail of each isotherm is expressed below.

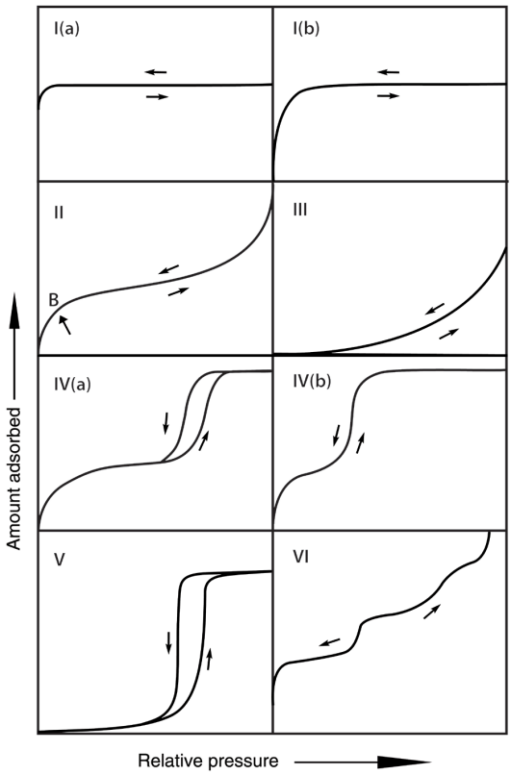

Figure 15 IUPAC Classification of physisorption isotherms

Type I- Microporous material. There is a larger increase at the first slope of isotherm at very low equilibrium pressure and it is saturated at higher pressure. The presence of first slope represent filling in micropores and it finally reached a saturation due to filling micropore rather than its internal surface. The difference between a and b type is the gradient. If the gradient is very steep at first, it means filling into narrow micropores mainly. For b type which has less steep gradient meaning filling in boarder range of wider micropores to narrow mesopores (< 2.5 nm).

Type II and Type III– Nonporous material or microporous material, there is a little slope at first in type II followed by gradual increase of volume occupied when pressure is increasing. This refers adsorbate is adsorbed onto the external surface. At high P/P_0 it has high knee of adsorption isotherm representing infinity multilayer of adsorption. The difference of type III compared to type II is there is no monolayer formation referring the adsorbate-adsorbent interactions are weak. The adsorbed molecules are agglomerated at the most favorable site first.

Type IV- Mesoporous material. From the IVa isotherm, it has a hysteresis loop of adsorption-desorption at moderate pressure to high pressure. It refers capillary condensation which is the identity of mesopores with the pore width larger than 4 nm. In type IVb the narrower mesopores than 4 nm are detected without capillary condensation.

Type V- This isotherm is similar to isotherm type III at the first slope where there is no clear slope. Increasing pressure increases volume uptake which caused by clustering of adsorbed molecules due to weak interactions between adsorbate-adsorbent. Then at higher pressure, the reversible isotherm has hysteresis loop due to presences of mesopores. This kind of isotherm was found in adsorption of water on hydrophobic microporous and mesoporous materials.

Type VI- Isotherm referred a material with non-porous uniform surface where the volume uptake was step-wisely increased. This was found on the adsorption of krypton or argon at low temperature on graphitized carbon black.

In addition, only physical adsorption isotherm does not provide enough information about pore structure. There is another point needed to be determined in isotherm, a hysteresis loop. The shapes of hysteresis loop present different characteristic of pore. It can also tell us about the shape of pore. Here, the detail of hysteresis loop suggested by IUPAC was explained below.

จุฬาลงกรณ์มหาวิทยาลัย

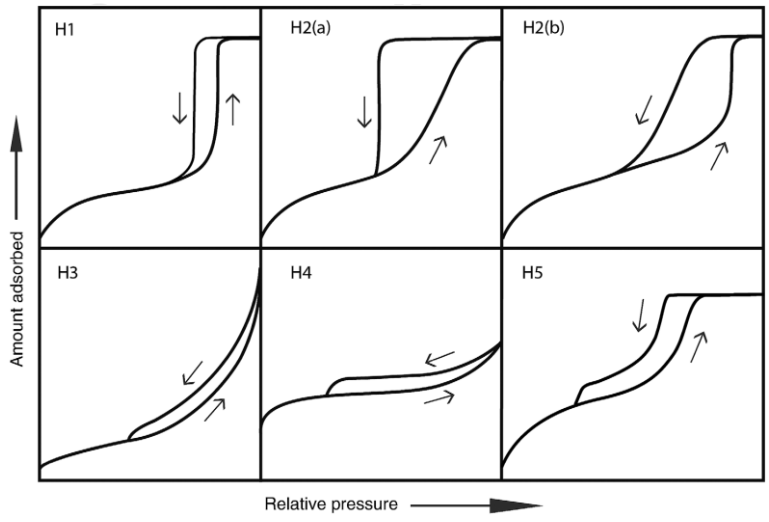

Figure 16 Classification of hysteresis loops

Hysteresis loop type H1 represents a material with narrow pore size distribution causing adsorption branch to be stepwise. A narrow reversible loop presents capillary condensation of pores where the neck size of pore is closed to pore width. This kind of loop can be found in highly ordered silicas (SBA-15, MCM-41, MCM-48)

For the boarder hysteresis loop type of H2 refers there is some blockage during desorption adsorbate out of the pore. This was caused by a much smaller neck of the pores compared to its pore width, so-called ink-bottle pore. At the adsorption branch compared to H1, it is gradually increasing meaning that pores have larger size distribution. The different between a-type and b-type is neck size distribution where a-type is more uniform than b-type. H2a was found in ordered mesoporous silica such as, SBA-16 and KIT-5 silicas, while type H2b was found in mesocellular silica foams.

The adsorption branch in H3 is similar to isotherm type II. H3 loop are representing non-rigid aggregates of plate-like particles or it refers interparticle pores.

The hysteresis loop of H4 is similar to type H3 but the difference is that the adsorption branch is composed of isotherm type I and type II where there is a filling in micropores. It was usually found in micro-mesoporous material.

The last type of hysteresis, H5, is different from the others and uncommon. The pore structure is more complicated where it is involving both open pores and blocked mesopores. It was reported to be found in plugged hexagonal templated silicas.

จุฬาลงกรณ์มหาวิทยาลัย
Chulalongkorn University

2.4 Swing adsorption process

In industrial level, the type of process is an important factor needed to be determined. For example, the post-combustion process should be integrated with continuous CO_2 adsorption process to operate flawlessly. However, the adsorbent after use for a while it must be saturated. Therefore, it needs regeneration which is a way to bring the saturated adsorbent back for next cycle of use to reduce the cost of

adsorbent. Thus, designing process is very important. From this part will be examples for different type of adsorption/desorption process which can operate continuously.

2.4.1 Temperature swing adsorption, TSA

This kind of process was done by the adsorption at low temperature. According to the nature of adsorption, which is exothermic in most cases, low temperature provides higher adsorption capacity as presented by adsorption isotherm at different temperatures shown in Figure 17. After it reached saturation, the regeneration is then followed at a condition of high temperature. At high temperature, the adsorbate has higher kinetic energy that is enough to escape from the surface of adsorbent. In addition, in the case of chemical adsorption high temperature is needed to provide sufficient energy to break the bond between adsorbate and adsorbent. The adsorbent used in this kind of process needed to be thermally stable for long-term use.

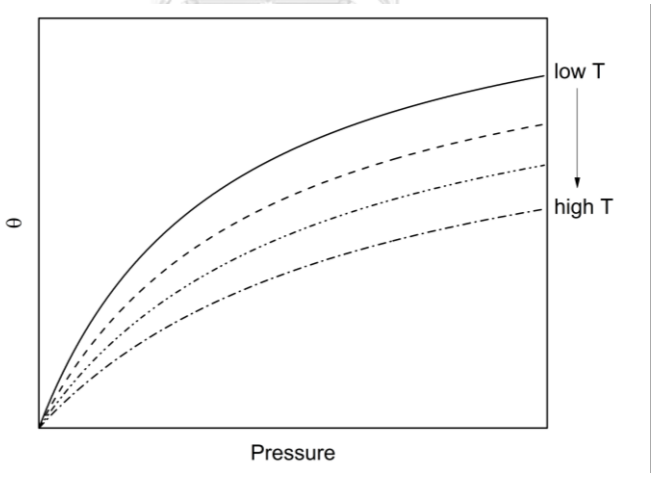

Figure 17 Adsorption isotherm at different temperatures

2.4.2 Pressure swing adsorption, PSA

Pressure swing adsorption is an operation that adsorption was done at high pressure in order to push adsorbate molecule to stay inside the adsorbent. While desorption was conducted at low pressure where the molecule at adsorbent's surface coming out because of pressure gradient. This was explained by adsorption

isotherm shown in Figure 18. Although, PSA needs high energy consumption for building up pressure, it also has advantage of low-temperature operation for the adsorbent that is not thermally stable at high temperature. Normally, the adsorbent used in PSA are physical adsorbents where the adsorption capacity dominated by surface area and operating pressure not the number of active sites.

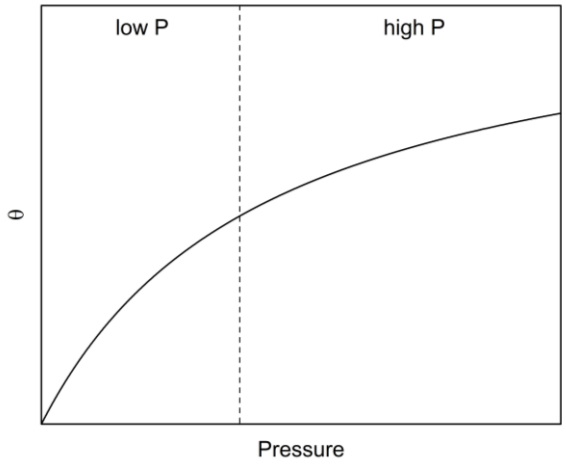

Figure 18 Adsorption isotherm at different regions of operating pressure

2.4.3 Vacuum swing adsorption, VSA

Similar to PSA, VSA was based on pressure swing but the adsorption occurs at atmospheric pressure and desorption operates under vacuum. From adsorption isotherm in Figure 18, at low pressure of adsorption has higher slope than high pressure region, meaning that at low pressure has greater influence to desorb molecule from saturated adsorbent. This could be done with TSA to increase the efficiency of regeneration.

2.4.4 Concentration swing adsorption, CSA

Concentration swing adsorption or purging is also used in industrial for regeneration process. It was done by adsorption at concentrated gas stream, then followed by purging of carrier gas. Consequently, the adsorbed molecules were forced to come out of saturated adsorbent's surface by concentration gradient as

driving forces. The purging gas should be unreactive which normally are nitrogen, helium and argon. Normally, purging must be done with help of increasing temperature for making molecules releasing from surface faster.

2.4.5 Hybrid process

From the processes above, they can be operated stand alone and also operated together to increase the efficiency. For example, TSA-VSA system that the adsorption occurs at low temperature and atmospheric pressure followed by regeneration at high temperature under vacuum condition. The efficiency of process should be optimized to get the condition that has the highest %recovery, low energy consumption and able to operate continuously.

2.5 Adsorption isotherm

To understand more about adsorption behavior and mechanism, the study of equilibrium isotherm is necessary. Equilibrium isotherm is a plot of surface coverage or adsorption capacity (q_e) at a particular temperature versus applied pressure(P). Then the shape of line will tell us about adsorption mechanism. There are many scientists invented math models which were derived with different assumptions to fit with experimental data. The well-known equilibrium isotherms will be presented here.

จุฬาลงกรณ์มหาวิทยาลัย
Chulalongkorn University

2.5.1 Langmuir isotherm

$$q_e = \frac{q_{l,max} K_l P}{1 + K_l P} \quad (1)$$

Langmuir isotherm [55] is a two-parameter model, in which $q_{l,max}$ is maximum adsorption capacity of a monolayer and K_l is the affinity related to the interactions between binding site of sorbent and sorbate molecule. This isotherm was derived from balancing the rate of adsorption and desorption in dynamic equilibrium state. It was designed for the adsorption that based on monolayer adsorption on

homogenous surface with a constant enthalpy of adsorption. The adsorption is proportional to the surface coverage and saturated at its full coverage.

2.5.2 Freundlich isotherm

$$q_e = K_f P^{n_f} \quad (2)$$

Another famous two-parameter model is Freundlich isotherm [56] which is presented in equation (2), where K_f is a constant related to the affinity of sorption and n_f is heterogeneity factor which associated to an exponential energy distribution of interactions between sorption site and sorbate molecule [57]. This isotherm was suggested to be an empirical isotherm with no theoretical background. However, Skopp, J [58] interestingly presented the derivation of Freundlich isotherm from fundamental kinetics and diffusion based properties. Generally, it describes the adsorption that occurs on heterogenous surface where stronger binding sites are occupied first. The adsorption capacity increases with equilibrium pressure refers a multilayer adsorption as well. However, this isotherm could not fit data well as it does not approach Henry's region at very low partial pressure [59]

2.5.3 Sips isotherm

จุฬาลงกรณ์มหาวิทยาลัย
CHULALONGKORN UNIVERSITY

$$q_e = \frac{q_{s,max}(K_s P)^{n_s}}{1+(K_s P)^{n_s}} \quad (3)$$

Sips isotherm [57, 60] is equated in equation (3). It was derived from a combination of Langmuir and Freundlich isotherms, where K_s is adsorption affinity related to equilibrium constant, n_s is Sips exponent or heterogeneity factor with a value between 0 to 1, and $q_{s,max}$ is maximal capacity. At infinite of dilution when P approaching 0, the equation is reduced to Freundlich isotherm, while at high pressure the adsorption is saturated at $q_{s,max}$ which represents Langmuir characteristic. The. When n_s is less than unity, it implies the adsorption on heterogeneous surface with different enthalpy of adsorption values of binding sites. The energy distribution of the binding sites is resembling to Gaussian distribution. On the other hand, n_s equals to 1, the equation reduced to Langmuir isotherm representing adsorption on

homogenous surface. However, Sips isotherm was derived from Freundlich equation. At low pressure to infinite dilution, it does not obey Henry's law which cannot reproduce Henry's constant from this equation accurately [59].

2.2.4 Toth isotherm

$$q_e = \frac{q_{t,max} K_t P}{[1+(K_t P)^{n_t}]^{1/n_t}} \quad (4)$$

For Toth isotherm [61] equated in equation (4), it was developed from monolayer adsorption model of Langmuir by adding heterogenous factor (n_t) where it is ranging from 0 to 1. The heterogenous factor indicates heterogeneity of surface. The lower value is, the more heterogenous. If n_t is equal to unity, it reduces to Langmuir equation meaning homogenous surface. The shape of adsorption energy on binding sites distribution expressed by Toth isotherm is an asymmetrical quasi-Gaussian distribution which is left-handed widened distribution. This means most sites of adsorption energy have binding energy lower than mean value.

However, using Toth's isotherm should be careful. In case n_t is much lower than 1, this model will overestimate saturated capacity when P approaches infinity value. This is incorrect in Thermodynamic aspect. Thus, correction is needed to be applied on isotherm with correction factor, χ_t. This correction is explained by Toth in his articles [62, 63]. For Toth isotherm χ_t is given by

จุฬาลงกรณ์มหาวิทยาลัย
Chulalongkorn University

$$\chi_t = \frac{1}{(K_t P_m)^{n_t}} + 1 \quad (5)$$

thus, the Toth's equation becomes:

$$q_e = \frac{\chi_t^{1/n_t} q_{t,mc} K_t P}{[1+(K_t P)^{n_t}]^{1/n_t}} \quad (6)$$

Where P_m stands for equilibrium pressure when surface is saturated and $q_{t,mc}$ is corrected monolayer capacity in mmol g^{-1}. The value of χ_t^{1/n_t} must be superior than 1, so that $q_{t,mc}$ is supposed to be lower than uncorrected value.

$$q_{t,mc} = \frac{q_{t,max}}{\chi_t^{1/n_t}} \quad (7)$$

At low n_t, the difference between $q_{t,mc}$ and $q_{t,max}$ is significant. This leads to overestimating in calculation of specific surface area [64]. With this correction, it does not violate old principle of dynamic equilibrium [62] and all thermodynamic parameters were not affected. The value of $q_{t,mc}$ is based on specific surface area of adsorbent (a^s, $m^2\ g^{-1}$) which was obtained from BET method. Then, the equation to calculate $q_{t,mc}$ is shown below [62].

$$q_{t,mc} = \frac{a_s}{602.3a_m} \tag{8}$$

Where a_m is the molecular cross-sectional area in nm^2. The estimation of a_m was suggested to obtain from liquid adsorptive density at adsorption temperature or critical point in which the shape and packing of molecules were assumed to be spherical and hexagonal close packing [65]. The formula is given by

$$a_m(cm^2) = 1.091 \left(\frac{M}{N\rho}\right)^{2/3} \tag{9}$$

with molar mass of adsorbate, M. N is Avogadro's constant, ρ is liquid density in gram per cubic centimeter at adsorption temperature or critical point.

2.6 Thermodynamics of adsorption

Another science that is necessary to explain what happen to the adsorption is Thermodynamics which includes 3 things. First, Thermodynamics studies the type of energy change of adsorption whether exothermic or endothermic. For the exothermic process, the process gives out energy from the reaction to the surroundings, while the endothermic is the process that take in energy from the surrounding. Second, it can also tell us about the entropy change of the system, more disordered or less disordered. The last thing is spontaneity of the system. According to the 2nd law of Thermodynamics stated that "For any spontaneous process, there must be an increase in total entropy change". If we could know the total entropy change, we could judge the process spontaneous or not. To find this in simpler way, Gibb's free energy change was introduced. Gibb's free energy is the free energy or available energy to do work which is involving in the process. For spontaneous process, there must be free energy given out and this energy can do

work. So that process should have ΔG with negative sign and also called this process as exergonic. Oppositely, if ΔG has the positive sign, the process cannot occur spontaneously, must take in energy or apply work to them to make it occur or it is called endogernic.

To classify the type of adsorption, enthalpy of adsorption needs to be found out. Since the enthalpy of adsorption is varied with the adsorbed amount of adsorbate on the sorbent, so we could find these values over the amount adsorbed by using isosteric method. Isosteric method is a way to find enthalpy of adsorption by using Clausius-Clapeyron equation, plotting isostere where it is a plot of logarithmic equilibrium pressure relative to standard pressure (ln [P]) versus reciprocal absolute temperature (1/T) when the loading amount is fixed, the equation was shown below:

$$R\left[\frac{d\ln[P]}{d(1/T)}\right]_q = \Delta H_{st}^{o} \qquad (10)$$

where R is a universal gas constant. The plot should give a straight line at a particular adsorbed amount. Then the isosteric enthalpy of adsorption can be obtained from gradient of the line. Moreover, the value of enthalpy of adsorption can tell us about type of adsorption where if enthalpy of adsorption is less than ≈-40 kJ mol^{-1} (0.4 eV per particle) the process will be physisorption which the adsorbate molecules were attracted by weak forces like Van der Waals forces. Oppositely, if the adsorbate and adsorbent interact interreact strongly or significantly change their electronic structure, such as via chemical bonding, this kind of adsorption becomes chemisorption which has ΔH_{ads}^{0} equal to or more negative than ≈-80 kJ mol^{-1} (0.8-8 eV per particle) [66].

From the previous part, with the isosteric method only could not achieve the enthalpy of adsorption at zero loading. Thus, another theory should be applied to figure out this. It is Henry's law region. Henry's law region is a principle that in most adsorption at very low pressure ($P \rightarrow 0$), the adsorbate-adsorbent forces are the most dominant. Thus, the affinity of adsorption could be obtained by Henry's constant which is a constant related directly to adsorbate-adsorbent interaction or

representing the affinity. To obtain Henry's constant, we use Virial equation [67] as expressed in equation below.

$$\frac{P}{q} = \frac{1}{K_H} \exp(2A_1 q + \frac{3}{2} A_2 q^2 + \ldots) \quad (11)$$

Where K_H is Henry's constant in mmol g^{-1} bar^{-1} P is pressure in bar, q is amount adsorbed in mmol g^{-1} and A_1, A_2 are the virial coefficients. The virial plot between ln (P/q) and q gives us a straight line approaching the axis ($q \rightarrow 0$). Thus, the intercept of a plot is -ln K_H. The other thermodynamic parameters, e.g. Gibb's free energy(ΔG^{o}_{ads}), enthalpy change of adsorption (ΔH^{o}_{ads}) and entropy change of adsorption(ΔS^{o}_{ads}), can be obtained by using Van't Hoff equation [68], Eq (12), combining with the fundamental Gibb's free energy equations (13) and (14), under the assumption that the enthalpy change and entropy change are essentially constant over small range of studied temperatures.

$$\frac{d \ln K_H}{d(1/T)} = -\Delta H^{o}_{ads} \quad (12)$$

$$\Delta G^{o}_{ads} = \Delta H^{o}_{ads} - T\Delta S^{o}_{ads} \quad (13)$$

$$\Delta G^{o}_{ads} = -RT \ln K_H \quad (14)$$

The Van't Hoff plot of is plotting of ln K_H versus reciprocal temperature gives us a straight line. Then gradient and intercept of the line is $-\Delta H^{o}_{ads}/R$ and $\Delta S^{o}_{ads}/R$, respectively.

CHULALONGKORN UNIVERSITY

2.7 Literature Review

Dura, G. and the group[16] studied CO_2 adsorption on microporous and mesoporous carbon sorbents. The activated charcoal (AC), which has higher microporosity, has lower CO_2 adsorption capacity than mesoporous carbon, Starbons®. They summarized that micropores play an important role to store CO_2 within pores. However, just only micropores could not achieve high capacity of CO_2. The adsorption capacity could be enhanced by the presence of mesopores that act as the pathway for CO_2 to access those micropores making kinetic of diffusion better. They also found that CO_2 adsorptions on AC and Starbons® are physisorption where CO_2 molecules attracted with pore with weak forces which has enthalpy of adsorption range of -14 to -22 kJ mol^{-1}. These values are between enthalpy of vaporization and enthalpy of sublimation of CO_2 of 10.3 kJ mol^{-1} and 26.1 kJ mol^{-1}, respectively. They also suggested that the presence of oxygen-containing functional groups survived after low-temperatured carbonization could adsorb CO_2 molecules with more negative enthalpy of adsorption. The selectivity of CO_2 over N_2 on these sorbents were reported that Starbons® gives higher selectivity than AC about 3 to 4 times.

Shafeeyan, M. S. and coworkers[25] investigated the effect of pre-oxidation followed by amination on nitrogen content of synthesized palm shell-based carbon. They have found that the pre-oxidation significantly enhanced the nitrogen content that doped on carbon framework by creating reactive sites on carbon surface that can be easier reacted with ammonia molecule or nitrogen-containing radical forming during treatment with ammonia at high temperature. They also studied the factors affecting CO_2 adsorption capacity. They suggested that microporosity is a predominant factor to adsorb CO_2 molecule at operating temperature of 30 °C. However, nitrogen content plays an important role at higher temperature by increasing the strength of binding forces to the sorbent's surface. Furthermore, they discovered that even the nitrogen content of the sorbents that treated at different temperatures are similar, but the type of nitrogen functional groups also affected CO_2 adsorption capacity. This suggestion was consistent to the research of Lim, G.

จุฬาลงกรณ์มหาวิทยาลัย
Chulalongkorn University

and group[23]. They studied the effect of N-containing functional groups on CO_2 adsorption on carbon by using density function theory (DFT). They calculated CO_2 adsorption energy between CO_2 molecule and different N-containing functional groups which are pyridone, pyridine, amine, quaternary, pyridine-N-oxide, cyanide and pyrrole. The results were shown that pyridonic-N and pyridinic-N have the most negative adsorption energies which referred to the strength of binding forces. For the pyridonic-N, it showed higher adsorption energy of eV compared to pyridinic-N of eV. The reason was explained by that hydrogen bonding between hydroxyl group on pyridone group and the electronegative oxygen atom of CO_2 molecule contributed in adsorption, which is stronger than Lewis acid-base interaction between CO_2 and lone pair electron on nitrogen atom of pyridine group. Moreover, they compared with N_2 adsorption which was shown that N_2 has weaker interaction to surface of sorbent due to its characteristic of smaller quadrupole moment and polarizability than CO_2 molecule.

Mangun, C. L. and team [69] studied the treatment of ammonia at various temperatures on activated carbon fiber derived from phenol-formaldehyde polymer. They investigated the effect of temperature on the type of nitrogen-containing functional groups using different techniques such as FT-IR, XPS, TGA and TPD. They had found that using treatment temperature at 500 ℃, the main types of nitrogen functional group are amide, aromatic amine, nitrile and protonated amide. While increasing treatment temperature to 600 to 700 ℃, there was a clear observation that the dominant type of nitrogen functional group changed to aromatic amine. Further increasing temperature to the level of 800 ℃ decreased the aromatic amine content. The predominant type becomes pyridinic-N functional group since there is an enough energy to nitride carbon rings. Moreover, there was an only slight decomposition of functional groups on carbon fiber over 500 ℃ and no significant change below 700 ℃. Thus, this material was suitable for regeneration at temperature below 500 ℃. Using higher temperature than 600 ℃ to promote formation of nitrogen incorporated with aromatic rings (e.g. pyridinic-N, pyrollic-N) was also confirmed by Pevida, C. and group [70]. They studied the heat treatment at different temperatures (200 ℃ to 800 ℃) on two commercial activated carbons, C

จุฬาลงกรณ์มหาวิทยาลัย
Chulalongkorn University

and R, under ammonia atmosphere. The type of nitrogen functional groups depends on treatment temperatures. At low temperatures, below 600 °C, the type of nitrogen-functionalities incorporated into the carbons were amides, amines, nitriles, and imines. Whereas, at higher temperature than 600 °C, the nitrogen is favorable to incorporate with aromatic rings forming pyridinic and pyrollic type which are thermally stable. Furthermore, the oxygen-functionalities has an influence to promote the reaction between carbon and ammonia, especially phenolic-like and ether-like functional groups.

Sreńscek-Nazzal, J. and group [71] investigated CO_2 adsorption on activated carbon, WG12, modified with $ZnCl_2$ and KOH at high pressure. They fitted experimental data with various isotherm models which were Langmuir, Freundlich, Sips, Toth, UNILAN, Ftitz–Schlunder, and Redlich–Peterson. They used five analysis of error functions: sum of the squares of errors, the hybrid fractional error function, the average relative error, the Marquardt's percent standard deviation, and the sum of the absolute errors to determine the best-fit model. The results were found that the consistency of tested equilibrium isotherm models putting in order from the best-fit to the least were Sips > Unilan > Langmuir > Toth > Fritz–Schlunder > Radke–Prausnitz > Freundlich, for WG. While both WG12_$ZnCl_2$ and WG12_KOH is Sipis > Toth > Unilan > Fritz–Schlunder > Radke–Prausnitz > Langmuir > Freundlich. The optimizations and error function analysis were found that sum of the squares errors and hybrid fractional error function were the best for overall results. They also suggested that the adsorption that fitted with Sips model can explain the adsorption behavior that the adsorption was occurred the heterogeneous surface by looking at the value of ns not equal to 1. Moreover, the treatment by KOH did not change the heterogeneity of surface, while treatment with $ZnCl_2$ made surface becoming more homogeneous.

จุฬาลงกรณ์มหาวิทยาลัย
Chulalongkorn University

CHATPER III

EXPERIMENTAL

3.1 Chemicals

Benzene (C_6H_6), Hexane (C_6H_{14}) and Ethanol (C_2H_5OH, purity 99.9%) were purchased from Quality Reagent Chemical (Qrec^{TM}). Nitrogen gas with ultra-high purity grade (N_2, 99.999%) and anhydrous ammonia gas (NH_3, 99.95%) were purchased from Thai-Japan Gas Co., Ltd., Thailand. Carbon dioxide (CO_2 99.99%) were obtained from Chubu Air Water Inc., Japan. All chemicals above were analytical grade and used without further purification. Metal-working fluid (DROMUS BA) was supported from Thai Houghton 1993 company. Its compositions are mainly composed of 80% of mineral oil, about 3% of dimethyl sulfoxide as a cosolvent, emulsifier and some additives (e.g. corrosion inhibitor, preservative and stabilizer) were also included.

3.2 Solution plasma process (SPP) set up

The solution plasma process was conducted at room temperature and pressure in a fuming cupboard. It was set up as follows. A pair of tungsten electrodes with a diameter of 1 mm was firstly sandpapered to clean the surface. Then it was insulated with ceramic tubes and fitted to the glass reactor vessel of 100 mL breaker using silicone bung. The gap between electrodes was set to be 1 mm. The electrodes were connected to bipolar pulse power supply. The operating parameters were set strictly as follows. The voltage, pulse width, applied pulse frequency were controlled to be 1.5 kV, 1.0 us, and 20 kHz, respectively. The schematic of SPP is displayed in Figure 19.

จุฬาลงกรณ์มหาวิทยาลัย
Chulalongkorn University

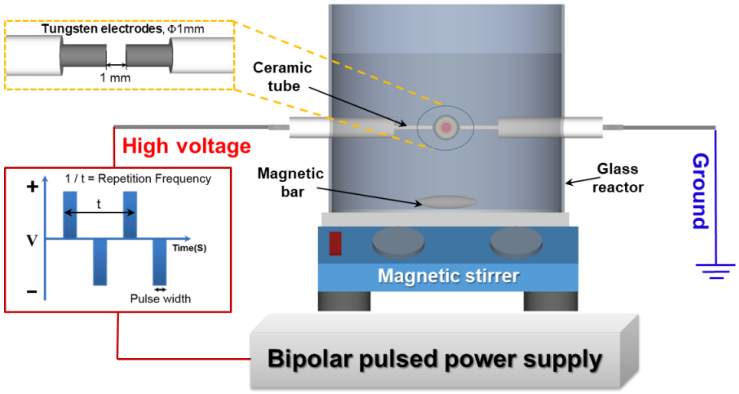

Figure 19 Schematic of solution plasma process

3.3 Preparation of nanocarbons

We prepared solutions for CNPs synthesis by using benzene mixed with MWF at different concentrations of 0, 5, 15 and 25 vol%. Briefly, 100 ml of solution was introduced into SPP reactor and then was discharged for 30 min without adjusting of temperature and pressure condition. The solution was changed from clear to deep-black after discharged. The resulting mixture was then separated by filtration under reduced pressure. It was washed with hexane until the washing turns colorless followed by washing with ethanol several times and dried in oven at 80 °C 12 h. About 500 mg of nanocarbon was obtained. The sorbent obtained by using only benzene was named as C and the sorbents synthesized from mixture of benzene and MWF were marked as oCX, when X denoted as vol% of MWF. For example, oC5 was prepared by a solution of benzene with 5 vol% of MWF.

จุฬาลงกรณ์มหาวิทยาลัย
Chulalongkorn University

3.4 Nitriding process

To modify the nanocarbons synthesized from previous step, nitriding process was introduced. About 2.0 grams of nanocarbons was placed in a quartz boat and then placed in to 38 mmD quartz tubular reactor. Heating up the reactor with heating rate of 15 °C/min by using horizontal splitting furnace to a target temperature (600, 700 and 800 °C) under N_2 atmosphere at 150 ml/min flowrate. Then it was stayed at target temperature for 15 minutes before changing it into NH_3 atmosphere at the same flowrate. The nitriding process was kept at target temperature for 2

hours. When the reactor was cooled down to 120 °C, it was changed back to N_2 atmosphere and continuously cooled down to room temperature. The nitride sorbents were kept in dark bottle and stored in desiccator for the next use. The nitride sorbents were marked as nC(Y) for nanocarbon prepared from pure benzene only and noCX(Y) for nanocarbon synthesized from mixture of benzene and MWF at X vol%, when Y was nitriding temperature. The operation procedure was graphically explained below

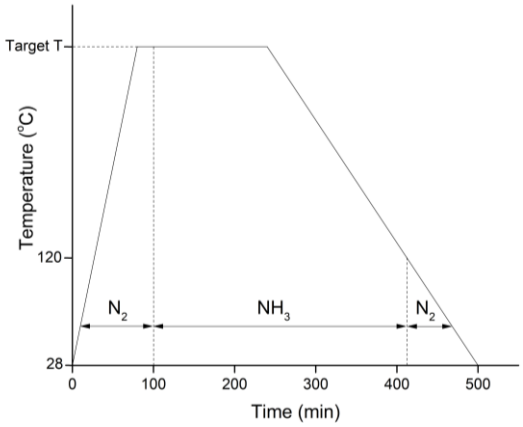

Figure 20 Temperature-time course utilized for nitriding process

3.5 CO_2 adsorption measurement

Static volumetric analyses were carried out on BELSORP-mini II (MicrotracBEL Corp., Japan) to collect the CO_2 adsorption isotherm of sorbents at adsorption temperature of 25 °C. The adsorption temperatures were controlled by water bath. About to 60 mg of sorbent were used for each batch of adsorption. Prior to the measurement, each sample were dried under vacuum at 120 °C overnight and followed by degassed at 150 °C for 2 hours. To calculate adsorption capacity, ideal gas equation was used.

3.6 Characterization

A Rigaku SmartLab diffractometer with monochromatic Cu Kα source (λ =0.154 nm) at 45 kV, 200 mA and 0.02° s^{-1} scan speed rate were used to record X-ray diffractograms (XRD) to identify the intrinsic crystallinity of the sorbents. The XRD

patterns were recorded over a 2θ range from 5–80°. The magnitude of the interlayer spacing (d_{002}) of carbon nanocrystallites was calculated from the peak at the (002) plane using the Bragg equation.

The N_2 adsorption/ desorption isotherm of sorbent(s) was determined via volumetric analysis on a BELSORP mini II analyzer at -196 ℃. The Brunauer-Emmett-Teller (BET) equation was used to calculate the specific surface area. The microporosity of samples was investigated using the t-plot calculated from the data series of N_2 adsorption isotherms based on Halsey's equation. Prior to measurement, moisture in the samples was eliminated by drying the sample in a vacuum oven at 100 ℃ for 12 h. The sample was then degassed under vacuum pressure at 150 ℃ for 2 h.

Raman spectra were recorded on a Raman Microscope (inVia confocal Raman Microscope, Renishaw Co. Ltd., UK) with an excitation wavelength of 532 nm over a Raman shift range from 500–2000 cm^{-1} at a resolution of 1.3 cm^{-1}. The in-plane (L_a) crystallite size was calculated based on the D/G peak intensity ratio.

After hand-grinding the sample to a fine powder, the powder was placed over a grid in order to analyze the morphology of the sorbent sample by transmission electron microscopy (TEM) using a JEM-2500SE (JEOL) microscope under an accelerating voltage of 200 kV. The selected area electron diffraction (SAED) was also performed on this instrument.

จุฬาลงกรณ์มหาวิทยาลัย
Chulalongkorn University

To evaluate the surface chemical state of the sorbent(s), X-ray photoelectron spectroscopy (XPS; JPS-9010MC, JEOL) was employed. Monochromatic Mg Kα radiation with 1253.6 eV was used as an excitation source. The emission current and the anode voltage were driven at 25 mA and 10 kV, respectively. The BE was calibrated using the C 1s peak at 284.5 eV for pristine carbon. An 80:20 Gaussian-Lorentzian ratio of line function with subtraction of Shirley background was used to fit the curve.

The total amount of nitrogen on the sorbent(s) was examined via CHNS/O elemental analyzer (Perkin Elmer 2400 Series II) with a thermal conductivity detector. The sample (2 mg) on aluminium foil was accurately weighed and then placed in the

sample chamber before being combusted in a pure oxygen stream under a static condition. Each sample was analyzed at least three times and the results are reported in terms of an average of the concordant results.

3.7 Thermodynamic studies

To reveal CO_2 adsorption behavior of synthesized sorbent, a sorbent with the highest CO_2 adsorption capacity at 25 °C was chosen to compare with the pristine carbon without modification, C. The further CO_2 adsorption experiments were conducted to obtain adsorption isotherms at different temperature. The operating step was the same as mentioned above except the reactor temperature. Four levels of reactor temperature were controlled at 25, 35, 45 and 55 °C by water bath. The dead-volume of sample vessel was also considered in each measurement. Then, the essential thermodynamic parameters, which are isosteric enthalpy of adsorption (ΔH_{st}^{o}), Henry's constant (K_H), enthalpy change of adsorption at zero loading (ΔH_{ads}^{o}), entropy change of adsorption (ΔS_{ads}^{o}) and Gibb's free energy (ΔG_{ads}^{o}) were calculated using equations as described in part II.

3.8 Isotherm studies

Isotherm studies were conducted to obtain more information of adsorption behavior. The experimental data were fitted with chosen isotherm models which were Langmuir, Freundlich, Sips and Toth models by using nonlinear least square (curve fitting) with help of Origin software. The best fit model was selected based on the highest value of coefficient of determination (R^2), the lowest values of Marquardt's Percent Standard Deviation (MPSD) [72] and Error function based on the normalized standard deviation (%Err). Also, all of model parameters must be non-negative value. The equation of them are shown in equation (15), (16) and (17), respectively.

$$R^2=1-\left[\frac{\sum_{i=1}^{n}(q_{e,exp}-q_{e,calc})^2}{\sum_{i=1}^{n}(q_{e,exp}-q_{m,exp})^2}\right] \qquad (15)$$

$$MPSD=\sqrt{\frac{1}{n-p}\sum_{i=1}^{n}\left[\frac{\left(q_{e,exp}-q_{e,calc}\right)^2}{q_{e,exp}}\right]} \quad (16)$$

$$Err(\%)=\sqrt{\frac{\sum_{i=1}^{n}\left[\frac{\left(q_{e,exp}-q_{e,calc}\right)}{q_{e,exp}}\right]^2}{n-1}}\times 100 \quad (17)$$

Where $q_{e,exp}$ is experimental equilibrium capacity, $q_{m,exp}$ is experimental mean equilibrium capacity and $q_{e,calc}$ is equilibrium capacity calculated from isotherm model which all of those are presenting in mmol g^{-1}. n is number of data used and p is number of parameters of isotherm (Langmuir and Freundlich are two-parameter, while Sips and Toth are three-parameter).

3.9 Regeneration test

The regeneration of spent sorbent was also studied. It was done by heated spent sorbent to temperature of 130 ℃ under vacuum condition (<0.1 bar) and keep it stays for 2 hours. Then, it follows the adsorption procedure as mentioned before to obtain the 2nd cycle adsorption capacity. This procedure was repeated until 5th cycle capacity was obtained.

จุฬาลงกรณ์มหาวิทยาลัย
Chulalongkorn University

3.10 Statistical analyses

The statistical analyses were done by using JMP®Pro13 software (SAS Institute Inc., United States) including the analysis of variance (ANOVA), effect estimates, the studentized residual by row number plot and the residual plot. The statistical significance level was set at 95% confidential level where the differences in means was accepted at the P-value less than 0.05. The calculated sums of squares from software were based on type-III sum of square where the order dependency is removed to determine estimates of factor in a model.

CHAPTER IV
RESULTS AND DISCUSSION

In this part, the results obtained from experiments are showing and discussing here. There are 5 parts including characterizations and CO_2 measurement of synthesized sorbent, thermodynamic studies, Isotherm studies, statistical analysis to determine the main effect on CO_2 adsorption capacity and deeper studies explaining the influence of micropore and nitrogen content on N-doped carbon.

4.1 Characterization of synthesized sorbent

4.1.1 Crystallinity determination by XRD technique

The synthesized nanocarbons were examined by several techniques. For the study of crystallinity of samples had been done by XRD. The representative of XRD patterns of carbon synthesized from pure benzene (C) and mixture of benzene with MWF at different ratios (oC5, oC15 and oC25), shown in Figure 21a, showed that there were three main peaks. The peak at a 2θ of 24° corresponded to the (002) plane of the turbostratic carbon [23], while that at 43° was the (100)/(101) plane of carbon, reflecting the hexagonal ring structure of carbon (JCPDS card no. 75-1621). Another peak was found at 2θ of 37° representing tungsten carbide at plane of 111 (WC1-x111) that was formed by sputtering of tungsten electrodes during discharging plasma in solution plasma process. Considering the peak at 2θ of 24° for nanocarbons, there was slight shifting of this peak to the lower 2θ from 24° to 23.5°, 23.2° and 22.9° when the ratio of MWF increased from 5 to 25 vol% for oC5, oC15 and oC25, respectively. This means expansion of interlayer of carbon frameworks due to that some oxygen atoms were doped into carbon frameworks. Corresponding to d-spacing of C002 plane calculated from Bragg's equation, the results were shown in Table 1. The d002 of C was increased from 0.370 to 0.388 nm with increasing MWF ratio from 0 to 25 vol% in the mixture. Then, each sample were nitridied at different temperature of 600 °C to 800 °C. After nitriding, C samples at different nitrided temperatures, nC(600), nC(700) and nC(800), showed a shifting of peak C002 located

จุฬาลงกรณ์มหาวิทยาลัย
Chulalongkorn University

at 2θ of 24° to lower degree. Whereas oC samples demonstrated opposite trend. The peak of C002 of samples were shifted to higher value of 2θ. This refers the mechanism of nitriding on nanocarbons with and without MWF were different. The shifting to lower 2θ on C sample series might be caused by adding nitrogen atom into carbon framework creating defect sites causing interlayer to be expanded. On the other hand, in oC sample series, nitriding at high temperature also removes oxygen functional groups and doping nitrogen atoms to carbon structure, but the amount of elimination of oxygen functional groups are greater causing interlayer spacing closer. All synthesized sorbents have the d002 values greater than the 0.335 nm which is an interlayer spacing of ideal graphite, thus they have lower degree of graphitization. In addition, after nitriding, the peak at a 2θ of 37° was slightly shifted to a larger 2θ value and became broader, because the phase of tungsten carbide might have been reduced by hydrogen gas [73] produced from the decomposition of NH_3. This effect became more obvious at the higher temperature of nitridation since ammonia decomposes to H_2 more at higher temperature.

Table 1 Structural properties obtained from XRD technique

Sample	XRD	
	2θ of C002 (degree)	d-spacing (nm)
C	24.0	0.370
oC5	23.5	0.379
oC15	23.2	0.383
oC25	22.9	0.388

จุฬาลงกรณ์มหาวิทยาลัย
Chulalongkorn University

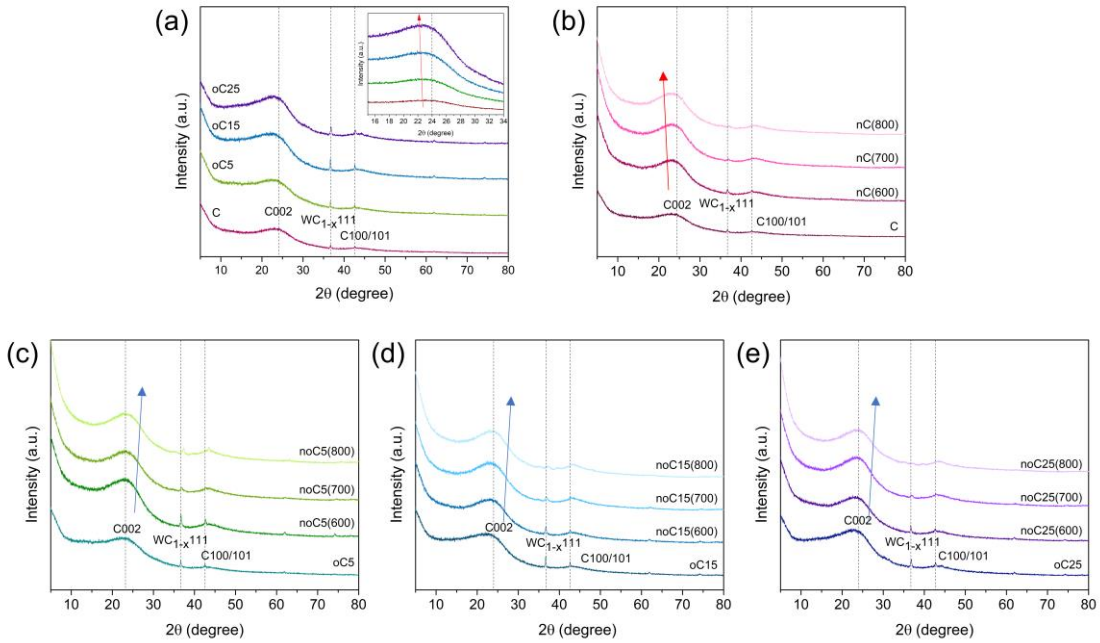

Figure 21 XRD patterns of synthetic nanocarbons at (a) different MWF ratio and different nitriding temperatures of (b) C series, (c) oC5 series, (d) oC15 series and (e) oC25 series

4.1.2 Bulk and surface elemental composition

The bulk and surface elemental analyses were conducted by CHNS/O elemental analyzer and XPS technique, respectively. The results were presenting in Table 2 showing that main component in sorbents was carbon. The samples without nitridation, the oxygen density was proportional to the ratio of MWF mixed in solution from 4.12% to 10.05at% at MWF ratio of 0 vol% to 25%vol. This confirmed mixing MWF with benzene and discharging in solution plasma process would enhance oxygen content on nanocarbon. After nitridation at temperature of 600 °C, all samples of C, oC5, oC15 and oC25 showed the presence of nitrogen atom. Doping nitrogen atom into carbon framework was done by reaction between active species of ammonia molecules which are NH and NH_2 radical and oxygen-containing functional groups on carbon framework as described in [74, 75]. The nitrogen content on samples were 1.6, 2.4, 2.6, and 1.9 wt%, for nC(600), noC5(600), noC15(600) and noC25(600), respectively. Increasing MWF ratio also increased oxygen density in

carbon framework which was beneficial for doping N atom into carbon framework due to that oxygen functionalities act as more reactive site for doping N compared to pristine carbon. However, there was a decrease in nitrogen content from 2.6 wt% when activating on oC15 to 1.9 wt% on oC25. This might be caused by the excess MWF remained on oC25 after washing with hexane followed by ethanol several times. So those oxygen atoms were not in carbon framework but just excess MWF that was covering the surface which the excess MWF were observed during nitriding oC25 samples. There was residue oil remaining in nitridation reactor. Increasing nitridation temperature to 700 °C increased nitrogen content significantly on all nanocarbon. The maximum N content was achieved at 4.1% on noC15(700) sample. Further increase nitriding temperature to 800 °C decreased nitrogen content due to decomposition of nitrogen functionalities, especially at the edges of carbon framework. The nitrogen contents on samples at 800 °C of nitridation were 1.8, 3.1, 2.8, and 2.8 wt% for nC(800), noC5(800), noC15(800) and noC25(800), respectively. Addition of MWF to the level 25 vol% seemed to be not beneficial in term of increasing nitrogen content on carbon framework due to blockage of excess MWF.

จุฬาลงกรณ์มหาวิทยาลัย
Chulalongkorn University

Table 2 Elemental composition of SPP-derived carbons

Sample	XPS			CHN		
	Surface elemental analysis			Bulk elemental analysis (wt%)		
	C (at%)	O (at%)	N (at%)	C	H	N (wt%)
C	95.8	4.2	0.0	93.0	1.4	0.0
nC(600)	97.5	1.4	1.2	92.9	1.0	1.6
nC(700)	95.3	2.4	2.4	89.0	0.9	2.9
nC(800)	97.1	1.7	1.3	89.2	1.0	1.8
oC5	94.4	5.6	0.0	89.9	2.1	0.0
noC5(600)	95.4	2.8	1.8	89.6	1.1	2.4
noC5(700)	96.0	1.1	2.9	85.6	1.1	3.6
noC5(800)	95.8	1.8	2.4	84.9	1.3	3.1
oC15	92.8	7.2	0.0	88.1	2.8	0.0
noC15(600)	95.7	2.3	2.0	88.6	1.2	2.6
noC15(700)	95.2	1.4	3.5	85.6	1.1	4.1
noC15(800)	95.4	2.4	2.3	82.4	1.5	2.8
oC25	90.0	10.1	0.0	89.1	2.3	0.0
noC25(600)	94.4	4.2	1.4	90.9	1.1	1.9
noC25(700)	95.6	1.4	3.0	86.2	1.0	3.7
noC25(800)	95.0	2.7	2.3	84.1	1.3	2.8

4.1.3 Textural properties of synthesized nanocarbons

The textural properties of synthesized sorbents were analyzed by volumetric N_2 adsorption-desorption at -196 °C. The N_2 adsorption-desorption isotherms of before and after nitrided samples were present in Figure 22. For non-nitrided samples, C, oC5, oC15 and oC25, showed a combination of isotherm type II and type IV according to IUPAC classifications of nanopores [76]. This refers the nanocarbons were nonporous. At high P/P0 of 0.8 to 1.0, there was a large increase in N_2 uptake without saturation representing filling in non-uniform macropores. In addition, there

was a hysteresis loop at high relative pressure in each N_2 adsorption-desorption isotherm. The origin of hysteresis loop was a capillary condensation of nitrogen which referring the identity of presence of mesopores. However, the shape of hysteresis loop was categorized as type H3 according to IUPAC classifications reflecting the presence of interparticle mesopores formed by aggregation of carbon particles. After nitridation, the isotherms were changed to a combination of type I and type IV with H3 hysteresis referring nitridation changed the textural properties of nanocarbons to microporous while interparticle mesopores still present. Nitridation developed microporosity to all samples with greater extent at higher temperature. The increases in gradient of first slope of isotherm of nitrided carbons reflected that micropores had been developed, especially ultramicropores where its pore diameter less than 0.7 nm. After the first slope, there was a gradual increase in slope of isotherm from P/P0 of 0.1 to 0.6. This refers the presence of supermicropore with the wider pore width larger than ultramicropore with diameter in range of 0.7 to to 2 nm. This similar trend was also found in oC5, oC15 and oC25 samples.

Table 3 shows surface area (S_{BET}) that were calculated from isotherms using a well-known BET equation purposed by Stephen Brunauer, Paul Hugh Emmett, and Edward Teller [77]. Without nitridation, S_{BET} of C was around 190 m^2 g^{-1}. Adding MWF to the mixture for SPP generated nanocarbon with different textural properties compared to nanocarbon from pure benzene. With MWF ratio of 5 vol% and 15 vol% exhibited similar surface area of 136, and 138 m^2 g^{-1} for oC5 and oC15, respectively. This confirmed synthesizing nanocarbon from different kinds of solution could provide different textures. Further increasing MWF ratio to 25 vol%, surface area obviously decreased to 115 m^2 g^{-1} confirming the presence of excess MWF remained after washing that might clogged in pore resulting smaller surface area. Addition of MWF to the solution also affected average pore size. Comparison with and without MWF, average pore size increased from 19.7 nm in C to 27.8 nm in oC5. It refers the morphology of C and oC5 were totally different. This might be because of that synthesizing nanocarbon from mixture of benzene and MWF which contains long-chained hydrocarbon making the structure more branched which pushes carbon framework further away. Increasing MWF ratio to 15 vol% decreased average pore

size to 22.4 nm. An increase in oxygen functionalities might increase hindrance between carbon plane that would create smaller pores resulting lower average pore size. Further increase MWF ratio to 25 vol% slightly increased average pore size. Due to the presence of excess MWF that would cover small pores making average pore width on sample larger and it might be inserted between carbon layers, confirmed by XRD patterns. After modified nanocarbons with nitridation under ammonia atmosphere at high temperatures, they showed a significant change in their texture and morphology. S_{BET} increased about 2-folded at nitridation temperature of 600 °C compared to non-nitrided samples for all oC5, oC15, and oC25 series. While average pore size had been decreased from developing small pores by nitridation. Nitridation became more effective at higher temperature, it increased surface area and decreased average pore size by more vigorous reaction between carbon and ammonia molecules at higher temperature. This results the greatest microporosity at nitriding temperature of 800 °C. However, there was an unusual trend for oC25 series, an increase in microporosity at nitriding temperature of 600 °C was less effective than oC5, and oC15 series because the excess MWF was covering on surface needed to be removed first. So, it was blocking nitridation. However, after increasing temperature to 700 °C, noC25(700) showed the same trend with no5(700), and noC15(700). At nitriding temperature of 800 °C microporosity had been the most developed. The clogging MWF was completely boiled away leaving small pores behind making larger surface area and more micropores. The detailed information of microporosity were shown in Table 3 with t-plot analysis. However, t-plot analyses cannot be applied to non-nitrided samples because of nonporosity. From t-plot results, micropore volume increased with MWF ratio and nitriding temperature. The maximum micropore volume was achieved at 0.174 $cm^3\ g^{-1}$ on noC25(800). In addition, it also showed similar trend on total pore volume that it increased with MWF ratio and nitriding temperature. Although the total pore volume of noC5(800) and noC15(800) were similar, but micropore volume of noC15(800) was higher. This led to noC15(800) had greater microporosity than noC5(800) in character according to V_{micro}/V_{total} ratio of 0.097 and 0.125 for noC5(800) and noC15(800), respectively. Even noC25(800) showed higher total pore volume and micropore volume than noC15(800), but it had

จุฬาลงกรณ์มหาวิทยาลัย
Chulalongkorn University

similar V_{micro}/V_{total} ratio (0.124) indicating that addition of MWF ratio to 25 vol% did not help in increasing microporosity in character after nitrided at 800 °C.

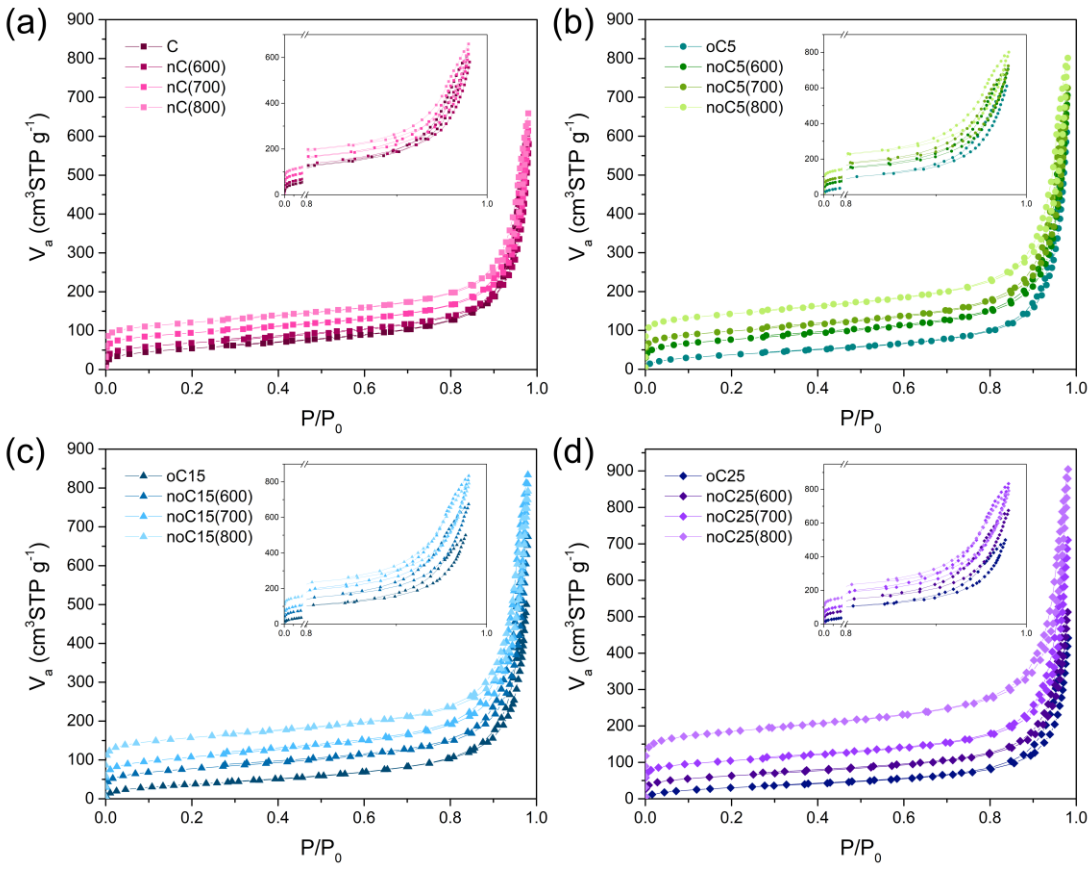

Figure 22 N_2 adsorption-desorption isotherm of synthetic nanocarbons at -196 °C for (a) C series, (b) oC5 series, (c) oC15 series and (d) oC25 series

จุฬาลงกรณ์มหาวิทยาลัย
CHULALONGKORN UNIVERSITY

Table 3 Textural properties calculated by BET and t-plot methods

Sample	BET		Total Pore Volume	t-plot		
	Specific surface area	Average Pore size		Micropore volume	Meso+Macro pore volume	V_{micro}/V_{total}
	($m^2 g^{-1}$)	(nm)	($cm^3 g^{-1}$)	($cm^3 g^{-1}$)	($cm^3 g^{-1}$)	
C	190.8	19.7	0.937	-	0.937	-
nC(600)	245.5	14.6	0.897	0.023	0.873	0.026
nC(700)	333.2	11.4	0.950	0.021	0.929	0.022
nC(800)	437.8	9.3	1.019	0.056	0.962	0.055
oC5	135.9	27.8	0.943	-	0.943	-
noC5(600)	269.1	16.2	1.090	0.036	1.054	0.033
noC5(700)	349.2	12.8	1.119	0.065	1.054	0.058
noC5(800)	513.3	9.7	1.238	0.120	1.118	0.097
oC15	138.4	22.4	0.773	-	0.773	-
noC15(600)	273.1	15.3	1.043	0.041	1.003	0.039
noC15(700)	378.5	13.6	1.289	0.072	1.217	0.056
noC15(800)	569.7	8.6	1.224	0.153	1.071	0.125
oC25	115.3	23.7	0.683	-	0.683	-
noC25(600)	222.4	14.3	0.793	0.029	0.764	0.036
noC25(700)	376.5	11.7	1.098	0.079	1.019	0.072
noC25(800)	679.7	8.2	1.399	0.174	1.225	0.124

จุฬาลงกรณ์มหาวิทยาลัย
Chulalongkorn University

4.1.4 CO_2 adsorption experiment

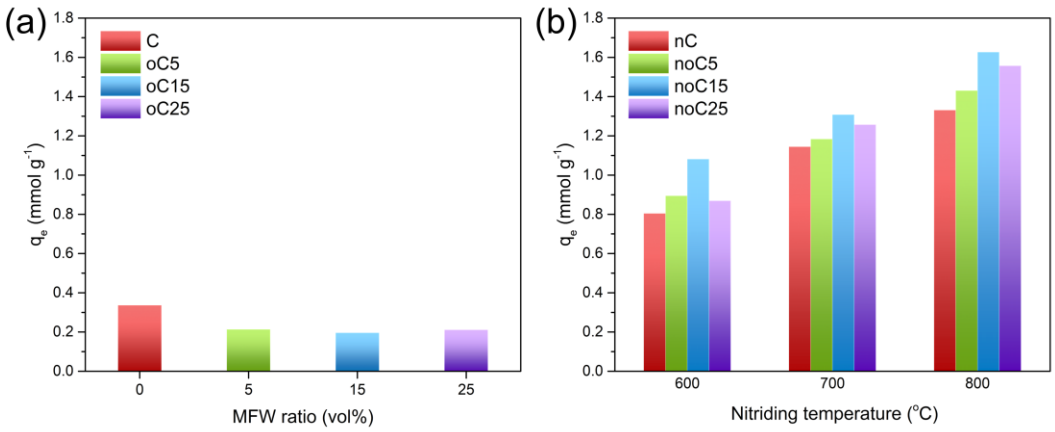

Figure 23 CO_2 adsorption capacities of SPP-derived carbons at 25 °C for (a) non-nitrided samples and (b) nitrided samples at different temperatures

The CO_2 adsorption capacity on samples were tested using volumetric analysis at 25 °C of adsorption temperature. The samples were divided into 2 groups, untreated and treated with NH_3. The adsorption capacities of un-treated and treated samples are shown in Figure 23a and Figure 23b, respectively. For untreated group, the adsorption capacity was influenced by surface area. C exhibited the highest surface area in this group of 190.8 m^2 g^{-1} showed the best capacity at 0.34 mmol g^{-1} while other samples, oC5, oC15 and oC25, showed similar adsorption capacity at about 0.2 mmol g^{-1} at specific area of 135.9, 138.4 and 115.3 m^2 g^{-1}, respectively. The adsorption capacity of samples prepared at different MWF ratios and nitriding temperatures was shown in Figure 23b. The adsorption capacity increased with nitriding temperature from 600 C° to 800 C°, for all oC5, oC15 and oC25 series. The maximum adsorption capacity was achieved on noC15(800) at the level of 1.63 mmol g^{-1}. Although noC25(800) had the largest surface area and micropore volume, its capacity was like noC15(800) due to similar microporosity (V_{micro}/V_{total} of 0.125 for noC15(800) and V_{micro}/V_{total} of 0.124 for noC25(800)). This confirmed that increasing MWF ratio in sample up to 25 vol% was ineffective for increasing adsorption capacity. Moreover, the CO_2 adsorption on carbon structure does not only rely on its micropore volume acting as storage for CO_2 molecules, but it needed to be balanced

with diffusion rate of CO_2 into micropores. Those mesopores and macropores played an important role to transport CO_2 molecule to micropores in carbon framework. Thus, the indifference on V_{micro}/V_{total} leaded to similar adsorption capacities of both noC15(800) and noC25(800).

Many studies revealed that nitrogen atom on carbon framework does enhance adsorption performance of CO_2. Our samples showed similar trend of nitrogen content on CO_2 adsorption capacity. However, further increasing nitriding temperature from 700 C° to 800 C° reduced nitrogen density due to decomposition of nitrogen functionalities at higher temperature. The adsorption capacities of samples nitrided at 800 C° did not decrease because of increasing in microporosiy. This contradiction leads to a question that whether microporosity or nitrogen content has greater influence on CO_2 adsorption capacity of our samples which this will be explained by using statistical analysis in later part.

From this point, only 4 sorbents were selected from the highest capacity in each group of nanocarbons prepared from pure benzene, nC(800), and mixture of benzene and MWF, noC15(800), to compare with non-nitrided samples, C and oC15.

4.1.5 Raman spectroscopy

Representative Raman spectra of the C, oC15, nC(800) and noC15(800) samples are shown in Figure 24. Only two bands were found in the spectra; the G band at around 1585 cm^{-1} and the D band at around 1335 cm^{-1}. The G band represents the vibration of sp^2 orderly bonded carbons, while the D band corresponds to the vibration of sp^3 carbon atoms, indicating the defects on the graphene layer. The intensity ratio of the D and G bands (I_D/I_G) was used to evaluate the degree of defection or disorder on the carbon framework [78, 79], with the results summarized in Table 4. The C and oC15 samples showed a similar I_D/I_G ratio value of around 0.83 and 0.81, respectively. After nitriding at a high temperature to obtain nC(800) and noC15(800), the I_D/I_G ratio was increased to 0.93 for nC(800) and 0.97 for noC15(800). This indicated that nitrogen doping caused defects on the carbon framework [80] and then the structure became less crystalline. A slight shift

จุฬาลงกรณ์มหาวิทยาลัย
Chulalongkorn University

to the right of the G band was found in the spectra of the nC(800) and noC15(800) compared to that in the C and oC15, respectively. The inverse of I_D/I_G ratio was applied to calculate the size of the in-plane crystallite, L_a, via the Tuinstra-Koenig relationship [81] as shown in eq.(18):

$$L_a(\text{nm}) = C\lambda^4(I_D/I_G)^{-1} \quad (18)$$

where C is a constant (2.4×10^{-10} nm^{-3}) and λ is the excitation laser wavelength (532.1 nm). From Table 4, the L_a crystallite diameter of C was around 23.18 nm, while it was around 23.75 nm for oC15. Thus, an increase in the magnitude of L_a was found when doping oxygen on the carbon framework. After nitriding, the crystallite diameter became smaller, being 20.69 nm for nC(800) and 19.83 nm for noC15(800), which might be due to the decomposition of the carbon during nitriding at a high temperature.

Table 4 Degree of graphitization expressed in term I_d/I_g and in-plane crystallite size

Sample	Raman spectroscopy	
	I_D/I_G	L_a (nm)
C	0.83	23.18
oC15	0.81	23.75
nC(800)	0.93	20.69
noC15(800)	0.97	19.83

จุฬาลงกรณ์มหาวิทยาลัย
CHULALONGKORN UNIVERSITY

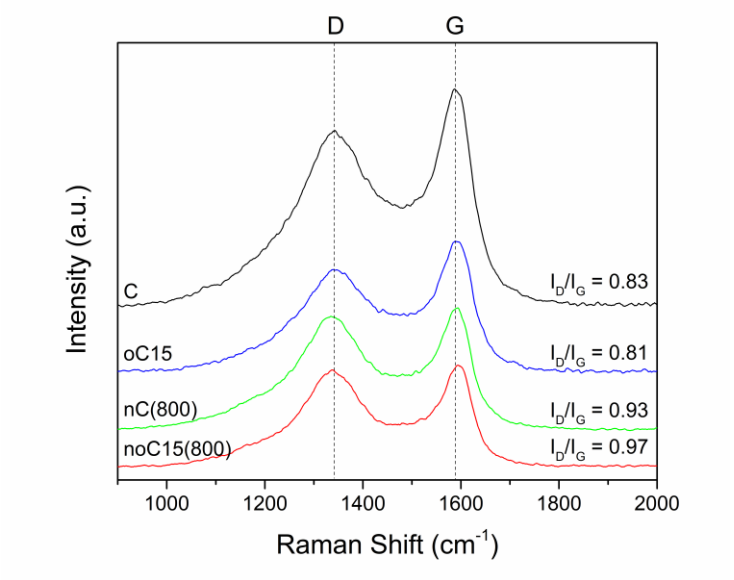

Figure 24 Representative Raman spectra of the different adsorbents

4.1.6 Transmission electron microscopy

Representative TEM images of the different types of particles are shown in Figure 25. The size of these particles was less than 50 nm, indicating they are nanoparticles. From the negative bright field images of the C, oC15, nC(800) and noC15(800) samples, the fringes were in a non-directive arrangement. This contributes to the 002 plane of carbon surrounded by an amorphous phase. However, the skeleton carbon in each particle were similar to each other. As can be seen from the SAED images of C (Figure 25c), nC(800) (Figure 25f), oC15 (Figure 25i) and noC15(800) (Figure 25l), the structure of the particles was mainly amorphous with some polycrystalline. Compared to the SAED of the C and oC15 samples, more blurred bright onion rings were observed in the SAED of the oC15 sample since some oxygen confounded with the carbon framework, while nC(800) and noC15(800) showed more blurred bright onion rings than C and oC15. During nitriding, some nitrogen atoms passed into the carbon framework, while some carbon atoms at the edge reacted with active species of NH_3 at high temperature. Thus, the crystallinity of the nitrided samples was decreased and they became more amorphous.

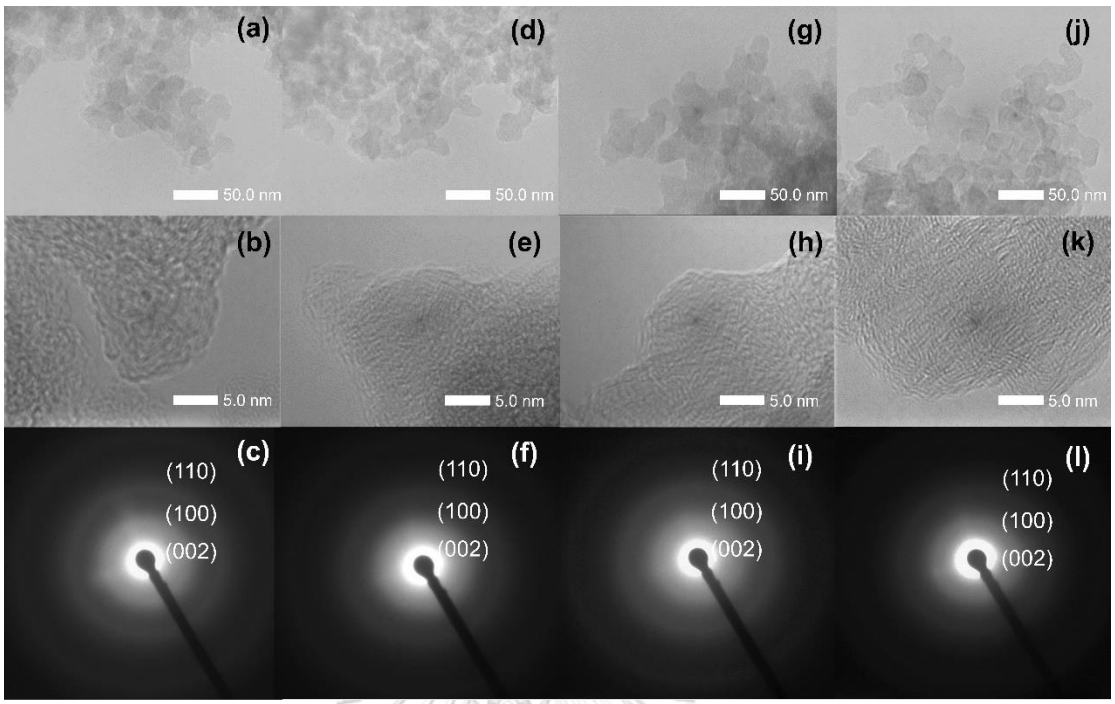

Figure 25 Representative TEM images of (a, b) C, (d, e) nC(800), (g, h) oC15 and (j, k) noC15(800) and SAED patterns of (c) C, (f) nC(800) (i) oC15 and (l) noC15(800)

4.1.7 Chemical state of heteroatom on nanocarbons examined by XPS

Representative XPS spectra of C 1s, O 1s and N 1s are shown in Figure 26 and summarized in Table 5. For the C 1s region, the major bands represent the C–C sp^2 bonding at a BE of 284.5 eV and C–C sp^3 ordering at a BE of 285.4 eV. This implies that the carbon framework of the samples was composed of graphitic and amorphous carbon. A long-tail peak in the C 1s region refers to the heteroatom bonds of C–O at 286.5 ± 0.1 eV, C=O at 288.1 ± 0.2 eV and O–C=O at 289.9 ± 0.2 eV. The C–N band at 285.8 eV was found in the spectra of nC(800) and noC15(800), supporting the successful synthesis of nC(800) and noC15(800) via nitridation. For the O 1s region, the XPS spectra revealed quinone at 530.2 eV, O=C–OH at 531.4 ± 0.2 eV, C=O at 532.3 ± 0.1 eV, C–OH at 533.3 ± 0.1 eV, C–O at 534.0 ± 0.2 eV and O–H at 535.5 eV. The presence of the O–H bond was due to the moisture adsorbed on the sample. Only the spectra of the nitriding samples expressed the N 1s region, which represented various N-forms on the surface, such as pyridinic at 384 ± 0.1 eV, pyrrolic-N at 400.2 ± 0.1 eV, graphitic-N at 401.3 ± 0.2 eV and pyridinic N-oxide at

403.5 ± 0.2 eV. Most of N-contribution belonged to nitrogen bonding on the edge, at around 90.4% for nC(800) and 84.2% for noC15(800), whereas the nitrogen chemical bond in the bulk (graphitic-N) existed at about 9.6% and 15.8%, respectively. Doping nitrogen at the edge was done by replacing the surface oxygen-functional group with the active species of NH_3 (NH and NH_2 radicals) [74, 75]. There is some difficulty to dope nitrogen atoms on the bulk due to the requirement to break the strong bonds of the carbon matrix [80]. The major N-contribution in the N 1s region of the nC(800) and noC15(800) samples was the pyridinic form, which is attributed to its adsorption performance. Moreover, the W4f band of elemental tungsten at a BE of around 33 eV was not observed in the XPS spectra of all samples, since the amount of contaminated tungsten was quite low.

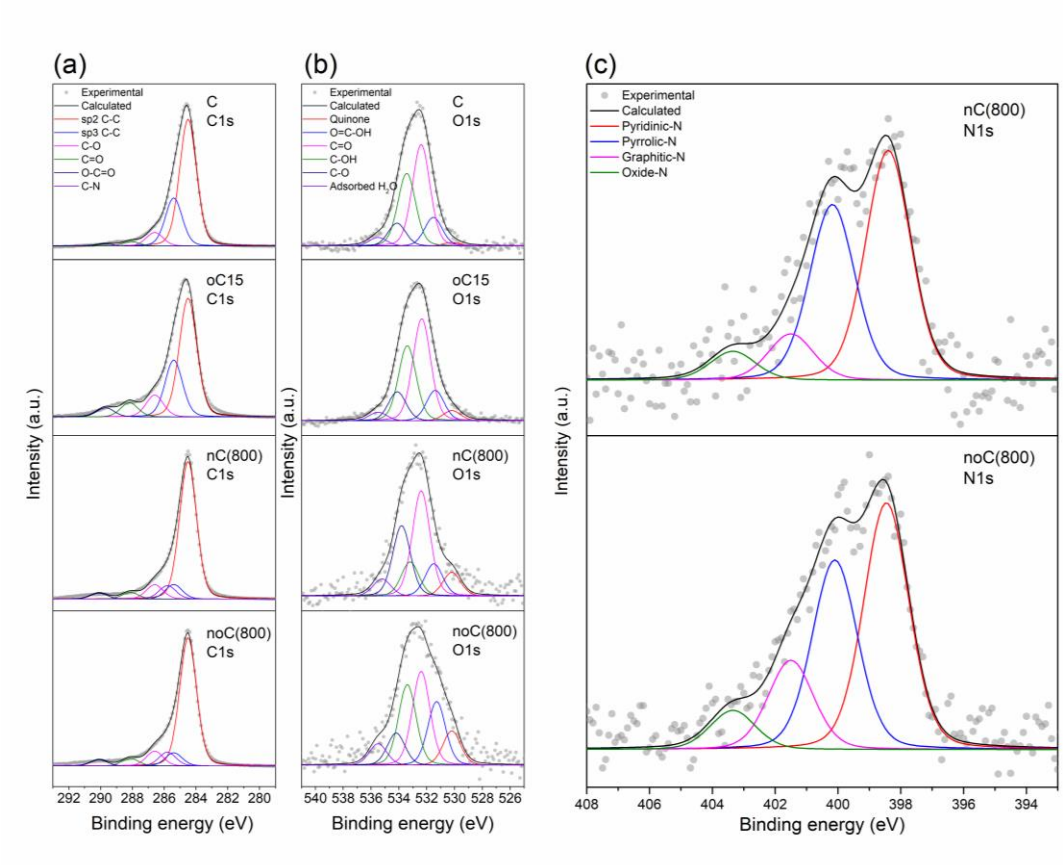

Figure 26 Representative XPS spectra of the C, oC15, nC(800) and noC15(800) samples for the (a) C 1s, (b) O 1s and (c) N 1s regions of the nitrided samples (nC(800) and noC15(800))

Table 5 Deconvolution results of the XPS spectra at C 1s, O 1s and N 1s for synthesized samples

Region	Bonding	Position (eV)	Relative percentage (%)			
			C	oC15	nC(800)	noC15(800)
C 1s	C—C sp^2	284.5	65.0	53.7	71.5	69.7
	C—C sp^3	285.4	24.7	25.8	7.5	7.2
	C—N	285.8	-	-	7.0	7.5
	C—O	286.4–286.6	7.0	9.9	7.5	8.1
	C=O	287.9–288.3	2.3	6.5	3.4	4.2
	O—C=O	289.7–290.1	1.0	4.2	3.1	3.4
O 1s	Quinone	530.2	1.5	4.0	8.4	10.5
	O=C—OH	531.2–-531.6	12.1	11.9	11.4	19.5
	C=O	532.2–532.4	42.6	40.0	37.2	28.8
	C—OH	533.2–533.4	30.6	29.4	12.1	24.7
	C—O	533.8–534.2	9.6	11.4	24.9	9.9
	Water adsorbed	535	3.6	3.3	6.1	6.6
N 1s	Pyridinic	398.4–398.6	-	-	47.8	43.7
	Pyrrolic-N	400.1–400.3	-	-	36.6	33.6
	Graphitic-N	401.1–401.5	-	-	9.6	15.8
	Pyridinic N-oxide	403.3–403.7	-	-	6.0	6.9

จุฬาลงกรณ์มหาวิทยาลัย
Chulalongkorn University

4.2 Thermodynamic studies

In this section, the thermodynamic studies are revealed in order to investigate the adsorption behavior. Starting from the study on the effect of the temperature on the CO_2 adsorption capacity of C and noC15(800) at various pressures is shown in Figure 27. It can be seen clearly that, at the same equilibrium pressure, the CO_2 adsorption was decreased from 1.63 mmol g^{-1} to 1.37, 1.18 and 0.99 mmol g^{-1} for noC15(800), and from 0.34 mmol g^{-1} to 0.32, 0.28 and 0.24 mmol g^{-1} for C, as the

temperature increased from 25 °C to 35, 45 and 55 °C, respectively. The effect of pressure on the CO_2 adsorption capacity differed from that of the temperature. The pressure played an important role on the thermodynamic driving force to push the adsorption forward and so the CO_2 adsorption capacity increased with increasing pressure. For the temperature, a decrease in CO_2 adsorption capacity was observed with increasing temperatures. Increasing the temperature caused the CO_2 molecules to diffuse faster and so fewer molecules were able to interact with the active site of the adsorbent. Moreover, at higher temperatures, the surface CO_2 molecules were desorbed into the surrounding gas once there was adequate energy to overcome the gas-solid interaction [43]. Therefore, increasing the temperature attenuated the CO_2 uptake, in agreement with the exothermic nature of the process. That the CO_2 adsorption capacity of noC15(800) was greater than that of C at the same pressure and temperature, reflects that these adsorbents have different active sites for CO_2 binding on their surface. It also infers that CO_2 has stronger interactions with the active sites on noC15(800) than on C, and so more CO_2 moleules covered the surface of noC15(800) leading to a higher CO_2 adsorption capacity.

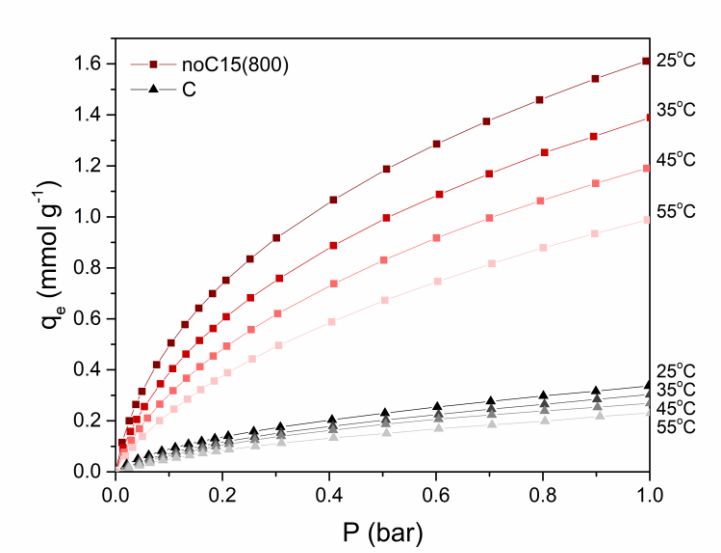

Figure 27 CO_2 adsorption capacity as a function of the pressure at various temperatures

4.2.1 Isosteric enthalpy of adsorption

To gain a deeper insight into the adsorption process, the isosteric enthalpy of adsorption ΔH_{st}^{o}) at a certain amount of CO_2 adsorbed was then considered. The ΔH_{st}^{o} deals with the overall interaction forces between CO_2 molecules and active sites on the surface of adsorbent and is determined via the Clausius-Clapeyron equation [44], as shown in equation (10). The difference in each adsorption temperature interval should not exceed 10 K. Firstly, a graph of the natural logarithm function of pressure as a function of the reciprocal absolute temperature at a constant amount of CO_2 adsorbed on the C and noC15(800) were plotted (Figure 28). They expressed a straight line of isostere with a negative slope. This also supported that the nature of the adsorption process on C and noC15(800) was exothermic. A shallower slope was found when more CO_2 covered the surface of the adsorbents. The ΔH_{st}^{o} was then calculated from the slope, since the slope of the line is equal to the ΔH_{st}^{o} to gas constant (R) ratio.

A decreased magnitude of the slope represents a decreased magnitude of ΔH_{st}^{o}, when more CO_2 adsorbed on the adsorbent surface. The calculated ΔH_{st}^{o} values were plotted against the equilibrium CO_2 adsorption capacity (Figure 29). The magnitude of ΔH_{st}^{o} ranged from 23–27 kJ mol^{-1} for C and from 30–32 kJ mol^{-1} for noC15(800). Normally, the magnitude of ΔH_{st}^{o} can be used to identify the type of adsorption, where it is classified as a pure physical interaction when the absolute magnitude of ΔH_{st}^{o} is less than 40 kJ mol^{-1}, and a strong chemical interaction when ΔH_{st}^{o} is greater than 80 kJ mol^{-1} [45]. From the derived ΔH_{st}^{o} values of C and noC15(800), the major mechanism of CO_2 adsorption was physisorption. The absolute value of ΔH_{st}^{o} for noC15(800) was greater than for C due to the higher degree of heterogeneity and stronger bonding forces between CO_2 and the noC15(800) surface. The decreased absolute value of ΔH_{st}^{o} implies that the surface of the sorbent is heterogeneous. This heterogeneity is caused by defects on the carbon structures due to the edge defect and oxygen and/or nitrogen substitution [29].

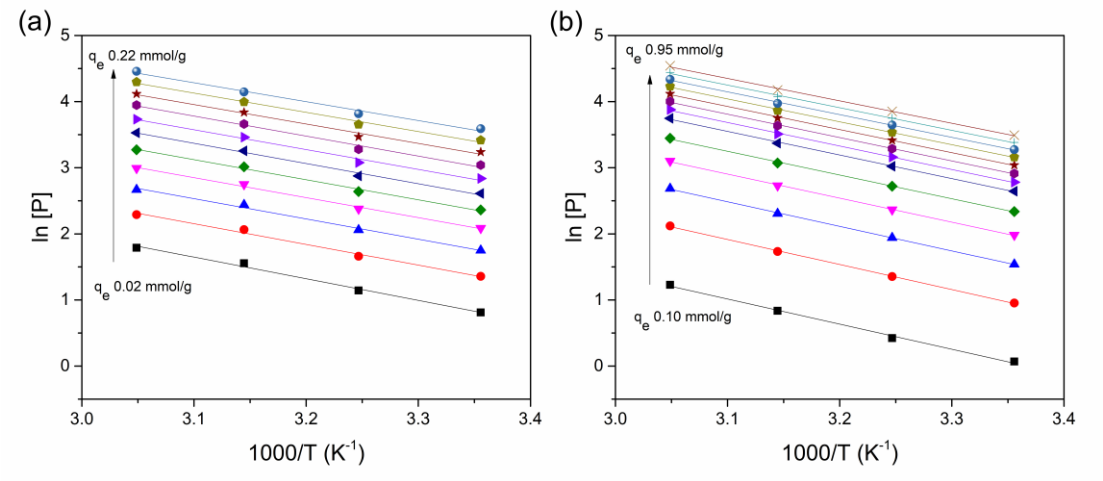

Figure 28 Isostere plots of (a) C and (b) noC15(800)

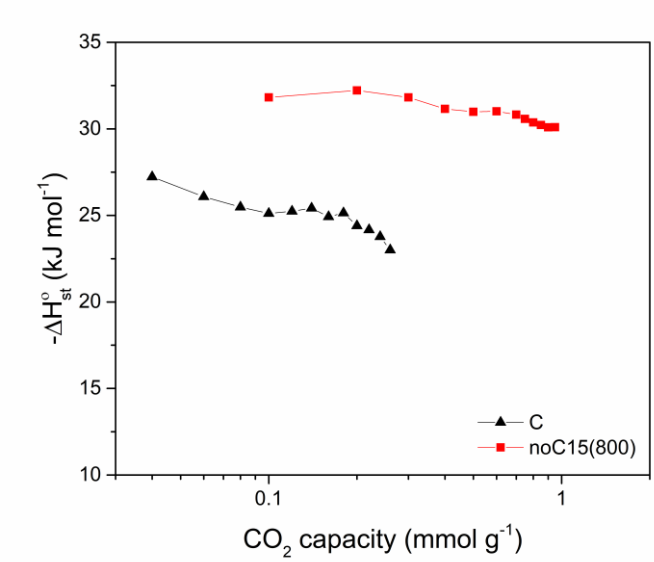

CHULALONGKORN UNIVERSITY

Figure 29 Isosteric enthalpy of adsorption over CO_2 loading on (a) C and (b) noC15(800)

4.2.2 Henry's law region

The study of isosteric enthalpy of adsorption using Clausius-Clapeyron equation could provide good information about binding energies at different amount adsorbed on surface. However, with this method, it could not obtain the thermodynamic parameters of the fresh adsorbent with no coverage of adsorbate (Figure 29). In principle, at a very low pressure ($P \rightarrow 0$) the adsorbate-adsorbent forces are the most dominant and so we can apply Henry's law (Henry's law region).

Henry's constant is directly related to the adsorbate-adsorbent interaction and represents the affinity. To obtain Henry's constant, we used the Virial equation [46] as expressed in equation (11) in part II.

The virial plot between the natural logarithm function of the ratio of P to q (P/q) and q gives a straight line approaching the axis ($q \rightarrow 0$), where -ln K_H is obtained from the intercept. The K_H at different temperatures of CO_2 adsorption on C and noC15(800) are shown in Table 6. Over the whole temperature range, higher Henry's constants for adsorption were found on noC15(800), which means that noC15(800) exhibited a greater affinity for CO_2 adsorption than C. It is noticed that the value of K_H became smaller with increasing temperatures, inferring that CO_2 adsorption on the adsorbent was less favorable at higher temperatures, and so the CO_2 capacity was decreased in accord with the temperature effect on the capacity, as discussed above.

To understand the nature of the adsorption phenomenon and type of adsorption, the other thermodynamic parameters were investigated via (i) Van't Hoff equation for the enthalpy change of adsorption (ΔH^{o}_{ads}) [47] , as shown in Eq. (12); (ii) the fundamental Gibb's free energy equations, for Gibb's free energy (ΔG^{o}_{ads}) as shown in Eq. (13) and for the entropy change of adsorption (ΔS^{o}_{ads}) as shown in Eq. (14). The assumption is that the enthalpy and entropy changes are essentially constant over the small range of studied temperatures. These thermodynamic parameters can be used as a crucial key to characterize the adsorption process, and are reported in Table 6.

จุฬาลงกรณ์มหาวิทยาลัย
Chulalongkorn University

The Van't Hoff plot (natural logarithm function of K_H as a function of the reciprocal temperature) was a straight line (Figure 30), where the gradient and intercept of the line were $-\Delta H^{o}_{ads}/R$ and $\Delta S^{o}_{ads}/R$, respectively. The thermodynamic parameters are shown in Table 6. At 25 °C, C and noC15(800) had negative ΔG^{o}_{ads} values, which means the adsorption of CO_2 on both sorbents was spontaneous at this temperature. The ΔG^{o}_{ads} values for noC15(800) at different temperatures were more negative than those for C, confirming that the CO_2 adsorption on noC15(800) is more thermodynamically feasible. Nitridation at a high temperature caused

micropore development and doped nitrogen atoms on the surface, which then enhanced the CO_2 adsorption capacity. When increasing the temperature, the ΔG^{o}_{ads} from noC15(800) and C became less negative, which means that the adsorption had a lower degree of spontaneity at higher temperatures. At lower temperatures, the CO_2 molecules diffused to the more energetically favorable active sites on the surface of adsorbent to form a surface layer of CO_2 molecules. Consequently, a higher adsorption capacity was obtained at a lower temperature, as discussed above. At a higher temperature, CO_2 diffuses faster and CO_2 molecules with a weaker interaction with the less energetically favorable active sites on the sorbent surface can then desorb and diffuse back to the gaseous bulk phase.

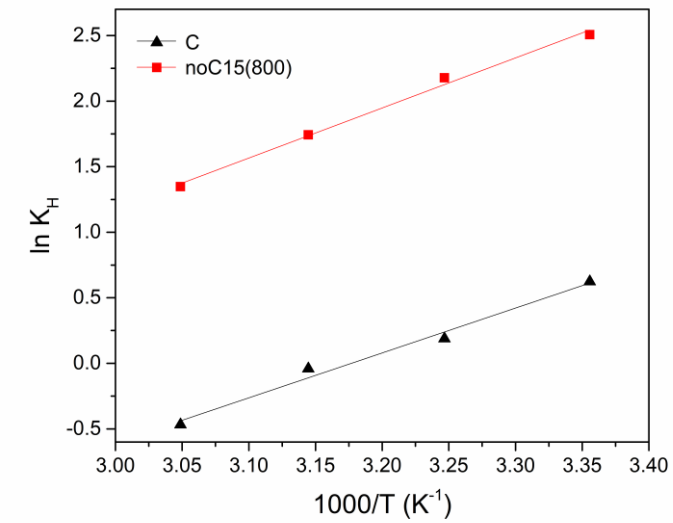

CHULALONGKORN UNIVERSITY

Figure 30 Van't Hoff plot of C and noC15(800)

The sign of ΔH^{o}_{ads} indicates the heat inflow/outflow to the adsorption system, where the negative sign meant that the nature of the adsorption process on C and noC15(800) was exothermic. Since the total energy released during formation of a bond between CO_2 and the active sites on the sorbent was greater than the total energy used in breaking the adsorbed CO_2 bond. That the absolute value of ΔH^{o}_{ads} from noC15(800) was greater than that from C means a larger amount of heat energy is released to the surrounding after adsorbing CO_2 molecules on the noC15(800) surface, reflecting the stronger nitrogen active site on noC15(800). Moreover, the absolute magnitude of ΔH^{o}_{ads} also revealed the type of adsorption, where ΔH^{o}_{ads} is <

40 kJ mol^{-1} and > 80 kJ mol^{-1} for physisorption and strong chemisorption, respectively, [45]. Thus, the major mechanism of CO_2 adsorption on C and noC15(800) was physisorption, in agreement with the ΔH_{st}^{o} values. This also confirm the heterogeneous surface adsorption. Thus, the CO_2 molecule and the active sites on the adsorbent's surface are attracted by weak Van der Waals forces.

For ΔS_{ads}^{o}, the sign corresponded to the degree of randomness of the adsorption process. It was clearly seen (Table 6) that a lower randomness of the system was observed during the CO_2 adsorption onto noC15(800) than on the C surface. The gaseous CO_2 in the bulk phase moved randomly, while the CO_2 adsorbed on the surface could not move freely due to their interaction force. The stronger interaction force between CO_2 and the nitrogen active site on the noC15(800) caused a more ordered stage with less randomness.

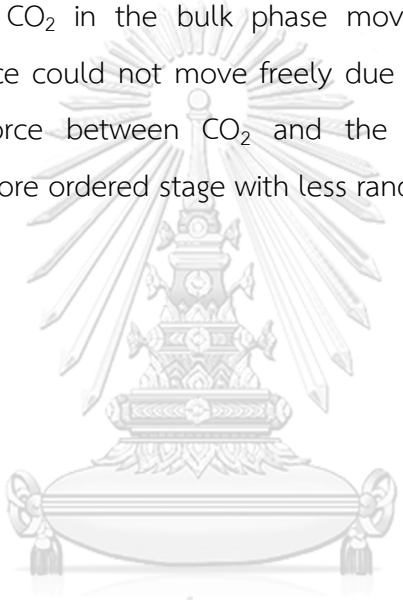

จุฬาลงกรณ์มหาวิทยาลัย
CHULALONGKORN UNIVERSITY

Table 6 Thermodynamic parameters of CO_2 adsorption on C and noC15(800) at different temperatures

Adsorption temperature (°C)	C					noC15(800)				
	ln K_H	K_H (mmol g^{-1} bar^{-1})	ΔG^o_{ads} (kJ mol^{-1})	ΔH^o_{ads} (kJ mol^{-1})	ΔS^o_{ads} (J mol^{-1} K^{-1})	ln K_H	K_H (mmol g^{-1} bar^{-1})	ΔG^o_{ads} (kJ mol^{-1})	ΔH^o_{ads} (kJ mol^{-1})	ΔS^o_{ads} (J mol^{-1} K^{-1})
25	0.62	1.86	-1.52	-28.45	-90.39	2.51	12.26	-6.30	-31.73	-85.36
35	0.19	1.21	-0.61			2.18	8.82	-5.44		
45	-0.04	0.96	0.29			1.74	5.71	-4.59		
55	-0.47	0.63	1.20			1.35	3.85	-3.74		

จุฬาลงกรณ์มหาวิทยาลัย
Chulalongkorn University

4.2.3 Selectivity of CO_2 over N_2

In general, adsorption would not occur to the pure gas steam, but it would separate specified gas from mixture of gases. Another important property of sorbent is a selectivity of specified gas from the mixture. Herein, the selectivity of CO_2 over N_2 gas on C and noC15(800) were studied by using Henry's constant, $K_{H,CO_2}/K_{H,N_2}$. From adsorption isotherms in Figure 31, both C and noC15(800) showed higher adsorption capacity of CO_2 than N_2. N_2 adsorption capacity had increased from 0.02 mmol g^{-1} to 0.21 mmol g^{-1}, while CO_2 adsorption capacity was changed from 0.34 mmol g^{-1} to 1.63 mmol g^{-1} for C and noC15(800), respectively. K_{H,N_2}, $K_{H,CO_2}$and the selectivity, which were summarized in Table 7. After nitriding, K_{H,N_2} increased from 0.11 to 0.42 and K_{H,CO_2}increased from 1.86 to 12.26 for C to noC15(800), respectively. It refers noC15(800) had greater affinity to CO_2 and N_2 than C. This can be explained by micropore development which improves the adsorption capacity of both N_2 and CO_2. However, the increase in K_{H,CO_2} was about 6.6 times which increased with greater extent than K_{H,N_2}. Not only micropores had been developed from nitridation, but there was also nitrogen doping to the carbon structure which enhanced the CO_2 adsorption affinity. This trend was in good agreement with selectivities of CO_2 over N_2 of C and noC15(800) which were obtained to be 16.29 and 29.22, respectively. It was about 2-folded increased. All of these based on the reason that CO_2 was attached to the surface of sorbent with stronger induced dipole interactions than N_2 because of its greater amount of electron in molecule. Moreover, CO_2 and N_2 are nonpolar molecules, but CO_2 has higher polarizability and quadrupole moment [82] which are 4.3 $\times 10^{-26}$ esu·cm^2 and 26.5 $\times$ 10^{-25} cm^3 for CO_2 and 1.52 $\times$ 10^{-26} esu·cm^2 and 17.6 $\times$ 10^{-25} cm^3 for N_2, respectively. Thus, the carbon surface could form stronger interactions at π-system and/or lone pair electron of N atom in case of N-doped carbon. Both are electron-rich region. So, it attracts at the position of $C^{\delta+}$ of CO_2 stronger than with N_2.

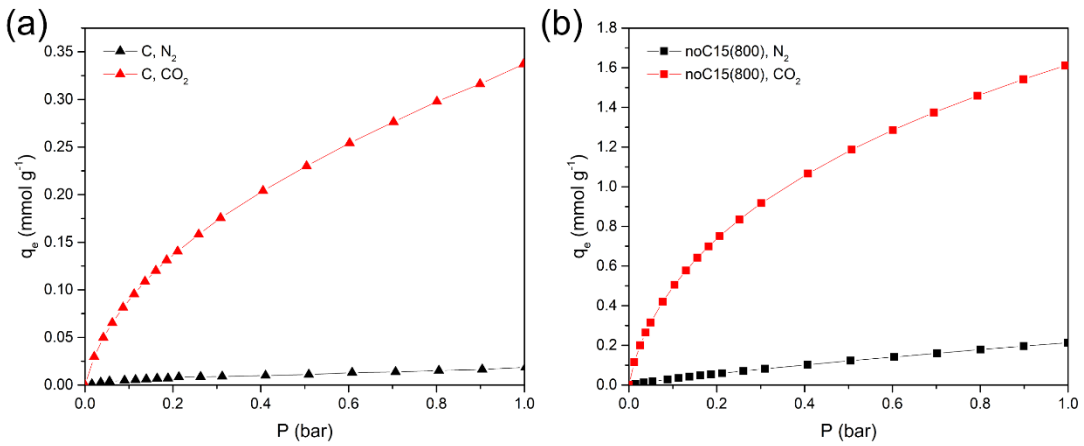

Figure 31 N_2 and CO_2 adsorption isotherm at 25 °C on (a) C and (b) noC15(800)

Table 7 Henry constants on N_2 and CO_2 adsorption and selectivity

Sample	K_{H,CO_2}	K_{H,N_2}	Selectivity $K_{H,CO_2}/K_{H,N_2}$
C	1.86	0.11	16.29
noC15(800)	12.26	0.42	29.22

4.2.4 Regenerability and stability test

From previous part revealed that the CO_2 adsorption on noC15(800) was physisorption where CO_2 molecule weakly attracted by Van der Waals forces. This leads to a high possibility for regeneration of sorbent. Regeneration is an essential factor to make the sorbent economical to use. It reduces resource requirement by regenerating spent sorbent and reuse for adsorption application. To test regeneration of noC15(800), the multi-cycled experiments were conducted. A fresh sorbent was used to saturation in adsorption procedure as mentioned. After the adsorption completed, the sorbent was regenerated at temperature of 130 °C in a vacuum condition (<0.1 bar) for 2 hours and followed the same CO_2 adsorption procedure again. The recycling results were shown in Figure 32. It shows that the adsorption capacities over 5 cycles of use were similar with less than 5 % different. This means over than 95% of adsorption capacities were recovered under this condition. This

จุฬาลงกรณ์มหาวิทยาลัย
Chulalongkorn University

implies that the noC15(800) has a good stability to withstand the multicycle of adsorption and evacuation.

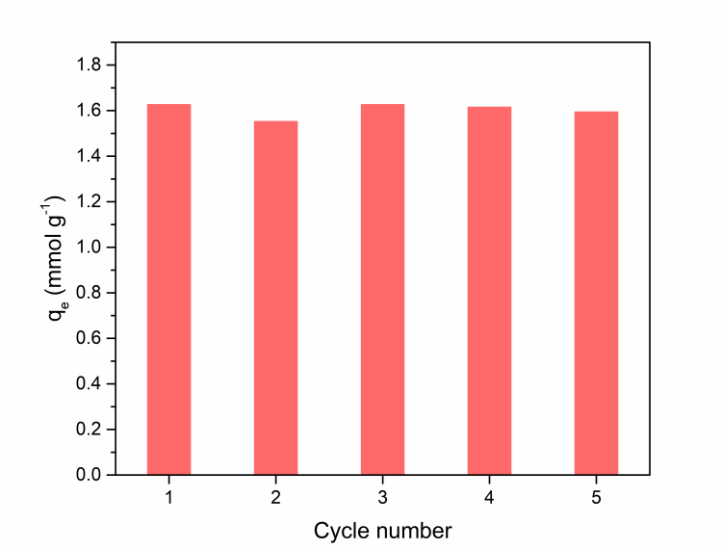

Figure 32 CO_2 adsorption capacities on noC15(800) over 5 cycles of use

4.3 Isotherm studies

Further investigation on mechanism was done by isotherm study. The adsorption isotherms express a relationship between the amount of CO_2 adsorbed on the solid adsorbent and the equilibrium pressure when the temperature is kept constant. In this part, only the CO_2 adsorption on noC15(800) was studied due to its maximum adsorption capacity. The experimental data was fitted to the two-parameter isotherm models of Langmuir and Freundlich, and to the three-parameter isotherm, Sips and Toth models. The best-fit model would give the information about adsorption mechanism based on their assumptions. Briefly, the adsorption that fitted to Langmuir isotherm is monolayer adsorption on homogeneous surface where the enthalpy of adsorption was constant for all binding sites. Freundlich model express the multilayer adsorption on heterogeneous surface. Sips was developed from Langmuir and Freundlich where the adsorption was on heterogenous surface with Freundlich's character at low equilibrium pressure, while it becomes saturated at high pressure reflecting by Langmuir's character. Toth was modified from Langmuir model by adding Toth constant, n_t, which describes heterogeneity when $n_t < 1$. The

equations of these model were expressed in part II, in equation (1) to (4) for Langmuir, Freundlich, Sips and Toth model, respectively. The best-fit model was chosen from the model that has the highest value of coefficient of determination (R^2), the lowest values of Marquardt's Percent Standard Deviation (MPSD) and Error function (%Err). Each model parameter and the magnitude of the three different tests of fitting the data for noC15(800) to the isotherm models are shown in. All models exhibited an R^2 of more than 0.99 and a MPSD less than 0.15, but the Toth model had the lowest %Err suggesting the better fitting of the data to the Toth model. Thus, the adsorption isotherm on noC15(800) over the whole pressure range at all temperatures can be characterized via the Toth isotherm. The fitness of different models on experimental data was shown in Figure 33.

The affinity constant (K) of each isotherm decreased with an increasing temperature (Table 8), inferring that the adsorption becomes less favorable at higher temperatures. A descent in the maximal capacity of each isotherm, except for the Freundlich model, was also observed with increasing temperature, meaning less CO_2 was adsorbed at higher temperatures, supporting that the CO_2 adsorption process on noC15(800) was exothermic. The degree of heterogeneity from each model, except for Langmuir, suggested that the adsorption occurred on heterogeneous active sites on the sorbent surface with different BEs. However, the value of n_t obtained from model fitting were quite low for all temperatures. This leads to overestimation of maximum capacity due to incorrect thermodynamic standpoint. To avoid this, the model should be corrected by multiplying χ_t, Toth's correction factor to the model and becoming corrected Toth model as expressed in equation (6), explained in previous part. After correction was done, a corrected maximum capacity, $q_{t,mc}$, was obtained as well as prediction of saturated pressure, P_m, where it is equilibrium pressure when the surface of sorbent is saturated with monolayer adsorption. The example of misuse of Toth model without correction was shown in Figure 34, that the maximum capacity without correction was much higher than corrected value and it was incorrect since this value obtained when P approaches infinity value which is thermodynamically impossible. The trend in the P_m value was to decrease at temperatures higher than 25 °C, which infers that the application of a higher pressure

is required to achieve a higher adsorption capacity when the adsorption was done at a higher temperature. This further supported that the CO_2 adsorption is less favorable at higher temperatures.

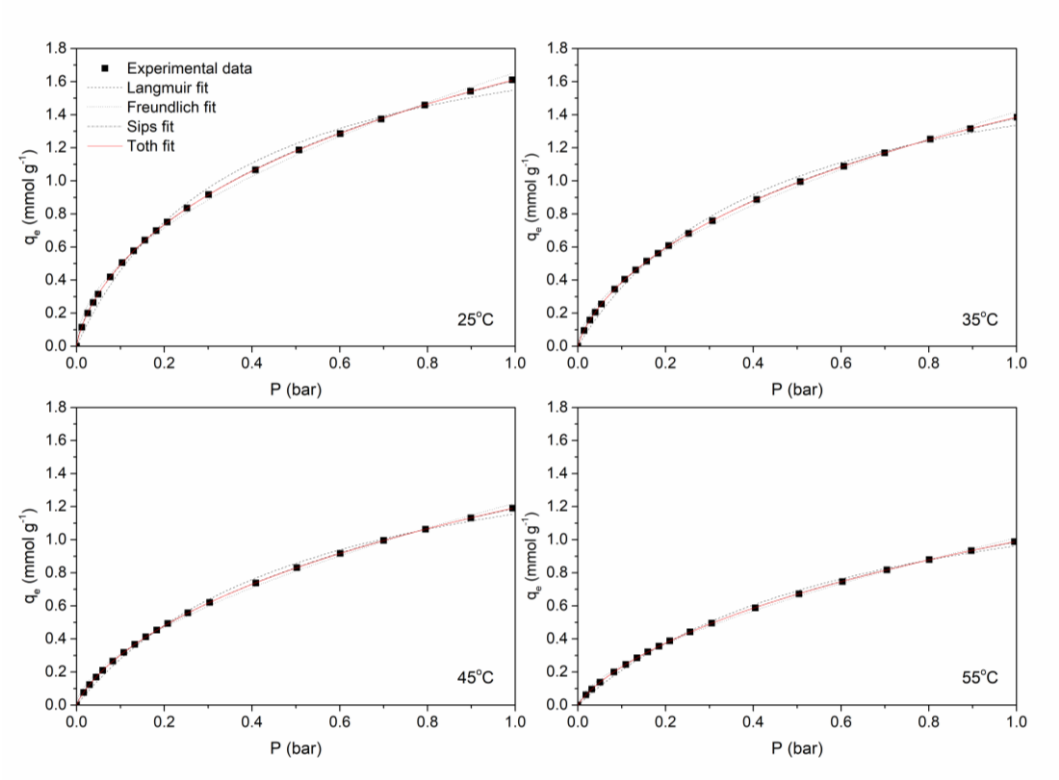

Figure 33 Fitting of CO_2 adsorption isotherms of noC15(800) at different temperatures with four selected isotherm models

จุฬาลงกรณ์มหาวิทยาลัย

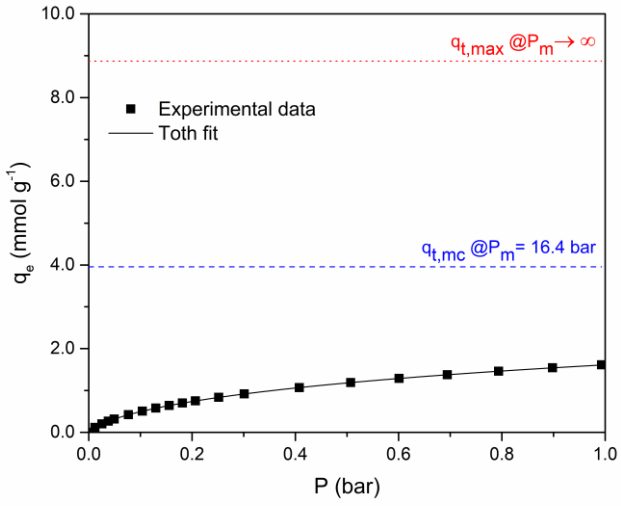

Figure 34 Overestimation of maximum capacity when using model without correction

Table 8 Parameters of fitting the CO_2 adsorption on noC15(800) data

Isotherm models		Fitting parameters	Adsorption temperature (°C)			
			25	35	45	55
Two-parameter isotherm	Langmuir	K_l	2.770	2.278	1.864	1.532
		$q_{l,max}$	2.109	1.924	1.777	1.593
		R^2	0.9933	0.9949	0.9963	0.9973
		MPSD	0.149	0.139	0.122	0.109
		%Err	14.5	13.5	11.9	10.6
	Freundlich	K_f	1.656	1.419	1.222	1.011
		n_f	0.520	0.555	0.593	0.624
		R^2	0.9971	0.9975	0.9979	0.9983
		MPSD	0.132	0.121	0.116	0.113
		%Err	12.9	11.8	11.3	11.0
Three-parameters isotherm	Sips	K_s	0.638	0.562	0.503	0.435
		n_s	0.695	0.724	0.756	0.779
		$q_{s,max}$	3.803	3.475	3.19	2.876
		R^2	0.9999	0.9999	0.9999	0.9999
		MPSD	0.025	0.018	0.018	0.020
		%Err	2.4	1.7	1.7	1.9
	Toth	K_t	2.629	1.653	1.055	0.707
		n_t	0.322	0.336	0.357	0.366
		$q_{t,max}$	8.872	8.564	8.115	7.868
		$q_{t,mc}$	3.960	2.990	2.990	2.990
		χ_t	1.297	1.424	1.428	1.425
		P_m (bar)	16.4	7.7	10.2	14.6
		R^2	0.9999	1.0000	1.0000	1.0000
		MPSD	0.0052	0.0023	0.0020	0.0027
		%Err	0.49	0.21	0.19	0.25

จุฬาลงกรณ์มหาวิทยาลัย
CHULALONGKORN UNIVERSITY

4.4 Statistical analyses

From the section 4.1.4 revealed that the factors affecting CO_2 adsorption capacity were microporosity and nitrogen content. This brings us to the question that which factor would affect CO_2 adsorption capacity between microporosity and nitrogen content. If any, which factor would have greater influence? To answer this question statistical analyses were used. The analyses were done by using statistical software, JMP® Pro 13. The analyses included analysis of variance (ANOVA), effect estimates, the studentized residual by row number plot and the residual plot. The statistical significance level was set at 95% confidential level where the differences in means was accepted at the P-value less than 0.05. The calculated sums of squares from software were based on type-III sum of square where the order dependency is removed to determine estimates of factor in a model. The sorbents were divided into two groups which are before nitriding and after nitriding. The CO_2 adsorption capacities of all samples were obtained at the adsorption temperature of 25 °C. We set response (y) to be CO_2 adsorption capacity (noted as capacity, mmol g^{-1}). Then we selected 4 factors that could possibly affect the response which are nitriding temperature (Temp, °C), MWF ratio (MWF, vol%), micropore volume (Vmicro, cm^3 g^{-1}), and nitrogen content obtained from XPS (%N, at%). The result of analyses was described below.

จุฬาลงกรณ์มหาวิทยาลัย
Chulalongkorn University

4.4.1 First screening

The first screening was done to see significance of 4 studied factors. This analysis was done on 12 observations that excluded samples without nitridation to see the contribution of nitriding temperature. The condition, factor and response on each condition were listed in Table 9. The validity of model fitting to data was determined the P-value of model showing in ANOVA table (Table 10), which is less than 0.05, so the model was valid. It was in good agreement with high value of R^2 (0.9537) and R^2 adjusted (0.9273). Moreover, the residual plot (Figure 35a) demonstrated good and random distribution meaning that there was no bias to our data. The studentized residual by row number plot (Figure 35b) also show no data

was out of the red line referring they were in 95% Bonferroni limit, so that there was no outlier. Then the significance of studied factors was determined by P-value in Table. There is only Temp factor that has P-value less than 0.05, therefore it is significant to response. However, the F-ratio of Temp is much greater than the others. So, it could be possible that the significance of other factors was masked by the significance of Temp. To make it clear, second screening was introduced.

Table 9 Twelve observations and its condition used for making statistical analysis

Sample	MWF ratio (vol%)	Vmicro ($cm^3\ g^{-1}$)	%N (at%)	Temp (°C)	Capacity (mmol g^{-1})
nC(600)	0	0.0232	1.18	600	0.8
nC(700)	0	0.0208	2.35	700	1.14
nC(800)	0	0.0563	1.29	800	1.33
noC5(600)	5	0.0356	1.84	600	0.89
noC5(700)	5	0.065	2.87	700	1.18
noC5(800)	5	0.1204	2.37	800	1.43
noC15(600)	15	0.0407	2.04	600	1.08
noC15(700)	15	0.0719	3.47	700	1.31
noC15(800)	15	0.1533	2.29	800	1.63
noC25(600)	25	0.0288	1.39	600	0.87
noC25(700)	25	0.0792	3	700	1.26
noC25(800)	25	0.1735	2.32	800	1.56

จุฬาลงกรณ์มหาวิทยาลัย
Chulalongkorn University

Table 10 ANOVA table of 1st screening

Source	DF	Sum of squares	Mean square	F ratio	P-value	
Model	4	0.7466	0.1867	36.0558	<.0001	<0.05
Residue	7	0.0362	0.0052			
C. Total	11	0.7829				
MWF ratio	1	0.0022		0.4191	0.5380	
Vmicro	1	0.0137		2.6512	0.1475	
Temp	1	0.0847		16.3605	0.0049	<0.05
%N	1	0.0190		3.6610	0.0973	
R^2	0.9537					
R^2 adjusted	0.9273					
Root Mean Square Error	0.0720					
Mean of Response	1.2067					
Observations	12					

จุฬาลงกรณ์มหาวิทยาลัย
CHULALONGKORN UNIVERSITY

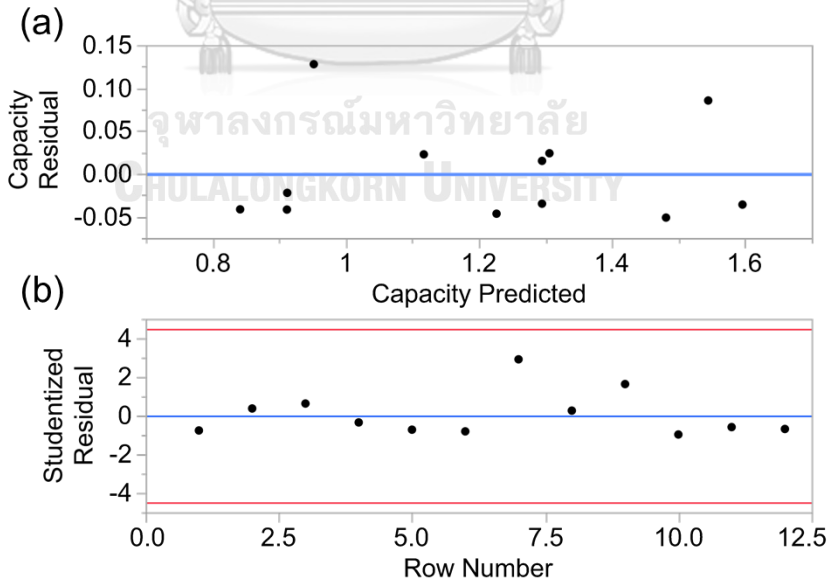

Figure 35 Residual plot (a) and Studentized residual by row number plot (b) for 1st screening analysis

4.4.2 Second screening

The second screening was conducted to test the effect of other factors excluded Temp factor. This time, the number of observations was increased to 16, in order to make the clearer data that containing Vmicro and %N at the level of zero by including CO_2 adsorption capacity of before-nitrided samples, showing in Table 11. Again, the results are presenting in ANOVA table in Table 12, residual plot in Figure 36a and studentized plot in Figure 36b. The analysis was again valid by considering high values of R^2 (0.9213) and R^2 adjusted (0.9017), P-value of model less than 0.05, and good distribution of data and they are within Bonferroni boundaries. After excluding activation Temp, Vmicro and %N become significant with P-value less than 0.05, while MWF is not significant by P-value greater than 0.05. This confirmed both Vmicro and %N affects the response, capacity, but they were masked by Temp which was highly significant. MWF is determined to be insignificant. Therefore, the next analysis will include these three main factors excluding MWF to analyze their interactions.

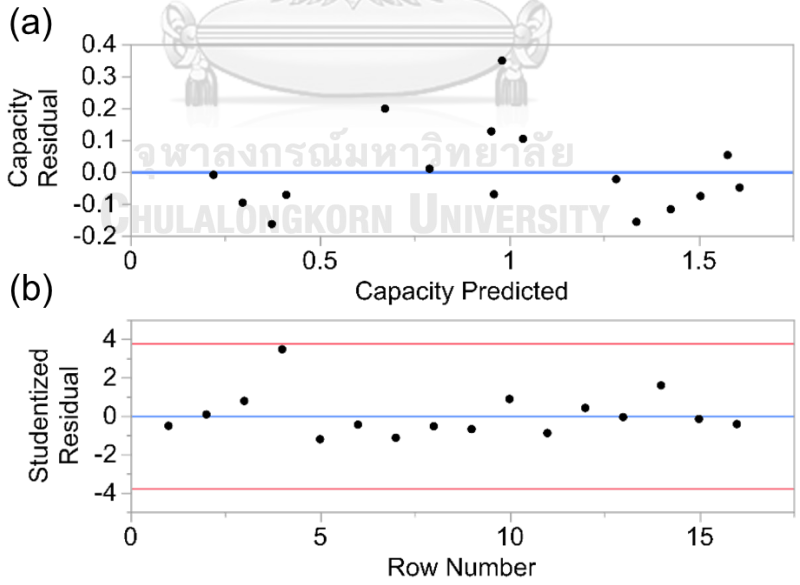

Figure 36 Residual plot (a) and Studentized residual by row number plot (b) for 2nd screening analysis

Table 11 Sixteen observations and its condition used for making statistical analysis

Sample	MWF ratio (vol%)	Vmicro ($cm^3\ g^{-1}$)	%N (at%)	Capacity (mmol g^{-1})
C	0	0.0000	0.00	0.34
nC(600)	0	0.0232	1.18	0.80
nC(700)	0	0.0208	2.35	1.14
nC(800)	0	0.0563	1.29	1.33
oC5	5	0.0000	0.00	0.21
noC5(600)	5	0.0356	1.84	0.89
noC5(700)	5	0.0650	2.87	1.18
noC5(800)	5	0.1204	2.37	1.43
oC15	15	0.0000	0.00	0.20
noC15(600)	15	0.0407	2.04	1.08
noC15(700)	15	0.0719	3.47	1.31
noC15(800)	15	0.1533	2.29	1.63
oC25	25	0.0000	0.00	0.21
noC25(600)	25	0.0288	1.39	0.87
noC25(700)	25	0.0792	3.00	1.26
noC25(800)	25	0.1735	2.32	1.56

จุฬาลงกรณ์มหาวิทยาลัย
Chulalongkorn University

Table 12 ANOVA table of 2nd screening

Source	DF	Sum of squares	Mean square	F ratio	P-value	
Model	3	3.3165	1.1055	46.8555	<.0001	<0.05
Residue	12	0.2831	0.0236			
C. Total	15	3.5996				
Vmicro	1	0.6033		25.5685	0.0003	<0.05
%N	1	0.5571		23.6113	0.0004	<0.05
MWF ratio	1	0.0796		3.3743	0.0911	
R^2	0.9213					
R^2 adjusted	0.9017					
Root Mean Square Error	0.1536					
Mean of Response	0.9650					
Observations	16					

4.4.3 Response surface methodology (RSM)

After screening processes were completed, next step is to investigate their contribution of 3 main effects, Temp, Vmicro and %N, and their interactions, Vmicro*Temp, Vmicro*%N, %N*Temp. The 12 observations were used again excluding samples without nitridation (Table 9). From ANOVA table in Table 13, shows that P-value is less than 0.05, with high level of R^2 and R^2 adjusted of 0.9722 and 0.9322, respectively. Furthermore, there is good and random distribution in residual plot (Figure 37a), and they are all in Bonferroni limits (Figure 37b). Thus, the model is valid, reliable, no bias and outlier.

To determine the contribution of factors, we made the assumptions to the analysis by assuming unequal variance and correlated. Since we know that from the experiment, Vmicro and %N were outcome from adjusting nitriding temperature. Thus, Vmicro and %N were not true dependent variables but correlating with dependent variable, nitriding temperature. The contribution of factors was

จุฬาลงกรณ์มหาวิทยาลัย
Chulalongkorn University

demonstrated by half-normal plot shown in Figure 38. It shows the deviation of factor from red line which has slope equal to 1. The factor with greater deviation will have greater contribution to the response. From the plot, the order of factor with decreasing in deviation is Vmicro, Vmicro*%N, %N, Vmicro*Temp, %N*Temp and Temp, respectively. From first screening temperature was the most significant factor, however when it was set to have correlation with Vmicro and %N, it was the least significant. This is because adjusting temperature would provide Vmicro and %N differently and the presence of those Vmicro and %N truly affects to the response with greater extent. The contribution of factors can be presented in Pareto plot, shown in Figure 39. It shows that Vmicro has the longest bar than the others meaning that Vmicro contributed response the most. From half normal plot and pareto plot, the answer was made that micropore volume had greater influence than nitrogen content on the sorbent in this study. Considering the sign on estimate of each factor, most of them have positive sign referring that they have positive effect to the response. While, the interaction between %N and Temp has negative effect.

The interaction of parameters was confirmed by interaction plot presenting in Figure 40. The presence of interaction between factors can be seen from those two lines in a graph that was unparalleled. The response surface of the interactions Vmicro*Temp, Vmicro*%N and %N*Temp are shown in Figure 41a, b, c, respectively. From Figure 41a, the higher capacity achieved when increasing Vmicro and Temp to the highest level. This is because increasing nitriding temperature developd more micropores, hence higher capacity. While, the interaction between Vmicro and %N expressed in Figure 41b showing a greater capacity when increasing both Vmicro and %N than its individual increasing. This confirmed the presence of synergistic effect between microporosity and nitrogen content with positively interactive effect. The negative interaction of %N and Temp is demonstrated in Figure 41c. The shape of surface is saddle-shaped reflecting curvature of the surface. The adsorption capacity increases with both Temp applied and %N on the sorbent to a maximum value, then it decreases when further increase Temp and %N. This contradiction caused by the fact that increasing nitriding temperature from 600 °C to 700 °C increased nitrogen content. However, further increasing temperature up to 800 °C decreased nitrogen

จุฬาลงกรณ์มหาวิทยาลัย
Chulalongkorn University

content. This is consistent to the report in previous section, 4.1.2 elemental analysis. So, decrease in nitrogen content would make CO_2 adsorption capacity lowered.

Table 13 ANOVA table of response surface analysis

Source	DF	Sum of squares	Mean square	F ratio	P-value	
Model	6	0.7611	0.1268	29.0896	0.001	<0.05
Residue	5	0.0218	0.0044			
C. Total	11	0.7829				
R^2	0.9722					
R^2 adjusted	0.9387					
Root Mean Square Error	0.0660					
Mean of Response	1.2067					
Observations	12					

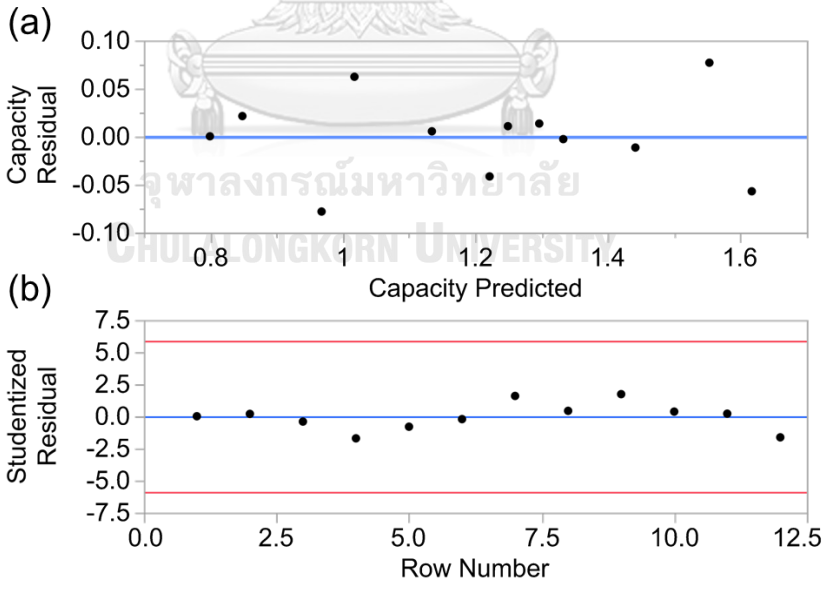

Figure 37 Residual plot (a) and Studentized residual by row number plot (b) for response surface analysis

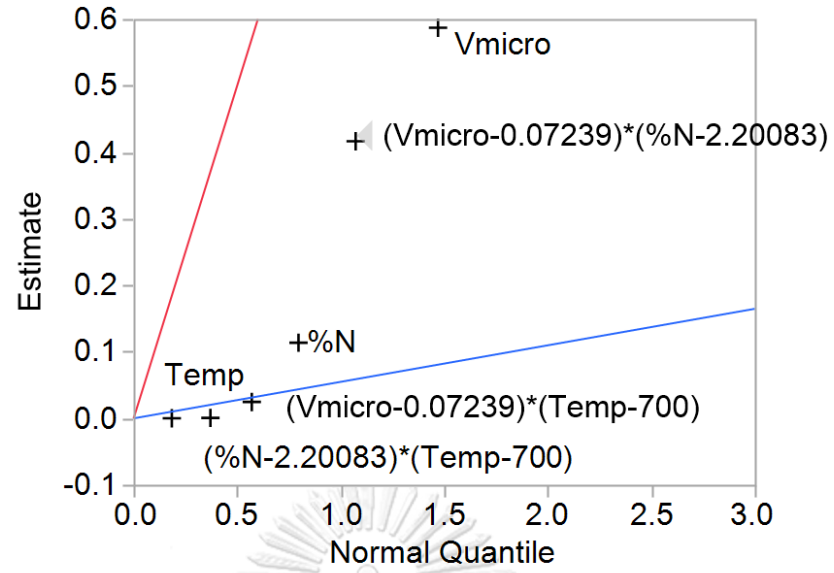

Blue line has slope equal to Lenth's PSE.
Red line has slope 1.

Figure 38 Half normal plot showing contribution of factors

Term	Estimate
Vmicro	0.5885453
(Vmicro-0.07239)*(%N-2.20083)	0.4179168
%N	0.1150754
(Vmicro-0.07239)*(Temp-700)	0.0260547
(%N-2.20083)*(Temp-700)	-0.0020138
Temp	0.0014838

Figure 39 Pareto plot

จุฬาลงกรณ์มหาวิทยาลัย
Chulalongkorn University

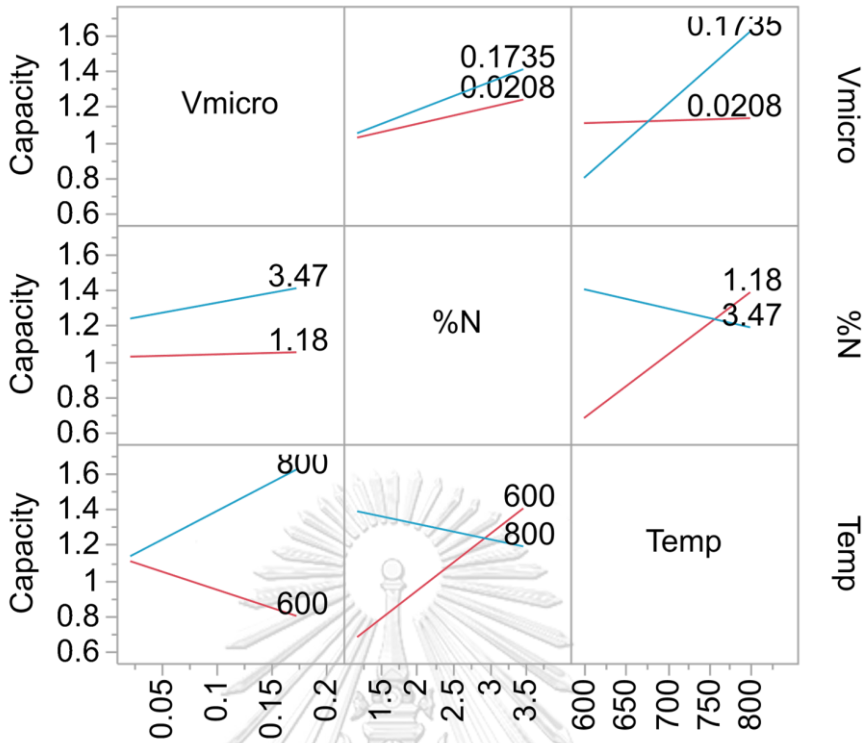

Figure 40 Interaction plot of 3 main effects

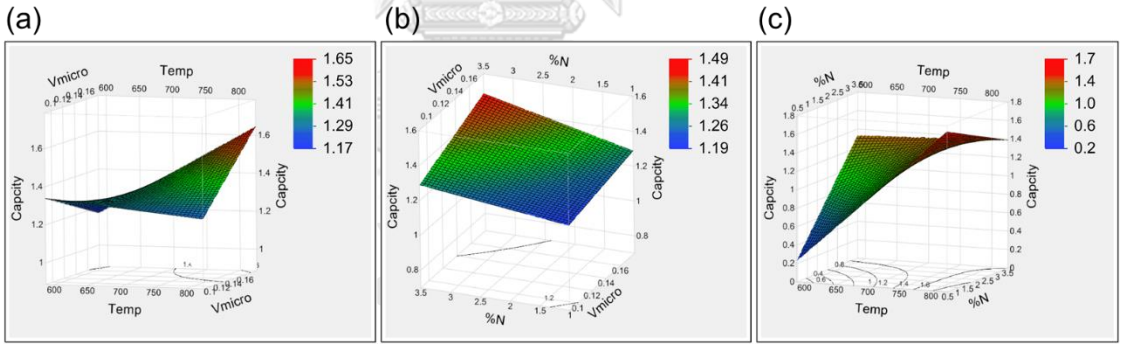

Figure 41 Surface response of interactions between (a) Vmicro and Temp, (b) Vmicro and %N (c) %N and Temp

The regression model was obtained from this analysis and its expression is shown in equation (19). This regression model was used to predict the response at different conditions. Then it was compared with actual value obtained from the experiment. The comparison and its percentage error were listed in Table 14. It was found that the predicted values from the model were in good agreement with actual value with percentage error less than 5%.

Capacity (y) = -0.183606832+0.5885453374*Vmicro
+ 0.1150753919*%N + 0.0014838195*Temp
+ (Vmicro-0.0723916667)*((%N-2.2008333333)*0.4179168137) (19)
+ (%N-2.2008333333)*((Temp-700)*-0.002013845)
+ (Vmicro-0.0723916667)*((Temp-700)*0.0260546817)

Table 14 Comparison of actual response and predicted response

Sample	Micropore volume ($cm^3\ g^{-1}$)	Nitriding temperature (°C)	%N (at%)	$q_{e,exp}$ (mmol g^{-1})	$q_{e,calc}$ (mmol g^{-1})	|%Err|
nC(700)	0.0208	700	2.35	1.14	1.13	0.48
nC(800)	0.0563	800	1.29	1.33	1.33	0.20
noC5(800)	0.1204	800	2.37	1.43	1.44	0.80
noC15(700)	0.0719	700	3.47	1.31	1.3	1.04
noC25(600)	0.0288	600	1.39	0.87	0.85	2.45

4.5 Deeper studies

From previous part, the major influence on CO_2 adsorption capacity was revealed. It was found that microporosity and nitrogen content played an important role to enhance adsorption capacity significantly. In this part, the contribution of them will be clarified below.

จุฬาลงกรณ์มหาวิทยาลัย
Chulalongkorn University

4.5.1 Influence of micropores on CO_2 adsorption potential

According to IUPAC classification of nanopores, micropore was defined to the pore with pore diameter (d_p) less than 0.2 nm. For mesopores, d_p is in range between 2 to 50 nm and lastly, macropore is above 50 nm. These different pore size attract CO_2 differently. This can be explained by the sorption potential purposed by Lennard-Jones model [83]. It is a plot of potential energy of sorbate molecule (**ε**) versus distance of separation of each pore size, showing in Figure 42. Generally, the potential energy decreases with the distance of sorbate closer to sorbent surface to

the minimum point, then it would drastically increase when it gets closer due to stronger repulsion between them. For Figure 42a, the adsorption in micropore has the strongest sorption potential. The sorbate molecule is superpositioned with greater extent by Van der Waals forces produced by two adjacent walls of pore which is the most stable compared to the other pore types. Adsorption in mesopore would give two minima potentials as shown in Figure 42b. These minima caused by sorbate molecule is close enough to a side of pore wall. At the center, potential energy is higher, but still lower than un-attracted. This refer sorbate molecule would be attracted partly with weaker attractive forces compared to the position near to the pore walls. For macropore sorption potential as described in Figure 42c, the potential energy is the highest compared to other pore types. Sorbate is weakly attracted by this kind of pore. In addition, adsorption of macropore is similar to the adsorption on the external surface which is the least preferred.

From the mentioned above, sorption potential of CO_2 increases with decreasing of pore. In our studies, CO_2 adsorption capacity increased after nanocarbon get nitrided. The development of microporosity enhance CO_2 adsorption efficiently due to that smaller pores had been created. This result was also consistent with thermodyncamic studies () that after nitrided, noC15(800) had lower isosteric enthalpy of adsorption than pristine carbon,C (∼-31 kJ mol^{-1} and ∼-25 kJ mol^{-1}, respectively). Moreover, isosteric enthalpy of adsorption decreases with increasing amount adsorbed. This refers the adsorption was filling into micropores first, with greater sorption potential, then it was followed by filling into larger pores, such as mesopores and macropores.

จุฬาลงกรณ์มหาวิทยาลัย
Chulalongkorn University

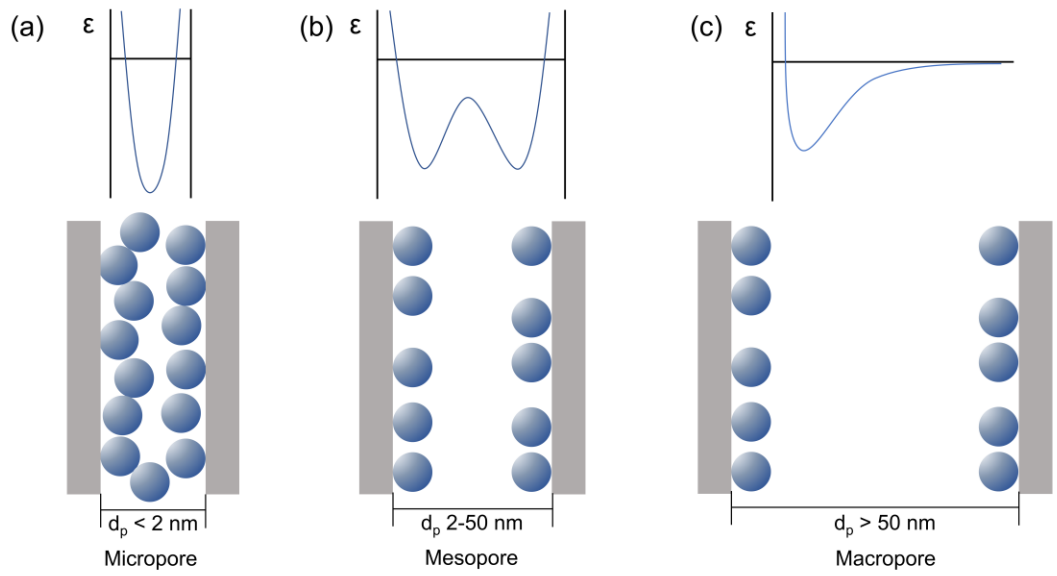

Figure 42 Sorption potentials on (a) micropore, (b) mesopore and (c) macropore

4.5.2 Influence of nitrogen atom in carbon framework on CO_2 adsorption mechanism

To clarify the contribution of nitrogen atom on CO_2 adsorption enhancement, the mechanism of CO_2 adsorption on noC15(800) was studied using the principles of classical chemistry. The major difference in the functional sites on the adsorbent surface were the presence of the bonding in the N 1s region on the noC15(800) surface. Nitrogen atoms in the carbon matrix have a greater affinity for CO_2 since the lone pair electron on the nitrogen atom, especially the pyridinic-N, acts as Lewis base while the C atom on CO_2 is an electrophile in nature [23], allowing them to form a Lewis acid-base interaction through N donating an electron to $C^{\delta+}$ on the CO_2 molecule. The adsorption of CO_2 on noC15(800) was mainly physisorption through weak forces. There was no change in the electronic properties of the CO_2-adsorbent complex and no significant change in the molecular orbital (MO) level [84]. So, from the perspective of quantum chemistry, electron donation and electron backdonation based on the highest occupied MO (HOMO) of the sorbent's surface interact attractively with the lowest unoccupied MO (LUMO) of the sorbate molecule. The MO of CO_2 is shown in Figure 43, while the interaction between the nitrogen atom on

the carbon structure and the C atom on CO_2 is shown in Figure 44. For electron donation, the electron pair in the non-bonding MO ($1\pi_g$), which is located on the oxygen atom of the CO_2 molecule, was donated to the LUMO on the C site of noC15(800). The electrons in the HOMO of the nitrogen atom of noC15(800) were then back donated to the LUMO of CO_2 ($2\pi_u$), which in this MO is mainly a $2p_{xC}$ [85]. That C, the pristine carbon without a nitrogen atom, had a higher adsorption barrier compared to noC15(800) was due to the larger energy gap between the HOMO and LUMO of C and the CO_2 adsorbate, leading to a lower adsorption capacity as described above. This also leads to a less favorable adsorption, which is in good agreement with the thermodynamic studies. The C has a lower Henry's constant than noC15(800), meaning that C has a lower CO_2 adsorption affinity. When nitrogen doped, the energy gap of the electron transfer between CO_2 and the adsorption site was reduced, which induces the local density of state below the Fermi level [24, 86].

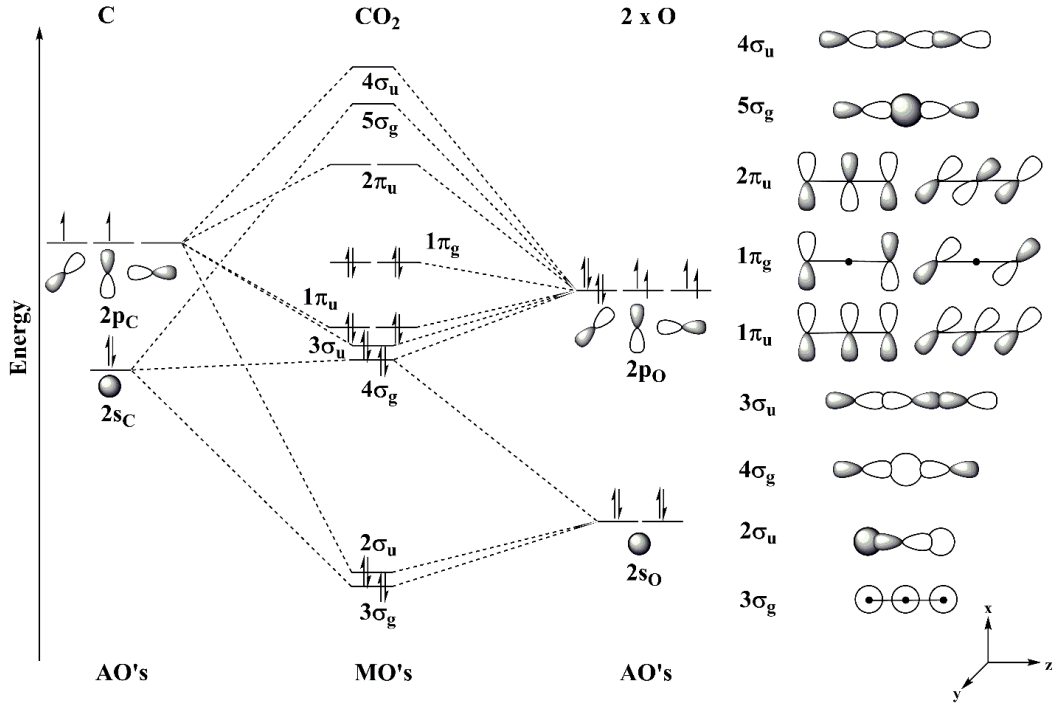

Figure 43 Molecular orbital diagram and the shape of orbitals of the CO_2 molecule [85, 87, 88]

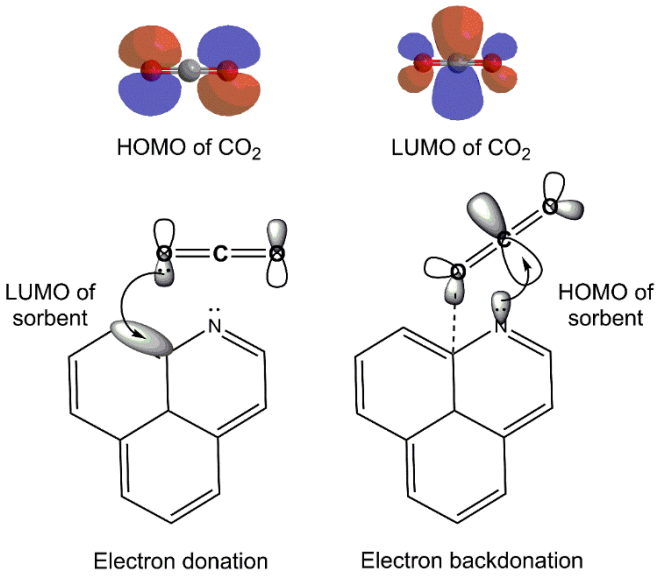

Figure 44 Adsorption mechanism of CO_2 on the noC15(800) adsorbent based on electron donation and backdonation

จุฬาลงกรณ์มหาวิทยาลัย
Chulalongkorn University

CHAPTER V
CONCLUSION

5.1 Synthesis of nanocarbon for CO_2 adsorption

In this dissertation, we successfully synthesized high performance of oxygen-doped nanocarbon from a mixture of benzene and metal working fluid via solution plasma process in a single step, which was then enhanced its CO_2 adsorption capacity by nitridation. Increase nitriding temperature from 600 °C to 700 °C, the maximum nitrogen content was achieved on 15 vol% of MWF mixed. Further increasing to 800 °C, the nitrogen content was decreased due to decomposition of nitrogen functionalities. Higher level of microporosity, particularly ultramicroporosity was received when increasing nitriding temperature. noC15(800) expressed the highest CO_2 adsorption capacity of 1.63 mmol g^{-1} at 25 °C of adsorption temperature.

5.2 CO_2 adsorption mechanism

From the studies of thermodynamics and isotherm, they revealed that the adsorption on noC15(800) was physisorption, exothermic, less spontaneous at higher temperature. The binding forces to CO_2 molecule on noC15(800) was stronger than pristine carbon, C, and it was on heterogeneous surface. Toth isotherm was the best-fit model to the CO_2 adsorption on noC15(800) over 25 °C to 55 °C range of adsorption temperature. Toth model explains that the adsorption was monolayer and on heterogenous surface. Nitridation not only increased CO_2 adsorption capacity but also enhanced selectivity of CO_2 over N_2. noC15(800) also showed good regenerability and stability over 5 cycles of use.

5.3 Influence of factors on CO_2 adsorption capacity

Investigation on contribution of studied parameters was done by using statistical analyses. The result showed that the presence of micropore influence more than nitrogen content on carbon framework. They also showed synergistic

จุฬาลงกรณ์มหาวิทยาลัย
Chulalongkorn University

effect to CO_2 adsorption capacity. The great influence of micropore was explained by strongest sorption potential due to the highest superposition extent of Van der Waals forces compared to the other pore types. While enhancement of CO_2 adsorption capacity by doping nitrogen was caused by creation of active site of nitrogen functionality which forms stronger binding forces via Lewis acid-base interaction or more affinity on electron donation and backdonation of LUMO and HOMO of sorbate and sorbent.

จุฬาลงกรณ์มหาวิทยาลัย
Chulalongkorn University

REFERENCES

[1] COP 21 Paris France Sustainable Innovation Forum 2015 working with United Nations Environment Programme (UNEP). [cited Jan 18, 2019]; Available from: http://www.cop21paris.org/about/cop21.

[2] Choi, S., Drese, J. H. and Jones, C. W. Adsorbent materials for carbon dioxide capture from large anthropogenic point sources. ChemSusChem 2 (2009): 796-854, doi:http://doi.org/10.1002/cssc.200900036.

[3] Xu, X. C., Andresen, J. M., Song, C. S., Miller, B. G. and Scaroni, A. W. Preparation of novel CO_2 "molecular basket" of polymer modified MCM-41. Abstracts of Papers of the American Chemical Society 223 (2002): U573-U573, doi:<Go to ISI>://WOS:000176296703142.

[4] Su, F. S., Lu, C. Y., Kuo, S. C. and Zeng, W. T. Adsorption of CO_2 on amine-functionalized Y-type zeolites. Energy & Fuels 24 (2010): 1441-1448, doi:http://doi.org/10.1021/ef901077k.

[5] Bhagiyalakshmi, M., Yun, L. J., Anuradha, R. and Jang, H. T. Synthesis of chloropropylamine grafted mesoporous MCM-41, MCM-48 and SBA-15 from rice husk ash: their application to CO_2 chemisorption. Journal of Porous Materials 17 (2009): 475-484, doi:https://doi.org/10.1007/s10934-009-9310-7.

[6] Xu, X. C., Song, C. S., Miller, B. G. and Scaroni, A. W. Influence of moisture on CO_2 separation from gas mixture by a nanoporous adsorbent based on polyethylenimine-modified molecular sieve MCM-41. Industrial & Engineering Chemistry Research 44 (2005): 8113-8119, doi:http://doi.org/10.1021/ie050382n.

[7] Houshmand, A., Daud, W. M. A. W., Lee, M.-G. and Shafeeyan, M. S. Carbon dioxide capture with amine-grafted activated carbon. Water, Air, & Soil Pollution 223 (2011): 827-835, doi:https://doi.org/10.1007/s11270-011-0905-7.

[8] Gray, M. L., et al. Parametric study of solid amine sorbents for the capture of carbon dioxide. Energy & Fuels 23 (2009): 4840-4844, doi:https://doi.org/10.1021/ef9001204.

[9] Veneman, R., Li, Z. S., Hogendoorn, J. A., Kersten, S. R. A. and Brilman, D. W. F.

จุฬาลงกรณ์มหาวิทยาลัย
Chulalongkorn University

Continuous CO_2 capture in a circulating fluidized bed using supported amine sorbents. Chemical Engineering Journal 207-208 (2012): 18-26, doi:http://doi.org/10.1016/j.cej.2012.06.100.

[10] Xu, X., Song, C., Andresen, J. M., Miller, B. G. and Scaroni, A. W. Novel Polyethylenimine-Modified Mesoporous Molecular Sieve of MCM-41 Type as High-Capacity Adsorbent for CO_2 Capture. Energy & Fuels 16 (2002): 1463-1469, doi:http://doi.org/10.1021/ef020058u.

[11] Yue, M. B., Chun, Y., Cao, Y., Dong, X. and Zhu, J. H. CO_2 Capture by As-Prepared SBA-15 with an Occluded Organic Template. Advanced Functional Materials 16 (2006): 1717-1722, doi:http://doi.org/10.1002/adfm.200600427.

[12] Wei, J., et al. A Controllable Synthesis of Rich Nitrogen-Doped Ordered Mesoporous Carbon for CO_2 Capture and Supercapacitors. Advanced Functional Materials 23 (2013): 2322-2328, doi:http://doi.org/10.1002/adfm.201202764.

[13] Zhao, X. C., et al. Synthesis and Electrochemical Performance of Heteroatom-Incorporated Ordered Mesoporous Carbons. Chemistry of Materials 22 (2010): 5463-5473, doi:http://doi.org/10.1021/cm101072z.

[14] Hao, G.-P., et al. Lysine-assisted rapid synthesis of crack-free hierarchical carbon monoliths with a hexagonal array of mesopores. Carbon 49 (2011): 3762-3772, doi:https://doi.org/10.1016/j.carbon.2011.05.010.

[15] Kang, J., Li, O. L. and Saito, N. Synthesis of structure-controlled carbon nano spheres by solution plasma process. Carbon 60 (2013): 292-298, doi:http://doi.org/10.1016/j.carbon.2013.04.040.

[16] Dura, G., et al. Importance of Micropore-Mesopore Interfaces in Carbon Dioxide Capture by Carbon-Based Materials. Angewandte Chemie International edition 55 (2016): 9173-9177, doi:https://doi.org/10.1002/anie.201602226.

[17] Presser, V., McDonough, J., Yeon, S.-H. and Gogotsi, Y. Effect of pore size on carbon dioxide sorption by carbide derived carbon. Energy & Environmental Science 4 (2011): 3059-3066, doi:http://doi.org/10.1039/c1ee01176f.

[18] Zhang, Z., et al. Critical role of small micropores in high CO_2 uptake. Physical Chemistry Chemical Physics 15 (2013): 2523-2529, doi:http://doi.org/10.1039/c2cp44436d.

จุฬาลงกรณ์มหาวิทยาลัย
Chulalongkorn University

[19] Yu, J., et al. One-pot synthesis of highly ordered nitrogen-containing mesoporous carbon with resorcinol–urea–formaldehyde resin for CO_2 capture. Carbon 69 (2014): 502-514, doi:http://doi.org/10.1016/j.carbon.2013.12.058.

[20] Yu, J., et al. Simple fabrication of an ordered nitrogen-doped mesoporous carbon with resorcinol–melamine–formaldehyde resin. Microporous and Mesoporous Materials 190 (2014): 117-127, doi:http://doi.org/10.1016/j.micromeso.2014.02.009.

[21] Jin, Z. Y., Xu, Y. Y., Sun, Q. and Lu, A. H. Evidence of Microporous Carbon Nanosheets Showing Fast Kinetics in both Gas Phase and Liquid Phase Environments. Small 11 (2015): 5151-5156, doi:https://doi.org/10.1002/smll.201501692.

[22] Hao, G.-P., et al. Porous carbon nanosheets with precisely tunable thickness and selective CO_2 adsorption properties. Energy & Environmental Science 6 (2013): 3740-3747, doi:https://doi.org/10.1039/c3ee41906a.

[23] Lim, G., Lee, K. B. and Ham, H. C. Effect of N-Containing Functional Groups on CO_2 Adsorption of Carbonaceous Materials: A Density Functional Theory Approach. The Journal of Physical Chemistry C 120 (2016): 8087-8095, doi:https://doi.org/10.1021/acs.jpcc.5b12090.

[24] Kiuchi, H., et al. Lewis Basicity of Nitrogen-Doped Graphite Observed by CO_2 Chemisorption. Nanoscale Research Letters 11 (2016): 127, doi:https://doi.org/10.1186/s11671-016-1344-6.

[25] Shafeeyan, M. S., Daud, W. M. A. W., Houshmand, A. and Arami-Niya, A. Ammonia modification of activated carbon to enhance carbon dioxide adsorption: Effect of pre-oxidation. Applied Surface Science 257 (2011): 3936-3942, doi:http://doi.org/10.1016/j.apsusc.2010.11.127.

[26] Ishizaki, T., Chiba, S., Kaneko, Y. and Panomsuwan, G. Electrocatalytic activity for the oxygen reduction reaction of oxygen-containing nanocarbon synthesized by solution plasma. Journal of Materials Chemistry A 2 (2014): 10589-10598 doi:https://doi.org/10.1039/c4ta01577k.

[27] Panomsuwan, G., Chiba, S., Kaneko, Y., Saito, N. and Ishizaki, T. In situ solution plasma synthesis of nitrogen-doped carbon nanoparticles as metal-free electrocatalysts for the oxygen reduction reaction. Journal of Materials Chemistry A 2 (2014): 18677-18686, doi:http://doi.org/10.1039/c4ta03010a.

จุฬาลงกรณ์มหาวิทยาลัย
Chulalongkorn University

[28] 2014. Climate Change 2014: Mitigation of Climate Change. Contribution of Working Group III to the Fifth Assessment Report of the Intergovernmental Panel on Climate Change. Edenhofer, O., R. Pichs-Madruga, Y. Sokona, E. Farahani, S. Kadner, K. Seyboth, A. Adler, I. Baum, S. Brunner, P. Eickemeier, B. Kriemann, J. Savolainen, S. Schlömer, C. von Stechow, T. Zwickel and J.C. Minx (Eds.). Press, C. U., Cambridge, United Kingdom and New York, NY, USA.

[29] Trends in Atmospheric Carbon Dioxide. [cited Jan 18, 2019]; Available from: http://www.esrl.noaa.gov/gmd/ccgg/trends/.

[30] Global Greenhouse Gas Emissions Data. [cited Jan 31, 2019]; Available from: https://www.epa.gov/ghgemissions/global-greenhouse-gas-emissions-data.

[31] Yu, C.-H. A Review of CO_2 Capture by Absorption and Adsorption. Aerosol and Air Quality Research 12 (2012): 745-769, doi:http://doi.org/10.4209/aaqr.2012.05.0132.

[32] Gui, M. M., Yap, Y. X., Chai, S.-P. and Mohamed, A. R. Multi-walled carbon nanotubes modified with (3-aminopropyl)triethoxysilane for effective carbon dioxide adsorption. International Journal of Greenhouse Gas Control 14 (2013): 65-73, doi:http://doi.org/10.1016/j.ijggc.2013.01.004.

[33] Su, F., Lu, C., Chung, A.-J. and Liao, C.-H. CO_2 capture with amine-loaded carbon nanotubes via a dual-column temperature/vacuum swing adsorption. Applied Energy 113 (2014): 706-712, doi:http://doi.org/10.1016/j.apenergy.2013.08.001.

[34] Park, H., Jung, Y. M., You, J. K., Hong, W. H. and Kim, J. N. Analysis of the CO_2 and NH3 reaction in an aqueous solution by 2D IR COS: formation of bicarbonate and carbamate. The Journal of Physical Chemistry A 112 (2008): 6558-6562, doi:https://www.ncbi.nlm.nih.gov/pubmed/18582024.

[35] Yu, J., et al. An examination of alkali-exchanged BEA zeolites as possible Lewis-acid catalysts. Microporous and Mesoporous Materials 225 (2016): 472-481, doi:https://doi.org/10.1016/j.micromeso.2016.01.039.

[36] Nalaparaju, A., Khurana, M., Farooq, S., Karimi, I. A. and Jiang, J. W. CO 2 capture in cation-exchanged metal–organic frameworks: Holistic modeling from molecular simulation to process optimization. Chemical Engineering Science 124 (2015): 70-78, doi:https://doi.org/10.1016/j.ces.2014.09.054.

[37] Kawamura, Y., Iwai, Y., Munakata, K. and Yamanishi, T. Effect of cation exchange

จุฬาลงกรณ์มหาวิทยาลัย
Chulalongkorn University

on hydrogen adsorption property of mordenite for isotope separation. Journal of Nuclear Materials 442 (2013): S455-S460, doi:https://doi.org/10.1016/j.jnucmat.2012.11.003.

[38] Abdullahi, T., Harun, Z. and Othman, M. H. D. A review on sustainable synthesis of zeolite from kaolinite resources via hydrothermal process. Advanced Powder Technology 28 (2017): 1827-1840, doi:http://dx.doi.org/10.1016/j.apt.2017.04.028.

[39] Alothman, Z. A Review: Fundamental Aspects of Silicate Mesoporous Materials. Materials 5 (2012): 2874-2902, doi:http://doi.org/10.3390/ma5122874.

[40] Knezevic, N., et al. Hard Template Synthesis of Nanomaterials Based on Mesoporous Silica. Metallurgical and Materials Engineering 24 (2018): 225-241, doi:https://doi.org/10.30544/400.

[41] Allotropes of carbon. [cited 1 Feb, 2019]; Available from: https://en.wikipedia.org/wiki/Allotropes_of_carbon.

[42] Antonio E. H. Machado, K. A. B., Tatiana A. Silva, Lidiaine M. Santos, Mariana F. Borges, Werick A. Machado, Bruno P. Caixeta, Marcela Dias França, Samuel M. Oliveira, Alam G. Trovó and Antonio O.T. Patrocínio, 2015. Applications of Mesoporous Ordered Semiconductor Materials — Case Study of TiO_2, in: Bello, S. R. (Ed.), Solar Radiation Applications. IntechOpen.

[43] Chen, C., et al. Template-free synthesis of hierarchical porous carbon with controlled morphology for CO_2 efficient capture. Chemical Engineering Journal 353 (2018): 584-594, doi:https://doi.org/10.1016/j.cej.2018.07.161.

[44] Rabbani, M. G. and El-Kaderi, H. M. Template-Free Synthesis of a Highly Porous Benzimidazole-Linked Polymer for CO_2 Capture and H2Storage. Chemistry of Materials 23 (2011): 1650-1653, doi:http://doi.org/10.1021/cm200411p.

[45] Yao, C., Li, G., Wang, J., Xu, Y. and Chang, L. Template-free synthesis of porous carbon from triazine based polymers and their use in iodine adsorption and CO_2 capture. Scientific Reports 8 (2018): 1867, doi:http://doi.org/10.1038/s41598-018-20003-1.

[46] Zhang, S., Mandai, T., Ueno, K., Dokko, K. and Watanabe, M. Hydrogen-bonding supramolecular protic salt as an “all-in-one” precursor for nitrogen-doped mesoporous carbons for CO_2 adsorption. Nano Energy 13 (2015): 376-386,

จุฬาลงกรณ์มหาวิทยาลัย
Chulalongkorn University

doi:https://doi.org/10.1016/j.nanoen.2015.03.006.

[47] Narula, U., Tan, C. M. and Lai, C. S. Growth Mechanism for Low Temperature PVD Graphene Synthesis on Copper Using Amorphous Carbon. Scientific Reports 7 (2017): 44112, doi:https://www.ncbi.nlm.nih.gov/pubmed/28276475.

[48] Li, X., et al. Transfer of large-area graphene films for high-performance transparent conductive electrodes. Nano Letters 9 (2009): 4359-4363, doi:http://doi.org/10.1021/nl902623y.

[49] Li, X., et al. Large-area synthesis of high-quality and uniform graphene films on copper foils. Science 324 (2009): 1312-1314, doi:http://doi.org/10.1126/science.1171245.

[50] Bratescu, M. A., Cho, S.-P., Takai, O. and Saito, N. Size-Controlled Gold Nanoparticles Synthesized in Solution Plasma. The Journal of Physical Chemistry C 115 (2011): 24569-24576, doi:http://doi.org/10.1021/jp207447c.

[51] Heo, Y. K. and Lee, S. Y. Effects of the gap distance on the characteristics of gold nanoparticles in nanofluids synthesized using solution plasma processing. Metals and Materials International 17 (2011): 431-434, doi:http://doi/org/10.1007/s12540-011-0620-3.

[52] Takai, O. Fundamentals and Applications of Solution Plasma. Journal of Photopolymer Science and Technology 27 (2014): 379-384, doi:https://doi.org/10.2494/photopolymer.27.379.

[53] Morishita, T., et al. Fastest Formation Routes of Nanocarbons in Solution Plasma Processes. Scientific Reports 6 (2016): 36880, doi:http://doi.org/10.1038/srep36880.

[54] Saito, N., Bratescu, M. A. and Hashimi, K. Solution plasma: A new reaction field for nanomaterials synthesis. Japanese Journal of Applied Physics 57 (2018): doi:https://doi.org/10.7567/JJAP.57.0102A4.

[55] Langmuir, I. The Adsorption of Gases on Plane Surfaces of Glass, Mica and Platinum. Journal of the American Chemical Society 40 (1918): 1361-1403, doi:https://doi.org/10.1021/ja02242a004.

[56] Freundlich, H. Over the Adsorption in Solution. The Journal of Physical Chemistry 57 (1906): 385-470,

[57] Sips, R. On the Structure of a Catalyst Surface. The Journal of Chemical Physics 16 (1948): 490-495, doi:http://doi.org/10.1063/1.1746922.

จุฬาลงกรณ์มหาวิทยาลัย
Chulalongkorn University

[58] Skopp, J. Derivation of the Freundlich Adsorption Isotherm from Kinetics. Journal of Chemical Education 86 (2009): 1341, doi:http://doi.org/10.1021/ed086p1341.

[59] Saadi, R., Saadi, Z., Fazaeli, R. and Fard, N. E. Monolayer and multilayer adsorption isotherm models for sorption from aqueous media. Korean Journal of Chemical Engineering 32 (2015): 787-799, doi:http://doi.org/10.1007/s11814-015-0053-7.

[60] Sips, R. On the Structure of a Catalyst Surface II. The Journal of Chemical Physics 18 (1950): 1024-1026, doi:http://doi.org/10.1063/1.1747848.

[61] Tóth, J. Uniform interpretation of gas/solid adsorption. Advances in Colloid and Interface Science 55 (1995): 1-239, doi:http://doi.org/10.1016/0001-8686(94)00226-3.

[62] Tóth, J. Some Consequences of the Application of Incorrect Gas/Solid Adsorption Isotherm Equations. Journal of Colloid and Interface Science 185 (1997): 228-235, doi:http://doi.org/10.1006/jcis.1996.4562.

[63] Tóth, J. Modifications in Classic Relationships Corresponding to Gas/Solid Physical Adsorption. Journal of Colloid and Interface Science 191 (1997): 449-455, doi:http://doi.org/10.1006/jcis.1997.4973.

[64] Garnier, C., et al. Selection of coals of different maturities for CO_2 Storage by modelling of CH_4 and CO_2 adsorption isotherms. International Journal of Coal Geology 87 (2011): 80-86,

[65] McClellan, A. L. and Harnsberger, H. F. Cross-sectional areas of molecules adsorbed on solid surfaces. Journal of Colloid and Interface Science 23 (1967): 577-599, doi:https://doi.org/10.1016/0021-9797(67)90204-4.

[66] Jousten, K. Handbook of Vacuum Technology. Second. Wiley-VCH, 2016.

[67] Czepirski, L. and JagieŁŁo, J. Virial-type thermal equation of gas—solid adsorption. Chemical Engineering Science 44 (1989): 797-801, doi:https://doi.org/10.1016/0009-2509(89)85253-4.

[68] Neti, V. S. P. K., Wang, J., Deng, S. and Echegoyen, L. High and selective CO_2 adsorption by a phthalocyanine nanoporous polymer. Journal of Materials Chemistry A 3 (2015): 10284-10288, doi:http://doi.org/10.1039/c5ta00587f.

[69] Mangun, C. L., Benak, K. R., Economy, J. and Foster, K. L. Surface chemistry, pore sizes and adsorption properties of activated carbon fibers and precursors treated with ammonia. Carbon 39 (2001): 1809-1820, doi:http://doi.org/10.1016/s0008-

จุฬาลงกรณ์มหาวิทยาลัย
Chulalongkorn University

6223(00)00319-5.

[70] Pevida, C., et al. Surface modification of activated carbons for CO_2 capture. Applied Surface Science 254 (2008): 7165-7172, doi:http://doi.org/10.1016/j.apsusc.2008.05.239.

[71] Sreńscek-Nazzal, J., Narkiewicz, U., Morawski, A. W., Wróbel, R. J. and Michalkiewicz, B. Comparison of Optimized Isotherm Models and Error Functions for Carbon Dioxide Adsorption on Activated Carbon. Journal of Chemical & Engineering Data 60 (2015): 3148-3158, doi:https://doi.org/10.1021/acs.jced.5b00294.

[72] Marquardt, D. W. An Algorithm for Least-Squares Estimation of Nonlinear Parameters. Journal of the Society for Industrial and Applied Mathematics 11 (1963): 431-441, doi:http://doi.org/10.1137/0111030.

[73] Pansare, S. S., Torres, W. and Goodwin, J. G. Ammonia decomposition on tungsten carbide. Catalysis Communications 8 (2007): 649-654, doi:http://doi.org/10.1016/j.catcom.2006.08.016.

[74] Stöhr, B., Boehm, H. P. and Schlögl, R. Enhancement of the catalytic activity of activated carbons in oxidation reactions by thermal treatment with ammonia or hydrogen cyanide and observation of a superoxide species as a possible intermediate. Carbon 29 (1991): 707-720, doi:http://doi.org/10.1016/0008-6223(91)90006-5.

[75] Shafeeyan, M. S., Daud, W. M. A. W., Houshmand, A. and Shamiri, A. A review on surface modification of activated carbon for carbon dioxide adsorption. Journal of Analytical and Applied Pyrolysis 89 (2010): 143-151, doi:http://doi.org/10.1016/j.jaap.2010.07.006.

[76] Thommes, M., et al. Physisorption of gases, with special reference to the evaluation of surface area and pore size distribution (IUPAC Technical Report). Pure and Applied Chemistry 87 (2015): 1051-1069, doi:http://doi.org/10.1515/pac-2014-1117.

[77] Brunauer, S., Emmett, P. H. and Teller, E. Adsorption of Gases in Multimolecular Layers. Journal of the American Chemical Society 60 (1938): 309-319, doi:https://doi.org/10.1021/ja01269a023.

[78] Ferrari, A. C. and Basko, D. M. Raman spectroscopy as a versatile tool for studying the properties of graphene. Nature Nanotechnology 8 (2013): 235-246,

จุฬาลงกรณ์มหาวิทยาลัย
Chulalongkorn University

doi:https://doi.org/10.1038/nnano.2013.46.

[79] Dresselhaus, M. S., Jorio, A., Hofmann, M., Dresselhaus, G. and Saito, R. Perspectives on carbon nanotubes and graphene Raman spectroscopy. Nano Letters 10 (2010): 751-758, doi:https://doi.org/10.1021/nl904286r.

[80] Wang, H., Maiyalagan, T. and Wang, X. Review on Recent Progress in Nitrogen-Doped Graphene: Synthesis, Characterization, and Its Potential Applications. ACS Catalysis 2 (2012): 781-794, doi:http://doi.org/10.1021/cs200652y.

[81] Cançado, L. G., et al. General equation for the determination of the crystallite size La of nanographite by Raman spectroscopy. Applied Physics Letters 88 (2006): 163106, doi:https://doi.org/10.1063/1.2196057.

[82] Golden, T. C. and Sircar, S. Gas Adsorption on Silicalite. Journal of Colloid and Interface Science 162 (1994): 182-188, doi:http://doi.org/10.1006/jcis.1994.1023.

[83] Everett, D. H. and Powl, J. C. Adsorption in slit-like and cylindrical micropores in the henry's law region. A model for the microporosity of carbons. Journal of the Chemical Society, Faraday Transactions 1: Physical Chemistry in Condensed Phases 72 (1976): doi:http://doi.org/10.1039/F19767200619.

[84] Madyal, R. S. and Arora, J. S. DFT studies for the evaluation of amine functionalized polystyrene adsorbents for selective adsorption of carbon dioxide. RSC Advances 4 (2014): 20323-20333, doi:http://doi.org/10.1039/c4ra00444b.

[85] Aresta, M. and Angelini, A. Carbon Dioxide and Organometallics. (53), First. Topics in Organometallic Chemistry. New York: Springer International Publishing, 2016.

[86] Chai, G. L. and Guo, Z. X. Highly effective sites and selectivity of nitrogen-doped graphene/CNT catalysts for CO_2 electrochemical reduction. Chemical Science 7 (2016): 1268-1275, doi:https://doi.org/10.1039/c5sc03695j.

[87] Allan, C. J., et al. ESCA studies of CO_2, CS_2 and COS. Journal of Electron Spectroscopy and Related Phenomena 1 (1972): 131-151, doi:https://doi.org/10.1051/jphyscol:1971416.

[88] Paparo, A. and Okuda, J. Carbon dioxide complexes: Bonding modes and synthetic methods. Coordination Chemistry Reviews 334 (2017): 136-149, doi:https://doi.org/10.1016/j.ccr.2016.06.005.

จุฬาลงกรณ์มหาวิทยาลัย
Chulalongkorn University

จุฬาลงกรณ์มหาวิทยาลัย
Chulalongkorn University

จุฬาลงกรณ์มหาวิทยาลัย
Chulalongkorn University

VITA

NAME	Phuwadej Pornaroontham
DATE OF BIRTH	25 July 1989
PLACE OF BIRTH	Bangkok, Thailand
INSTITUTIONS ATTENDED	Department of Chemical Technology, Faculty of Science, Chulalongkorn University
HOME ADDRESS	187/4 Kanchanapisek Rd. Tha Kham Bangkhuntien Bangkok Thailand 10150
PUBLICATION	Publications: Enhancement of CO2 adsorption capacity on nanocarbons via nitrogen-oxygen-codoping synthesized by solution plasma process and nitridation (Preparing) Statistical analysis for nitrogen-oxygen-codoped nanocarbon derived from aromatic compounds via solution plasma and nitridation (Preparing) Conferences: Phuwadej Pornaroontham, Nagahiro Saito, and Sangobtip Pongstabodee, "Carbon dioxide Capture on Aminated Carbon Nanoparticle Derived from Aromatic Compounds via Solution Plasma Process". 2017 Workshop on Biomimetic Materials and Energy-Saving Materials (2017BMEM), Shanghai, China, November 2017. Phuwadej Pornaroontham, Sangobtip Pongstabodee, Nagahiro Saito, "Carbon dioxide Capture on Nitrogen-doped Carbon Nanoparticle Derived from Aromatic

จุฬาลงกรณ์มหาวิทยาลัย
Chulalongkorn University

Compounds via Solution Plasma and Nitriding Processes", The 3rd Seminar on JSPS Core-to-Core Program (B. Asia-Africa Science Platforms) “Establishment of Research Hub for Compact Mobility Model in the ASEAN Region”, Nagoya, Japan, February 2018.

จุฬาลงกรณ์มหาวิทยาลัย
Chulalongkorn University